Chapter 3
State of the Art and Future Perspectives of Ba Scandate Dispenser Cathodes

Georg Gaertner and Yiman Wang

Abstract So far Ba scandate cathodes have shown the highest emission capability of all thermionic cathodes and are promising for future applications, e.g., in thermionic converters, in high-power high-frequency tubes, especially in vacuum terahertz devices. They are essentially based on Ba dispenser matrix cathodes modified with differently distributed additions of scandia. In this review, the historical development of different types of Ba scandate cathodes is addressed. Then the Philips activities on Laser ablation deposition (LAD) top-layer scandate cathodes with Re and Ba scandates are presented, which were mainly aimed at increasing ion bombardment resistivity and hence lifetime, but also led to record saturated pulsed emission of up to 400 A/cm^2. Finally, the activities on nanosized-Scandia Doped Dispenser cathodes (SDD cathode) carried out more recently at Beijing University of Technology (BJUT) and Beijing Vacuum Electronics Research Institute (BVERI) in China, which mainly focused on application in high current density, long life advanced vacuum electron devices, are introduced. The outstanding emission capability and lifetime tested at both diodes and electron guns are presented and also basic investigations on the emission model are discussed. A further motivation for this review is to derive guidelines for more robust highly emissive Ba scandate cathodes suitable for future tube applications.

G. Gaertner (✉)
Consultant, Aachen, Germany
e-mail: georg.f.gaertner@t-online.de

Y. Wang
Beijing, China
e-mail: wangym0709@yahoo.com

G. Gaertner et al. (eds.), *Modern Developments in Vacuum Electron Sources*,
Topics in Applied Physics 135, https://doi.org/10.1007/978-3-030-47291-7_3

3.1 Introduction: Historical Development of Different Types of Ba Scandate Dispenser Cathodes and Application Perspectives

As we have already seen in Chap. 1, vacuum electron sources or cathodes are the crucial components of a wide range of vacuum electron devices (VEDs) such as cathode-ray tubes (CRTs), X-ray tubes, or microwave tubes [1, 2]. Despite the decline of CRTs, advanced microwave and terahertz devices with applications ranging from civilian communication and scientific research to military and space-based technologies are being continuously improved [1–3]. One of the development challenges for advanced high power VEDs are electron sources with high current densities and long lifetime. VEDs operating at millimeter-wave and in THz range require cathodes that provide space charge limited (SCL) current densities up to 100 A/cm^2 with good emission uniformity and more than 10,000 h of a lifetime at reasonable operating temperatures [3–5].

Since in high power microwave devices also substantial currents are needed, thermionic cathodes are the only candidates for this task at present. Among the currently available thermionic cathodes, Ba dispenser cathodes, including mixed matrix and M-type cathodes, have long lifetimes >20,000 h with current densities of 5–10 A/cm^2 [2, 5]. However, at current densities of $\geq$20 A/cm^2 their practicality becomes problematic, due to the high temperatures and excessive evaporation of cathode materials and hence shorter lifetime. Alloy cathodes such as Ir_2La and Ir_5Ce can provide pulsed current densities of 50–100 A/cm^2, but at very high operating temperatures of 1600–1800 °C and a lifetime in the order of 1000 h [6, 7]. Ba scandate cathodes, which are Ba dispenser cathodes with scandium oxide additions, also referred to as scandate cathodes, have attracted great attention in recent years thanks to their low work function and capability of providing high current densities at operating temperatures lower than that of Ba dispenser cathodes [8–10]. In the following, we will call impregnated cathodes without scandium *Ba dispenser cathodes* (also known as I or impregnated cathodes) and cathodes with scandium *Ba scandate dispenser cathodes* (or Ba scandate cathodes for short). The development of emission capabilities versus time has already been shown in Chap. 1, Fig. 1.12.

Since the discovery of the Ba scandate cathode by Figner et al. [11] in 1967, the first rapid development of this kind of cathode was for high-resolution CRTs, which required cathodes with DC current densities of more than 10 A/cm^2 and an operating temperature lower than that of Ba dispenser cathodes. To meet the demands, several types of Ba scandate cathodes, including impregnated, mixed matrix, pressed top-layer, and thin-film top-layer types, had been developed in 1970s–1990s [9, 12–22]. However, none of the above cathodes has found applications in CRTs before the decline of this industry.

Yet it is instructive to study the different types of Ba scandate cathodes with their respective peculiarities in the sequence of their introduction, which can be found in more detail in [2, 9]. Starting with the pressed scandate cathode, which is based on a patent of Figner from 1967 [11], van Oostrom et al. [12] in 1979 realized $i_0 = 10$

A/cm^2 at 950 °C(Mo-brightness) operating temperature (1017 °C true temperature). Comparable emission was achieved with the impregnated scandate cathode invented by Philips (van Stratum et al. [13]) in 1977, where Sc_2O_3 was added to the impregnant. Mixed-matrix scandate cathodes were first introduced by S. Yamamoto (Hitachi) in 1983 [14], where the matrix consisted of a mixture of tungsten and Sc_20_3: J. Hasker (Philips) improved this in 1989 by using W + ScH_2 as a starting powder mixture [16], yielding about 100 A/cm^2 at the standard operating temperature. In 1986 Hasker had also pioneered the top-layer scandate cathode [15], where a 5 μm layer on top of the porous W body consisted of a mixed matrix of W + Sc_2O_3, but was still prepared via powder metallurgy. Further variants of top-layer scandate cathodes were then introduced by sputter coating the W-base with W + Sc_2O_3 (1986) [17, 18] and later on with W + $Sc_2W_3O_{12}$ (1989) by Yamamoto et al. (Hitachi) [19]. This approach was also continued by R. Longo et al. from Hughes and by Y. Wang using pulsed laser depositing at BVERI (1996) [20, 21], but the results of Hasker were not surpassed. G. Gaertner et al. (Philips) also investigated top-layer scandate cathode preparation by plasma-activated CVD of W and Sc_2O_3 from WF_6/H_2 and $Sc(C_5H_7O_2)_3/O_2$ starting compounds in alternate layers. They managed to reduce the inevitable C and F content of the top layer significantly by modifications of the DC glow discharge CVD process and by further thermal treatment and realized about 60 A/cm^2 pulsed emission, which also was no real improvement [22]. U. van Slooten and P. Duine from Philips reported improved ion bombardment resistivity of a ee-coated mixed matrix scandate cathode in 1996 [23]. A common feature of all these types of Ba scandate cathodes was their nonuniformity and the low robustness under ion bombardment. From all these variants only impregnated scandate cathodes based on a Philips license are still produced by Spectra-Mat and others and were used in some microwave tubes [13, 24].

In the following subchapter we will first address LAD top-layer scandate cathodes as investigated by Philips for CRT applications, which were mainly aimed at increasing ion bombardment resistivity, but also led to record saturated pulsed emission of up to 400 A/cm^2 [9]. These cathodes differ from other variants, since the top layer coating prepared by laser ablation deposition (LAD) in the form of nanoparticles consisted of Re, scandia, and (411) impregnants doped with scandia. The details given here may help to trigger new research also with reference to cheaper production methods of this type.

In the next part the activities on a new type of Ba scandate cathode, the nanosized-Scandia Doped Dispenser cathodes (in short SDD cathode) developed about two decades ago first by Beijing University of Technology (BJUT) and Beijing Vacuum Electronics Research Institute (BVERI) and later continuously carried out at BJUT in China, which mainly focused on application in high current density, long life advanced vacuum electron devices, are presented [10]. They are now the current workhorse for new device applications. More recently, in the US a new initiative on Ba scandate cathode research has been started [25].

3.2 LAD Top-Layer Ba Scandate Dispenser Cathodes with Re on W Base Matrix (G. Gaertner)

3.2.1 Motivation

The main aims for developing top-layer LAD cathodes with Re and Ba scandate at Philips Research Aachen (PRA) were to increase ion bombardment resistivity and emission uniformity with operating time and hence lifetime. In order to also overcome disadvantages of I cathodes such as high operating temperature (high Ba production!) and limited current density, Philips Research realized a top-layer scandate cathode by laser ablation deposition (LAD), which reached unprecedented pulsed emission (saturated) current density of up to 400 A/cm^2 at the same operating (true) temperature as for I cathodes of 1030 °C [9]. Thus, a reduction of the LAD scandate cathode operating temperature and also new high-end applications become feasible. The top-layer scandate cathodes were prepared by Excimer LAD of ultrafine particles of W or Re and of Sc_2O_3 or Ba, Sc containing materials from respective targets on 411-impregnated W–I cathode bases, usually already mounted in Philips 0.65 W cathode units. The top layer of typically 100–500 nm thickness had a very fine-grained structure after activation, which is favorable for fast resupply of Ba and Sc to the surface. The preparation conditions will be presented in more detail in the next paragraph. The robustness under ion bombardment [28] and also the emission uniformity of this cathode was strongly improved over previous scandate cathode types. Methods for accelerated ion bombardment are presented and the superposition model is discussed. Further topics are emission properties such as lifetime, poisoning sensitivity, emission dependence on temperature [9], and roll-off in diode and gun configuration. Cathode surface investigations by SEM/EDX and SAM and elemental depth profiles have been carried out and are correlated to the emission properties.

3.2.2 Experimental Conditions

3.2.2.1 Cathode Preparation by LAD

A common idea of nearly all concepts and structures of scandate cathodes is to provide Sc sources near the cathode or on the cathode surface, since the Sc diffusion length is much smaller than the diffusion length for Ba, the other component needed for a Ba scandate cathode. Several groups at Hitachi [17, 19] and at Hughes [20] had studied the preparation of top-layer scandate cathodes by sputter-deposition of Scandia on impregnated cathode bases. The cathodes obtained showed saturated emission current densities of 100 A/cm^2 at 1030 °C true temperature, but only limited ion bombardment resistivity and were not really an improvement over the other types discussed in the historical section. This was partly due to the fact that the composition was not really suited. At Philips Research, therefore, a more controlled approach was

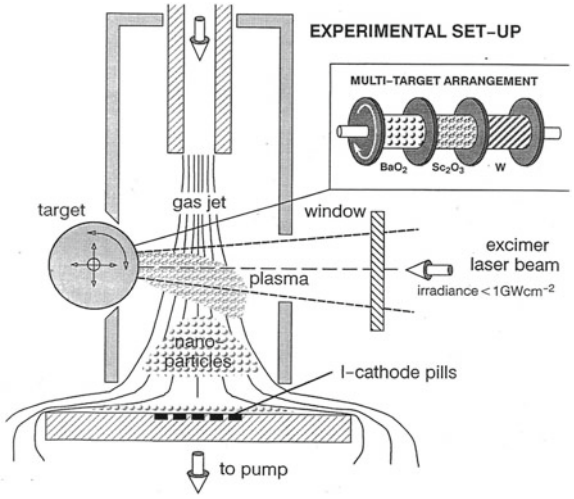

Fig. 3.1 Schematic view of the Excimer—LAD setup (first stage, static substrate); see [26]. Copyright Royal Philips N.V

used by laser ablation deposition (LAD) of thin layers of ultrafine particles and also the composition of these layers was varied [29]. This approach insured that Sc sources were in several nm distances to the emitting surface.

The LAD of top-layer scandate cathodes was carried out with a KrF Excimer laser (type EMG 202MSC, Lambda Physik; $\lambda = 248$ nm) of about 60 W average power and maximum pulse energy of 6 J, which is well suited not only for LAD of refractory metals such as W due to electronic instead of thermal excitation, but also for oxides. This setup had been used before for preparation of nanosized phosphor particles, e.g., consisting of yttria doped with Pr [26, 27] and was modified for the new task. The Excimer laser beam was guided into a stainless steel ablation chamber (UHV flanges) through a UV quartz window and hit a rotating cylindrical target. In Fig. 3.1 also a multi-target arrangement with 3 targets in a row is seen. A plasma plume with ablated nanoparticles formed above the target and the nanoparticles (also called ultrafine particles or UFPs, in the LAD case typically of 5–10 nm size) were carried by the carrier gas to the substrates. In the initial setup, the deposition was static with low yields [26, 27]. In a later stage a scale-up of deposition rates and efficiency was carried out by the addition of a nozzle above the substrate (see Fig. 3.2) and a meander scanning movement of the substrate relative to the nozzle. Also, LAD parameters such as gas flow, gas composition, and total pressure were adjusted in order to obtain improved uniformity. Thus, a UFP deposition yield of up to 60% of the ablated material was achieved. In the case of W-LAD, a major problem was the formation of W-oxide phases in the UFPs due to oxygen contaminations, despite using an inert carrier gas. During activation of the cathode, this leads to unwanted side effects such as WO_x loss by evaporation and/or formation of $BaWO_4$ (of negligible emission!) by reaction with atomic Ba. By several measures comprising the use of high purity

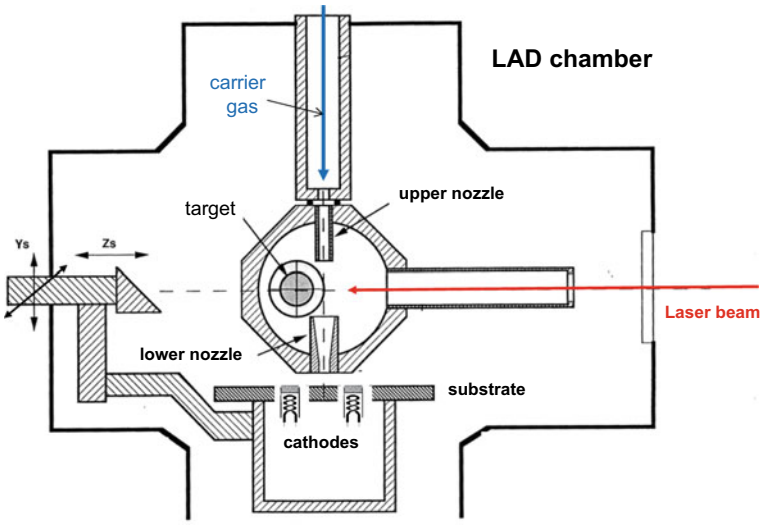

Fig. 3.2 LAD chamber (not to scale) with inner chamber and entrance nozzle for Ar carrier gas and exit (lower) nozzle (second stage of LAD setup, now dynamic; substrate with scanning movement). In holes in the substrate plate 4 I-cathode units are mounted

argon (Ar 6.0: 99.9999% purity), the addition of hydrogen (Ar/H_2 mixture), and heating of the cathode units during W deposition, the WO_x ($x \geq 2$) content could be reduced from 70% to about 20%, yet a much stronger improvement was obtained by replacing W by Re (Re-oxide content about 1%) [30].

A careful investigation of the I cathode bases (entry control) by SEM/EDX and STM [34] prior to the LAD coating revealed a varying contamination of the supplied W bases with BaO nanoparticles. These particles were remnants from the washing procedure of the pills and originated from the impregnant. After Re + Sc_2O_3 LAD it turned out, that there was a positive correlation between improved emission performance/fast ion bombardment recovery of the scandate cathodes thus obtained and the BaO nanoparticle base contamination in the range around 1.5 % Ba as determined by EDX. In conclusion G. Gaertner et al. at PRA introduced a similar artificial interface layer by LAD and investigated several Ba-oxide compounds [29–31], from targets not only such as BaO_2, $BaCO_3$, and also $Ba_3Sc_4O_9$, $Ba_2Sc_2O_5$, but also $Sc_2W_3O_{12}$, $4BaO_2{\cdot}CaAlO_4$, $8BaCO_3{\cdot}2CaCO_3{\cdot}1/2\ Sc_2O_3$. Yet the emission properties of all these layer variants were minor to the BaO-contaminated cathodes. By the way, the beneficial effect of an intermediate sputtered W + BaO layer below a sputtered W + $Sc_2W_3O_{12}$ layer on emission and its uniformity was later also shown by Sasaki et al. [35]. Therefore targets were directly prepared from the 411 impregnant melt, but with different additions of Scandia [30–33]. This approach resulted in a major breakthrough in emission capability and also in IB resistivity. It turned out that the optimum 411x target composition was about $4BaO{\cdot}CaO{\cdot}Al_2O_3{\cdot}1/3\ Sc_2O_3$ with acceptable performance also for the interval between x = 1/4 and 1/2. Yet there

Table 3.1 Mean j_{max} (1.7 kV) at operating temperature of 965 °C Mo-Br versus type of 411x target, the other layers are Re and ScOx

411x-target	Mean j_{max} [A/cm^2] and standard deviation	Number of cathodes
x = 1/4 (C)	268 ± 80	12
x = 1/3 (D)	227 ± 65	93
x = 1/2 (B)	196 ± 80	67
x = 1 (S)	208 ± 50	27
Without 411x layer	106 ± 20	16

was the tendency to get more stable targets for x ≥ ½ and better emission performance for x ≤ 1/3. As an alternative the same target compositions were prepared by sintering of pressed powder targets, but again stable targets were only obtained for x ≥ ½. Table 3.1 shows the influence of the target composition on the average emission results

Figure 3.3 shows some steps of the evolution of LAD layer structures as schematic views of the deposition sequence/layer structure of LAD top-layer scandate cathodes with alternate layers of Scandia and Re. The common porous tungsten base is impregnated with $4BaO{\cdot}CaO{\cdot}Al_2O_3$ (411). Figure 3.3b has an inverted layer structure compared to Fig. 3.3a, but here also the beneficial BaO surface contamination on W is shown schematically. A typical LAD top-layer deposition sequence (in a structural numbering #Cd$_0$122_3, in short CG1_3, one of the first cathode series with top emission) is listed below and is also schematically shown in Fig. 3.3: about 4000

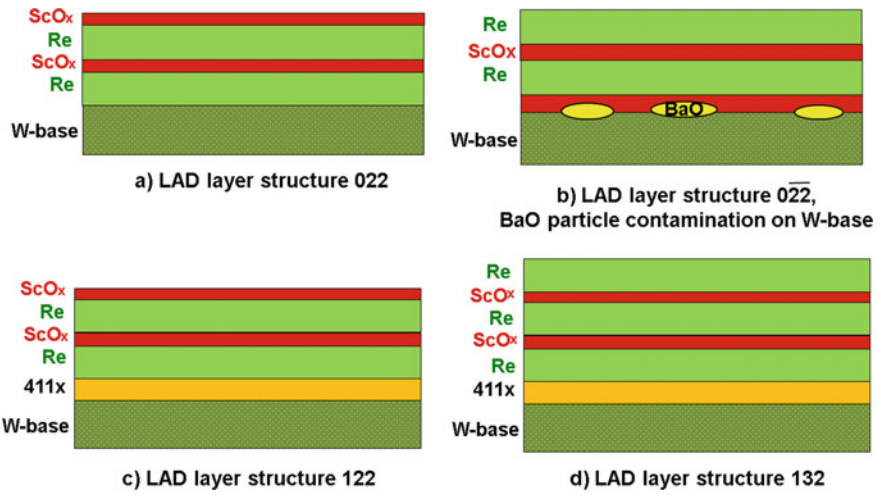

Fig. 3.3 Evolution of LAD layer structures: schematic views of the deposition sequence/layer structure of LAD top-layer scandate cathodes. The porous tungsten base is impregnated with $4BaO{\cdot}CaO{\cdot}Al_2O_3$ (411). In the following, we simply call <022>=:G0, <122>=:G1, <132>=:G2, and <132> with double thickness d_0<132>$2d_0$ = G2 + (structures see [29–33])

pulses of 411.1/4 (target C), then 6000 pulses Re, 2000 pulses Sc_2O_3, 6000 pulses Re, 2000 pulses Sc_2O_3, with the general conditions 0.4 slm Ar 6.0 carrier gas flow and a chamber pressure of 2.5–5 mbar depending on the target [29, 31]. The meander movement over the substrate was restricted to a total area of 16 mm × 16 mm. The whole process was computer controlled. The laser pulse energy was 400–460 mJ, with 4–6 Hz repetition frequency. The whole deposition then lasted about 75 min. The effective coating thickness (for 100% density) was calculated from EDX analysis referenced to the deposited mass. For CG1_3 one thus obtained about 120 nm for the 411x layer, 140 nm of Re, and 25 nm Sc_2O_3 mass equivalent layer thickness in total (assuming 100% density). Of course the layers are very porous and not 100% dense. After LAD smaller pores are covered and others are partly closed, as can be later seen in Fig. 3.21, they get open again after activation, when the structures become coarser due to grain growth. We achieved similar emission results with "132" top-layer structures (G2), where a top Re sub-layer was added, and with inverted structures, where the sequence of Sc_2O_3 and Re was inverted. The idea behind doubling the Re and Sc_2O_3 layers was to create a reservoir for ion bombardment. A doubling of the 411x layer only makes sense, if additionally a neighboring W layer is added, which implies an extension to a fourfold target arrangement.

Further improvements especially in ion bombardment resistivity were achieved by the "132" structure **and** by the so-called $2d_0$ layers, where the thickness of every sub-layer was increased by doubling the number of laser ablation pulses (e.g., #D2$d_0$132_1 = :DG2+). With the first cathode DG2+_1.2 of this series 27% of the specified ILD (ion lifetime dose) was reached!

We can see from Table 3.1, where cathodes have been classified with reference to the 411x target, disregarding their layer structure as in Fig. 3.3, that the lowest scandia content in 411x gave the best results. Yet we could not lower x further below 1/4, because the targets became mechanically unstable. The rather large scatter in the overall emission results, as judged from the j_{max}(1.7 kV) values at operating temperature shown in Table 3.1, is partly artificial, since not only variations of layer sequence and sub-layer thickness, but also changes in activation are contained in the respective groups. The sintered S targets showed less scatter, but could only be prepared for x > 0.5. For comparison in the table also results without 411x layer, only with LAD top layers of Re and ScO_x are given (G0 type), illustrating the strong improvement by introduction of this "magic" interlayer. In this reference case an average j_{max} of 106 A/cm^2 was obtained, where the saturated emission density $j_{10\%}$ is only about 40 A/cm^2. But also when all conditions were kept constant, there was still some scattering of results. Possible reasons are the target composition and the target properties (such as stability and porosity) and also changes of the target surfaces during subsequent ablations can contribute, since the same surface parts are hit several times by the laser beam in a spiraling movement, influencing the size distribution of nanoparticles. But also variations in the rest gas composition dependent on pumping down conditions can play a role or drift in the laser fluence due to internal window contamination or variation of the cathode base properties and some other not directly controlled conditions. Best conditions were achieved when the LAD setup was run continuously with 2–3 deposition runs per week and intermittent pumping-down

cycles. Technically the relevant parameters can be controlled better by improvements in the setup.

The industrialization prospects for top-layer scandate cathodes by using Excimer LAD are good in view of the deposition yield in the order of 50%. Excimer lasers are commercially available and—equipped with commercial chambers—are used for low-pressure LAD of thin compact layers. A change to a pressure range of several mbar as used here leads to the formation of UFP layers instead of compact layers. In the experiments 10–20 years ago at Philips Research Aachen, a KrF Excimer laser type EMG 202MSC of Lambda Physik with about 60 W average power was used. Yet only about 3 W were needed for the above deposition conditions for a top layer of about 300 nm thickness in total. Since the ablation rates scale with power, nowadays commercial Excimer lasers with 600 W average power and a maximum pulse repetition frequency of 600 Hz are available. Of course price predictions of LAD scandate I cathodes will strongly depend on the number of cathodes to be produced. As an alternative, the same layer structures as above could also be prepared by sputtering, since the subsequent thermal activation treatment will anyway change and roughen the surface structures as prepared.

3.2.2.2 Thermionic Emission Measurements

In the initial static stage of the LAD experiments a substrate plate with 32 circular holes was used, where impregnated cathode pills with 1 mm diameter D_c were sitting in the holes, see Fig. 3.1. This implied that these pills after LAD had to be mounted in 0.65 W Philips cathode units with heaters as shown in Fig. 3.4. In order to avoid possible damage to the LAD layer during mounting and processing, in the second stage of LAD experiments, four complete 0.65 W Philips I-cathode units were directly mounted (of course without Os/Ru layer, only W–I cathodes) under respective holes

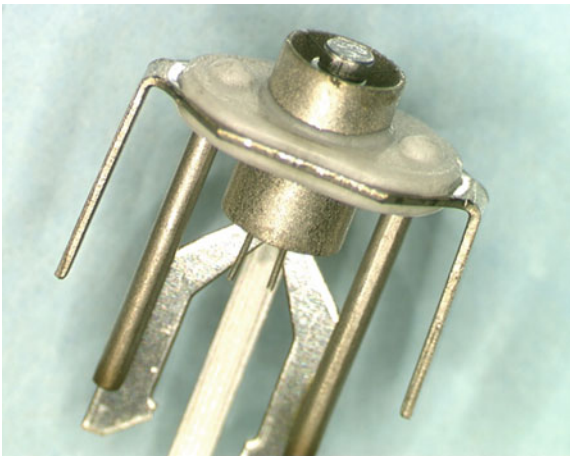

Fig. 3.4 Philips 0.65 W I-cathode unit; cathode pill diameter 1 mm; from [2], G. Gaertner, H. Koops, chapter 10 of "Vacuum Electronics, Components and Devices", Springer 2008, p. 440

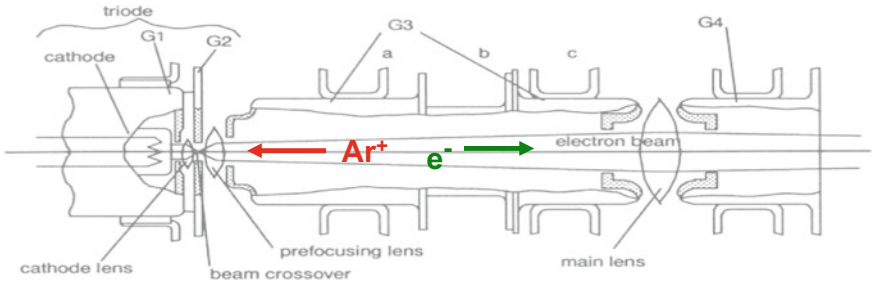

Fig. 3.5 Schematic longitudinal section of an electron gun (one electron beam). The electrons ionize the rest gas and ions (mainly Ar, N_2) are accelerated back to the cathode surface through the grid apertures: locally peaked ion beam profile! (see X. Zhang, G. Gaertner, presentation at IVESC 2002 and [44]; copyright Royal Philips N.V)

in a new substrate plate, with an additional central circular Mo reference substrate of 3 mm diameter used for layer characterization.

Electron emission measurements were carried out in either closed-spaced diode or electron gun configuration in a UHV (ultra-high vacuum) chamber, as can be seen in Fig. 3.5. In the close-spaced diode configuration the typical cathode to anode distance d_{CA} was 0.2–0.3 mm. Close-spaced diode implies that $d_{CA} \leq ¼\ D_c$ (see Hasker [38]), where D_c is the diameter of the cathode disk.

The cathode pill was mounted in a Mo cap, the side of which could be observed through a glass window for pyrometric determination of cathode temperature. The temperature could be adjusted by control of the heater voltage of 0.65 W unit. A typical setting for an operating temperature of 965 °C(Mo-brightness) or 1030 °C true temperature is a heater voltage of 6.4 V and a heater current of 103 mA. Despite heater calibration curves, the Mo-brightness temperature was determined in every measurement and corrected for window absorption.

The massive anode typically consisted of high melting Ta, in order to stand continuous heating by the electron current. The measurement of a current-voltage characteristic was done by starting with DC measurements from 10 to 100 V, then continuing with pulsed measurements in order to avoid excessive heating of the anode at higher voltages. Pulses were either delivered by a sawtooth pulser of up to 1.75 kV voltage and up to 3 A emission current, the pulse length being varied from 5 μs to 15, 50 or 100 μs, with a repetition frequency of 50 Hz, or by a rectangular pulser of up to 2 kV pulse height (pulse length 10 μs, repetition frequency 50 Hz, stepping up the voltage). In the original version (later on in parallel) of the sawtooth pulser the pulsed current–voltage characteristic could be observed as a stationary triggered sweep on an oscilloscope. During the whole project all emission measurements were computer controlled, the electronics being assembled in test racks. This implied an averaging of the pulsed sawtooth measurements over a chosen time interval. During the 25-year duration of several cathode projects, Philips Research Aachen (PRA) was equipped with up to 10 UHV chambers (32 diode test positions), including two chambers with Ar ion guns for ion bombardment investigations (see Fig. 3.6), additional dummy

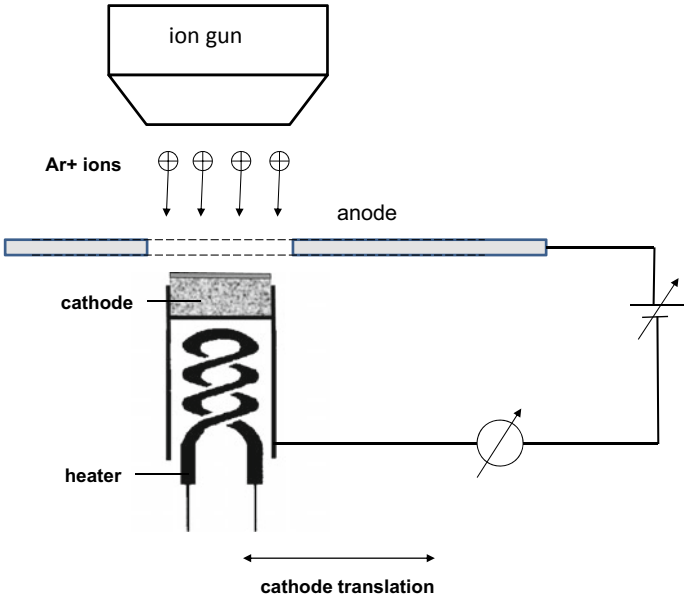

Fig. 3.6 Schematic diagram of the diode configuration with the differentially pumped Ar ion gun (Perkin-Elmer Φ 04): $d_{CA} = 0.3$ mm; the anode aperture has 2 mm diameter; the cathode can be translated to a planar diode test position (compare [44])

glass tubes for gun testing, and 4 emission test racks for measuring, e.g., current-voltage characteristics at a given temperature (status at PRA visit of IVESC 1996 participants). Cooling or heating effects under a given DC load were in most cases compensated via the heater voltage of the cathode.

Since scandate cathodes show anomalous behavior in the saturation range with only a small gradual deviation from the space charge limit (SCL) especially at higher temperatures, from the current voltage *I(U)* characteristics the 10% deviation point from SCL $I_{10\%}$ is used [9] as a good approximation of saturated emission current I_{sat} (see Manenschijn et al. [39]). For I cathodes $I_{10\%}$ is about 10% larger than I_{sat} obtained by fitting [39]. It has to be noted that the slope in a lg$I$ /lg$U$ plot in the SCL range is not 1.5, but according to Child-Langmuir theory (see formula (10.9), p. 433 in [2] and the calculation of diode characteristics by Hasker [40] and Scott [37]) varying between 1.35 and 1.45. The higher values of x are obtained for current densities in the range around 100 A/cm^2 [39]. For determination of $I_{10\%,}$ it is then required that the slope x in the SCL range is above 1.4. The current density limit $j_{10\%}$ is also a reasonable measure of electron emission capability for the typical applications in the space charge limited range as in CRTs [36, 39]. Interestingly, the saturation region of scandate cathodes can also be described by a power law with slopes lower than the SCL slope. This lends support to the superposition theory of scandate patch fields,

where their contribution is reduced by prolonged sputtering as in [28]. In this context one should keep in mind that also for standard Ba dispenser cathodes a theoretical description for the complete *I(U)* characteristic is missing. It only exists for the space charge limited range and at much higher voltages for the Schottky range. In the intermediate range in between a theoretical description in closed form is missing, apart from the approximation by Hasker [40] and the numerical solution by Scott [37].

In the electron gun configuration usually 3 cathodes (for red, green, and blue) were mounted in a Philips 45AX CRT gun, as can be seen in Fig. 3.5, where the distance to grid 1 typically was 80 μm. In the diode mode of the gun, only the emission to grid 1 outside the rectangular hole of 0.5×0.7 mm^2 size was measured. This was compared to roll-off measurements in the gun mode. The gun could either be mounted in a vacuum chamber or in a dummy tube (just the neck, without phosphor screen). The path of one electron beam in gun operation is also shown in Fig. 3.5, with a beam crossover in grid 1 region, which also gives a peaked ion beam hitting back onto the cathode surface. A potential distribution for such a gun was given by T. Spanjer et al. in Fig. 8, p. 353 of Philips Technical Review 44 [42].

Since a theoretical description of the *I(U)* characteristics of Ba scandate cathodes in the saturation range is still missing and hence zero field emission cannot be derived from a curve fit, the group at BJUT of Yiman Wang uses the deviation point I_{dev}, where deviation from SCL just starts [43]. These values are lower than the $I_{10\%}$ values. In a further method, the intersection point of the straight line fits (power law slopes) in SCL range and saturation range is determined in a double logarithmic plot of the characteristic. The projected point I_{is} on the characteristic is a good approximation of zero field emission, which is more in line with the $I_{10\%}$ value. Yet this method cannot be applied, if the voltage range is not reaching far enough into the "saturation" region. In this case, a clear recipe is needed for marking the transition from SCL to saturation. This problem does not occur for *I(U)* characteristics at lower temperatures, where there are only small deviations between $I_{10\%}$ and I_{is}, as we will see later during the evaluation of temperature-dependent *I(U)* characteristics.

It should be noted that the type of equipment used for emission measurements was also used at Philips Research Eindhoven and by Philips Display Components. The 45 AX guns in the tests were applied in several commercial Philips CRTs and their design was based on electron optical calculations (see [41, 42] and other articles in Philips Research Reports or Philips Technical Review). With this equipment all types of thermionic cathodes, including thoriated tungsten, oxide cathodes, and various types of impregnated and scandate cathodes, have been tested, results have been published and are consistent with the literature. The message is that the record emission is not due to peculiarities of the test equipment, as one might speculate, since quite regularly top emission of the same cathodes was ruined by accelerated ion bombardment or by deterioration during operation (see [28, 47]) and it took some years to reach the state of the art in 1994 and then improve further.

3.2.3 Summary of Emission Results

3.2.3.1 Top-Layer Scandate Cathode Activation

It is well known that impregnated dispenser cathodes need an activation process in vacuum, in order to start the Ba supply to the surface, where Ba is generated via a reaction of the impregnant with the tungsten of the pore walls. A typical activation scheme of an I cathode consists of some preheating steps and activation by heating at 1100 $°C_{Mo\text{-}Br}$ for half an hour. It turned out, that this scheme is not really suited for LAD top-layer scandate cathodes. Of course also some preheating steps are needed for degassing of the deposited layer. A typical preactivation sequence used was 5 min at 850 $°C_{Mo\text{-}Br}$, then followed by 5 min at 965 $°C_{Mo\text{-}Br,}$ under the condition that the total pressure in the chamber is kept below 10^{-7} mbar. Yet the high-temperature activation needs to happen at 40–60 °C lower temperature than for I cathodes, otherwise lifetime and survived ion dose are strongly reduced. The optimum activation conditions are obtained under the action of an electric field (typically 75 V at $d_{CA} = 0.25$ mm) at a temperature of about 1060 $°C_{Mo\text{-}Br.}$ with a duration of 60–120 min. Figure 3.7 shows the activation curves of cathode CG1_3.2 at an average temperature of about 1060 °C(Mo-Br.) with a constant electric field of 75 V/0.25 mm. Shown is current in log scale, either DC or pulsed, versus time in log scale. The dotted line is an estimation of activation continuing in the pulsed range; see [45]. During operation

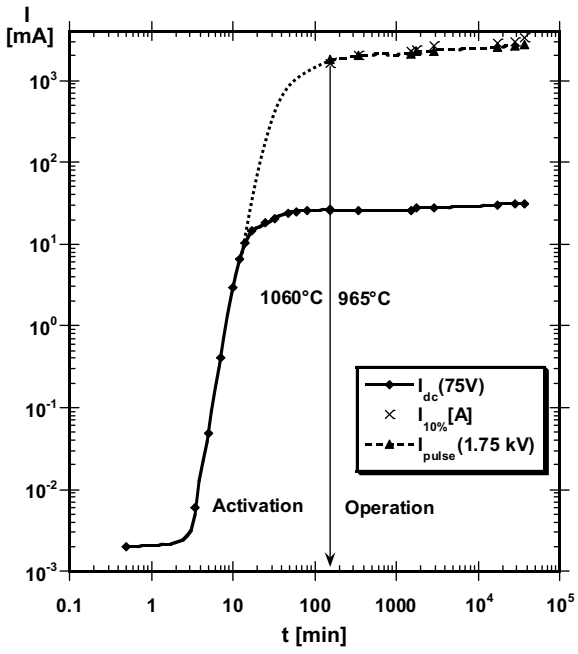

Fig. 3.7 Activation of cathode CG1_3.2 at an average temperature of about 1060 $°C_{Mo\text{-}Br.}$ with constant electric field of 75 V/0.25 mm. Shown is current in log scale, either DC or pulsed versus time in log scale; data based on [45]

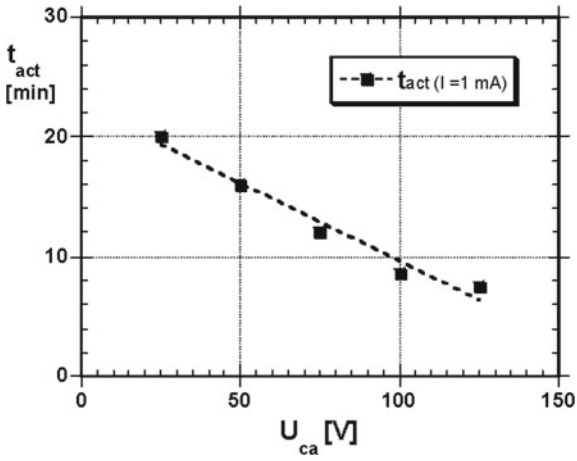

Fig. 3.8 Activation time (delay) to DC current level of 1 mA at a temperature of about 1060 °C for LAD scandate cathodes (BG1) as a function of applied voltage ($d_{CA} = 0.25$ mm); data based on [45]

of the cathode at 965 $°C_{Mo\text{-}Br.}$ following the activation interval in Fig. 3.7, one can still observe a slow further increase in the emission current.

The influence of the electric field on activation of LAD scandate cathodes of type BG1 at an activation temperature of about 1060 °C is shown in Fig. 3.8. Here we see that the lower the field strength the longer the activation time needed, but t_{act} (1 mA) has the character of a delay time, which is also dependent on the thickness of the LAD layer. It should be noted here, that for W–I, Re–I, or mixed matrix scandate cathodes, the initial delay is less than 2 min. Once a level around 0.1–1 mA has been reached, the further increase is at about the same rate as in Fig. 3.7. The influence of the electric field, especially in the higher voltage range of the *I(U)* characteristic, is consistent with the higher mobility of Sc shown in Auger experiments by J. Crombeen, where the application of a diode voltage of about 200 V would strongly increase the Sc/W signal ratio [16, 45]; he has also shown a strong influence of the oxygen concentration on activation. The advantageous action of an electric field is also known from the activation of oxide cathodes (see Chap. 4).

Of course, Ba supply during activation and on life can also be monitored by emission measurements. Here emission activation energy can be determined from the temperature dependence of activation times (e.g., time to reach half of the maximum or plateau value). Figure 3.9 shows results obtained for LAD Ba scandate cathodes with Re and uncoated impregnated (W–I) cathodes. It has to be noted that in the case of scandate cathodes two activation times can be observed, namely a fast activation—typical for Ba supply—to space charge limited emission in the low voltage range (DC-emission; Re–I characteristic!), and a slower activation to the final scandate *I(U)* characteristics in the high voltage range (pulsed emission) belonging to Ba-scandate complex formation ('Sc'). The Ba activation energy E_{act} (Ba) = 3.12 ± 0.1 eV is the same for both types of Ba dispenser cathodes. The activation times to the scandate characteristic are a factor 6 prolonged, but E_{act} ('Sc') = 3.35 ± 0.2 eV is

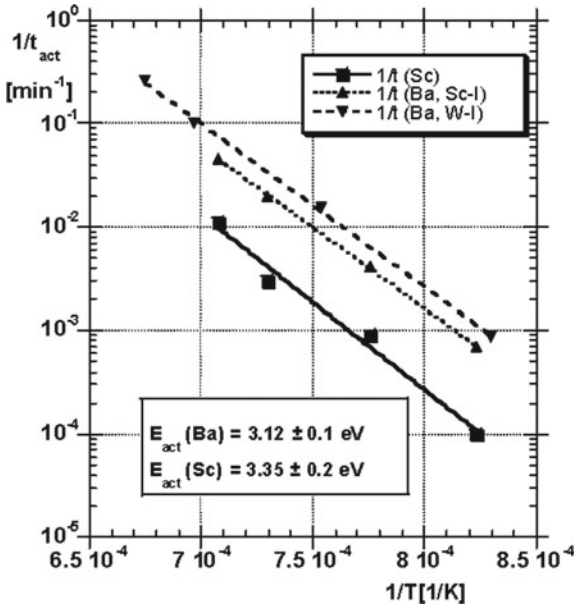

Fig. 3.9 Inverse activation times as a function of inverse true temperature for LAD Ba scandate cathodes with Re (series BG1, here denominated as Sc-I; with constant electric field), and B-type Ba dispenser cathodes (W–I); from [46] and [47], G. Gaertner et al., "Supply and Loss Mechanisms of Ba Dispenser Cathodes", Appl. Surf. Sci. 146, 22–30 (1999), with permission from Elsevier

(within the limits of accuracy) still consistent with Ba generation being the limiting factor [46, 47].

The activation times needed are dependent not only on temperature and electric field, but also on the layer thickness, the degree of oxidation of W or Re and other impurity contents, and may be prolonged by 1–2 orders of magnitude depending on the conditions, but we will not go into further details here.

3.2.3.2 Thermionic Emission Properties

The motivation for the investigation of scandate cathodes was to overcome the disadvantages of the I cathode such as high operating temperature (high Ba production!) and limited current density. Yet one of the common features of the development of different types of scandate cathodes was that they did not show a clear transition to saturation and a continuing current increase with voltage in this region instead. Since an accepted theoretical description is missing, more phenomenological practical approaches have been used, as we have already discussed in Sect. 3.2.2, namely the different transition criteria $I_{10\%}$, I_{is} and I_{dev}, where I_{dev} is marking the lower boarder of the transition range. The differences between these criteria get smaller at lower temperatures.

In Fig. 3.10 the current density versus voltage characteristics of a LAD top-layer scandate cathode type DG2, an Os/Ru–I cathode, and a W–I cathode at 965 °C Mo-brightness temperature (1030 °C_{true}), as determined in the diode mode in an electron gun configuration (45AX), are compared. The onset of saturation is given as a 10%

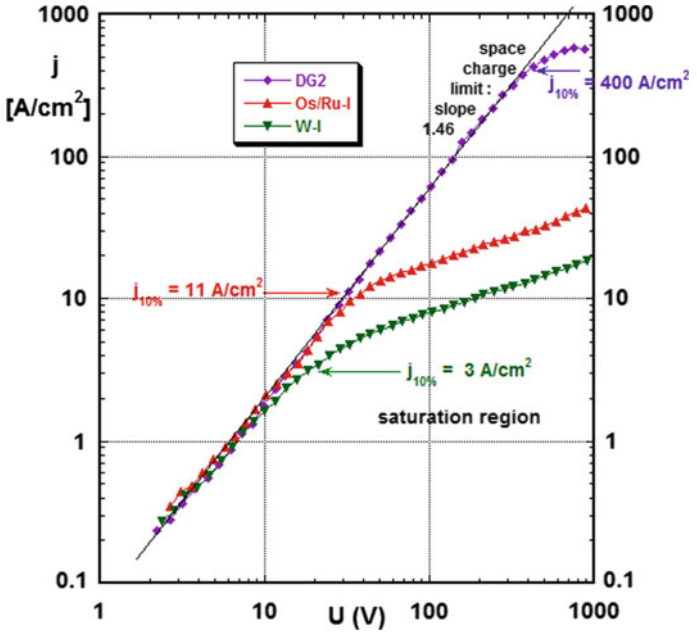

Fig. 3.10 Current density versus voltage characteristics of a LAD top-layer scandate cathode type DG2, an Os/Ru–I or M cathode and a W–I cathode at 965 °C Mo-brightness temperature, as determined in the diode mode in an electron gun configuration (d_{ca} ~ 80 μm). The onset of saturation is given as 10% deviation from the space charge limitation (slope 1.46 for DG2). For the Os/Ru–I cathode, the SCL slope is about 1.35 and the saturation slope 0.4. The graph is based on a re-evaluation of data presented in [57, 59]

deviation from the space charge limitation (slope 1.46 with second-order corrections) [57, 58]. For the Os/Ru–I cathode, the SCL slope is about 1.35 (compare [39]) and the saturation slope is 0.4. For the W–I cathode, the SCL slope is about 1.30 and the saturation slope is also 0.4. The gun data are consistent with diode measurements and the literature with reference to both types of I cathodes. In this plot also, practically no significant differences between the $j_{10\%}$ values and j_{dev} (of Wang et al. [43]) can be seen. We will discuss the correlations between gun and diode measurements later.

In Fig. 3.11 the emission current densities j of a BG1-type cathode are depicted versus diode voltage U in a double logarithmic plot at different temperatures [9]. These characteristics have been measured in a close-spaced diode configuration and are consistent with characteristics in the diode mode of a 45AX gun, where higher electric field strengths can be reached in pulsed measurements. There (Fig. 3.10) the emitting cathode area A_{cath} for determination of current density from current is A_{cath} = ($\pi \times 0.5^2$–0.35) mm^2 compared to $A_{cath} = \pi \times 0.5^2$ mm^2 = 0.7854 mm^2 in a planar diode. The power law slopes in saturation are shown at the right side of the curves. The respective $j_{10\%}$ values for the temperatures from 600 °C to 915 °C are

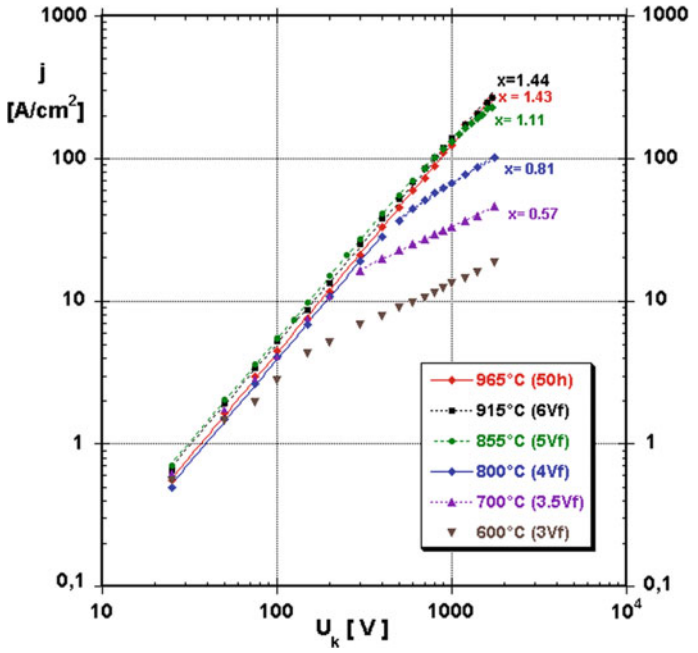

Fig. 3.11 lg j/lg U characteristics of BG1_2 cathode for different Mo-brightness temperatures in diode configuration (d_{ca} ~ 200 μm). The power law slopes x_s in the double logarithmic plot in saturation are shown at the right side of the curves. The graph is based on a re-evaluation of data presented in [9]

Table 3.2 Saturated emission of cathode type BG1_2 versus Mo-brightness temperature

T [°C $_{\text{Mo-Br.}}$]	600 °C	700 °C	800 °C	855 °C	915 °C
Heater voltage U_f [V]	3.0	3.5	4.0	5.0	6.0
$j_{10\%}$ [A/cm^2]	1.8	15	38	178	293
Slope x_s	0.57	0.57	0.81	1.11	

given in Table 3.2. Saturation cannot be determined at an operating temperature of 965 °C$_{\text{Mo-Br.}}$, since the maximum pulsed voltage is not high enough to see a deviation from space charge limit.

In a plot of saturation current density versus true temperature as in Fig. 3.12a, one can obtain a good overview of the optimization of LAD scandate cathodes. Here $j_{10\%}$ has been chosen as a good approximation for zero field emission or "saturation" current density. A general feature of all Ba scandate cathodes prepared by LAD is the work function of about 1.15 eV, as one can also derive from the Richardson plots of Fig. 3.13. The same holds also for SDD cathodes of Y. Wang and for sputtered top-layer scandate cathodes of S. Yamamoto. Only the Richardson constant A_R is

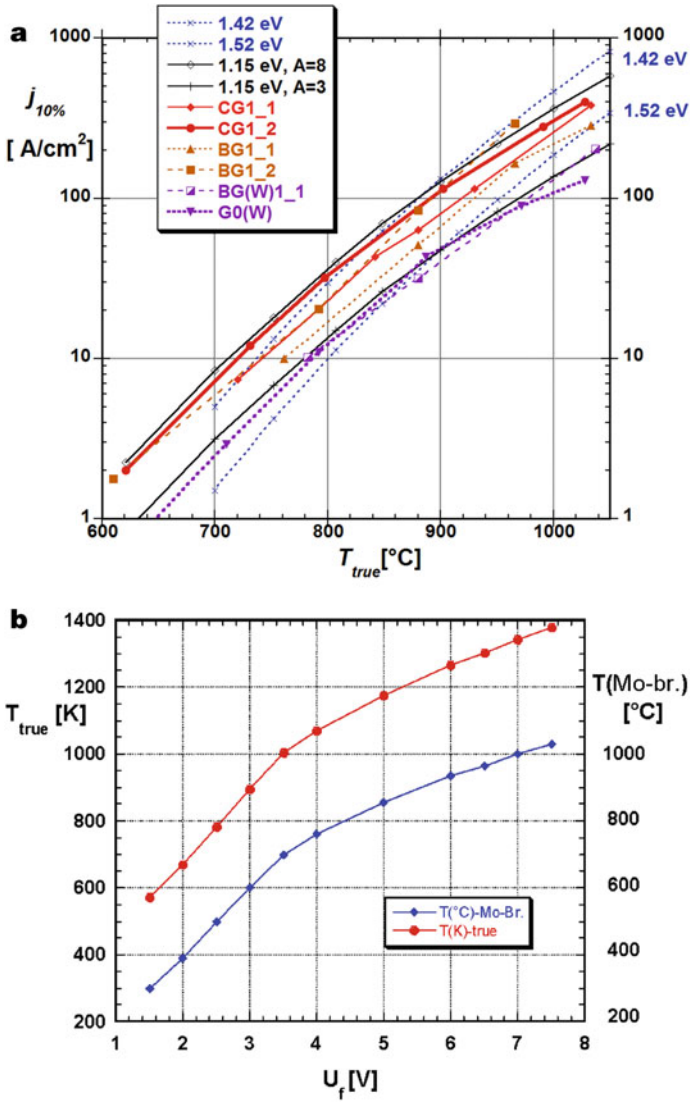

Fig. 3.12 **a** Saturation current density versus true temperature. A general feature of all Ba scandate cathodes prepared by LAD is the work function of about 1.15 eV, whereas the Richardson constant A_R is varying between 3 and 8 A/(cm^{2}K^2). For comparison, also the saturated emission density curves for work functions of 1.52 eV and 1.42 eV with the Richardson constant being the thermionic constant are shown. Results of [47, 59] are contained in this graph. **b** Temperature versus heater voltage for Philips I-cathode unit. The blue curve is the Mo-brightness temperature in °C and the red curve the true temperature in K. Measured Mo-brightness temperatures of individual units may deviate in the region of the working point 6.3 V_f by about $\pm$15 °C. During continuous DC load also, emission cooling has to be taken into account. These calibration curves are basis for the results given in [47, 59]

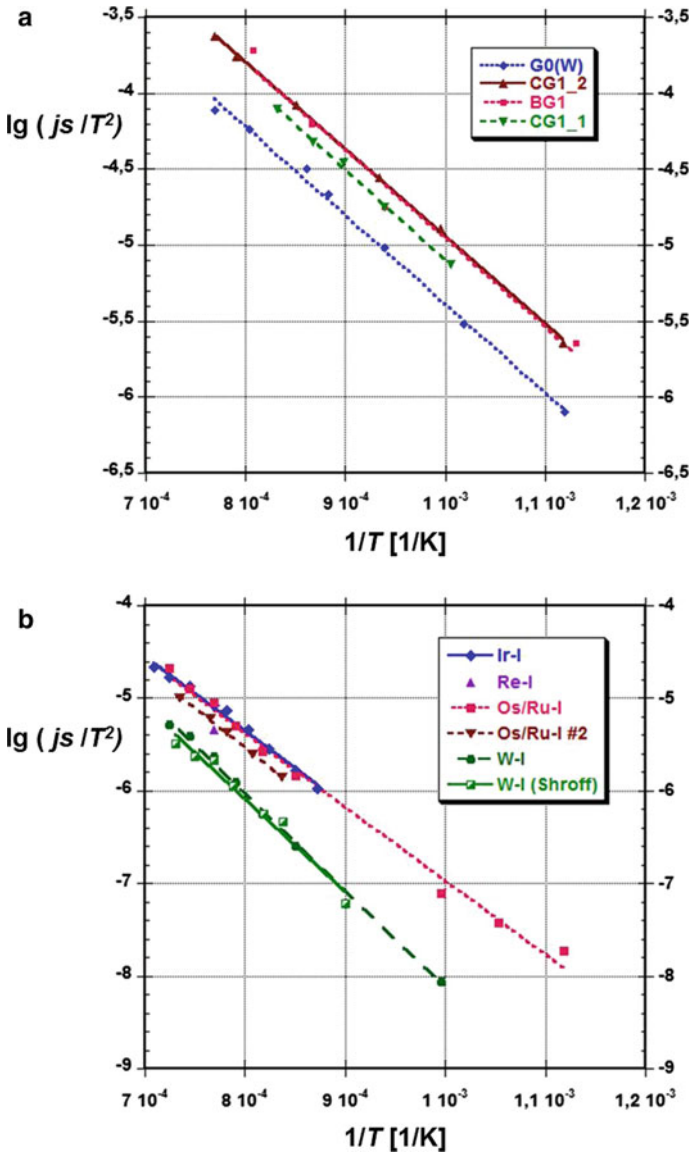

Fig. 3.13 **a** Richardson plot of LAD top-layer scandate cathodes G0 (without 411x layer), CG1_1 (x = 1/4), CG1_2 (x = 1/4), and BG1 (x = 1/2); compare [9, 58]. **b** Richardson plots of different types of Ba dispenser cathodes; see Table 3.3 and [39, 59, 61, 62]

varying between 3 and 8 A/(cm^{2}K^2), which is a measure of increasing coverage of the surface area (see Gilmour, p. 44 in [48]) and is also consistent with increasing ion bombardment resistivity when Ar = 8 A/(cm^{2}K^2) is approached. For comparison also the saturated emission density curves for work functions of 1.52 eV and 1.42 eV with the Richardson constant being the thermionic constant are shown in Fig. 3.12a,

but they do not deliver a good fit over a larger temperature interval. One can also see that only tungsten-based LAD cathodes without Re, namely BG(W)1_1 and G0(W), are located around $A_R = 3$ A/(cm^{2}K^2) at the lower boarder. In this context a Ba scandate cathode on W base has also been obtained by metal Sc-LAD on a W–I base with js in the same range (not shown here, literally Sc/W–I), where the W base is usually decorated with BaO nanoparticles as already mentioned [34]. Activation then leads to oxidation and scandate formation on a W–I base.

Very important for establishing a reliable plot as in Fig. 3.12a and also as a basis for the Richardson plots of Fig. 3.13 a + b is the determination of true temperature, which is not trivial. Such a calibration curve is given in Fig. 3.12b as a function of the heater voltage of the I-cathode unit. Of course the measured Mo-brightness temperatures of individual units may deviate, which can be about $\pm$ 15 °C in the region around the working point 6.3 V_f. During continuous DC load also electron emission cooling has to be taken into account. Thus at certain intervals during continuous runs or before/after *I(U)* characteristic measurements, the cathode temperature needs to be determined usually by optical pyrometry (visible or infrared). In regular intervals ($\leq$1 year) the pyrometer needs to be calibrated with either a tungsten ribbon lamp or a black body radiator. If the brightness temperature of the Mo cap is measured, not only the Mo emissivity as a function of temperature and observation wavelength has to be taken into account, but also the transmission of the viewing window. In case the observation spot is located on the part of the uncovered tungsten, W emissivity determines the correction.

We know from Chaps. 1 and 2 that the dependence of saturated electron emission current density on temperature is given by the Richardson–Dushman equation [2, 48], which is usually written in the form

$$j_s = A_R T^2 \exp\left(-e\phi_R / kT\right) \tag{3.1}$$

where A_R is the Richardson constant, which for real cathodes in most cases is smaller or much smaller than the thermionic constant $A_{th} = 120.4$ Acm^{-2} K^{-2} for the ideal case. $e\Phi_R$ [eV] is the Richardson work function in the form written by S. Dushman, Herring and Nichols, Nottingham, Scott [37], Hasker [40], and others [2], where within this book $e\Phi = \phi$ is used. j_s is the saturated emission current density in Acm^{-2}. From the measured dependence of j_s on true temperature T [K], one can determine work function and Richardson constant from a so-called Richardson plot [48] of log (j_s/T^2) versus *1/T*, where the physical quantities have been divided by their respective units

$$\lg\left(j_s / T^2\right) = \lg A_R - e\phi_R / (kT \ln 10) \tag{3.2}$$

It should be noted, that the Richardson constant A_R can also be expressed as a temperature dependence of work function $e\Phi = e\Phi_R + \alpha T$, with the coefficient $\alpha = k \ln (A_{th}/A_R)$. This of course only makes sense for uniform emitter surfaces.

Figure 3.13 a shows Richardson plots of LAD top-layer scandate cathodes of type G0 (without 411x layer, $\phi = 1.16$ eV, $A_{Rrel} = 2.8$), CG1_1 (x = 1/4, $\phi = 1.17$ eV, $A_{Rrel} = 6.3$), CG1_2 (x = 1/4, $\phi = 1.14$ eV, $A_{Rrel} = 6.2$), and BG1 (x = 1/2, $\phi = 1.15$ eV, $A_{Rrel} = 7.0$). The Richardson work function of about 1.16 $\pm$ 0.02 eV and a Richardson constant of $A_R = 6$ to 7 $Acm^{-2}K^{-2}$ gives a better fit to the experimental 'Sc'-I data than an effective work function of 1.4–1.45 eV ($A_R = A_{th} = 120.4$ $Acm^{-2}K^{-2}$). This illustrates the superior emission of the LAD scandate cathodes down to temperatures of 500 °C with about constant work function.

Here in Fig. 3.13a again as in Fig. 3.12a, the only tungsten-based LAD scandate cathode without Re, namely G0(W), is characterized by A_R of about 3 $A/(cm^2K^2)$, hence in the lower range.

In order to check the validity of this interpretation of the Richardson constants of scandate-type cathodes, it should be compared with the respective results for impregnated Ba dispenser cathodes, namely the W–I or Re–I cathode bases, which in general exhibit more uniform emission than scandate cathodes. Therefore in Fig. 13b Richardson plot data of Os/Ru–I, Ir–I, and W–I cathodes from Philips and a W–I cathode from Thomson have been evaluated. The results are listed in Table 3.3.

Unfortunately respective data for Re–I have not been published; from the comparison at the operating temperature at 965 °C(Mo-Br), the Re–I line is expected in the emission range 30–40% lower than Os/Ru–I cathodes. In conclusion much higher Richardson constants for Ba dispenser cathodes are obtained from this new evaluation compared to older references. The range of A_R for Os/Ru–I and Ir–I shows a rather good agreement. Reasons for disagreement with the older literature are mainly due to the systematic errors in the determination of zero field emission current density j_0 induced by Schottky extrapolation used at that time, especially at higher temperatures, as pointed out by Hasker [38, 40]. To some extent, it may also be due to rather

Table 3.3 Fitted results of Richardson plots for LAD scandate cathodes and Ba dispenser cathodes

Ba dispenser cathode type	Reference	Richardson work function $e\Phi_R$ [eV]	Richardson constant A_R [$Acm^{-2}K^{-2}$]
LAD scandate BG1 ('Sc'/Re–I)	Gaertner et al. [59, 61]	1.15	7.0
Os/Ru–I (M)	Gaertner et al. [59, 61]	1.58	10.5
Os/Ru–I (M), #2	Manenschijn et al. [39, 36]	1.71	22.1
Ir-I (M)	Geittner et al. [61, 62]	1.60	13.0
W–I (S)	Gaertner et al. [59, 61]	2.08	171
W–I (S)	Shroff et al. [64][a]	2.01	102.6

[a]See [64] A. Shroff et al., Applic. Surf. Sci. **8**, 36–49 (1981), p. 38, Fig. 1

small temperature intervals and to problems in determining true temperature. Especially the results of Manenschijn et al. for Os/Ru–I [39] are very reliable, since they have determined j_0 by application of the theory of Hasker for the transition range between space charge limited and Schottky emission [39, 40]. The values for the W–I cathodes should be checked again, despite that a value of the Richardson constant higher than the thermionic constant is not uncommon for certain crystal faces of pure metals and corresponds in the alternate picture to a negative temperature dependence of work function. In case of the values of Shroff, the Richardson plot exhibited a slight curvature. One has to keep in mind that the results for A_R and $e\Phi_R$ will also change with operation time.

3.2.3.3 Features of an Emission Model

One of the models to describe the current–voltage characteristics in this range is the semiconductor model of Raju and Maloney [50]. We do not doubt the usefulness of this model, but it was applied to very nonuniform scandate cathodes of minor emission performance. From simulation and from continuing ion bombardment experiments [28, 49], we found that scandate cathodes can be better described by a patch or superposition model, where the ideal scandate surface portion is in first approximation only space charge-limited, but with a lot of I cathode (in our case Re–I) patches in between. Depending on the relative fractions of the Ba scandate and Re–I part, the slope in a double logarithmic plot of I versus U is increasing from about 0.4–1.46 (space charge slope or power) with increasing scandate part. This behavior at operating temperature or below is linked to the fact that the Ba-scandate surface complex has a very low work function of about 1.15 eV compared to 2.02 eV for W–I and 1.93 eV for Re–I [51–53]. This superposition model is also backed by measurements of the local nonuniform emission distribution by Hasker [16] and by measurements of the local work function of sputtered top-layer scandate cathodes by Yamamoto with the field emission retarding potential (FERP) method, yielding 1.15 eV [54]. Also, the investigation of a model system by Zagwijn et al. [55] with Sc and Ba monolayers (ML) on W(001) surface with medium energy ion scattering (MEIS) resulted in a work function of 1.18 eV for O concentrations between 1 and 1.5 ML. It is consistent with the observation that the slope is increasing during activation, which takes longer for the Ba-scandate complex than for the I cathode parts. The same happens in the reverse direction after successive ion bombardment and during emission decline at the end of life, where the I cathode area portions now increase. Yet it has to be kept in mind, that the superposition model does not imply the simple addition of contributions, since there is also a mixed term by enlargement of the Ba scandate portion by space charge expansion within the space charge coupling length, which is also called the beamlet effect by Hasker [38]. In the first approximation, this coupling length is estimated to be related to the distance d_m of the space charge maximum in front of the cathode. For a cathode temperature of 1300 K and a current density of $j = 100$ A/cm^2, one obtains $d_\mathrm{m} = 0.6$ µm and for $j = 10$ A/cm^2, $d_\mathrm{m} = 1.6$ µm [56]. Due to this space charge leakage and the low

Schottky saturation contribution of the I cathode portions, one can observe a space charge like behavior with lower power (slope in log-log plot below the space charge limit slope of about 1.45). A complete theory of this "coupled superposition" still has to be established. Surface analysis of Sc-I cathodes after activation and during life typically shows spots with Sc and Ba enrichment with an extension below the grain sizes of about 3 μm on the average. It should be noted that the superposition model is not in contradiction with a still to be established emission model of the emitting (Ba, Sc, O) complex, eventually via a semiconductor type theory of a Ba–Sc mixed oxide compound with a Ba monolayer on top, but here in the form of patches.

3.2.3.4 Low-Temperature Thermionic Emission and Field Emission

Due to the low work function, thermionic emission could be measured down to about 200 °C, where the temperature was measured with an infrared pyrometer. Field emission (FE) was observed at room temperature and under moderate heating up to $1.5V_f$ (about 300 °C) for 'Sc'/Re–I, Re–I, and W–I cathodes. The threshold field strengths (reference level 1 nA) were 3.2 V/μm for 'Sc'/Re–I, 9 V/μm for Re–I and 11 V/μm for W–I [59]. In the range from 250 to 350 °C, thermal-assisted field emission is observed and the threshold vanishes [59–61, 63] as can be seen for the respective upper curves in Fig. 3.14. These results are discussed in more detail in

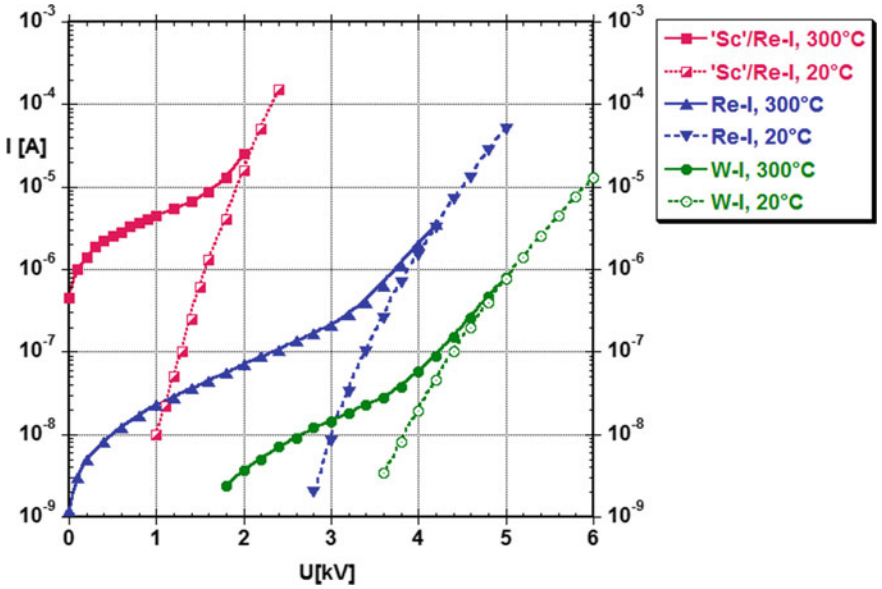

Fig. 3.14 Field emission characteristics at room temperature and low temperature *I(U)* characteristics for top-layer Re-Scandate = 'Sc'/Re–I, Re–I, and W–I cathodes; from G. Gaertner et al. [59], Copyright 2002, with permission from Elsevier

[59]. Unfortunately for stable field emission of scandate cathodes a very good UHV with chamber pressures in the order of 10^{-10} mbar is needed, including the baking of the chamber after cathode mounting. K. Jensen gives a theoretical description of the superposition of thermal and field emission in Chap. 8.

3.2.3.5 Life-Limiting Mechanisms and Experimental Results

As shown in [46, 47], the Ba evaporation rate for 'Sc'/Re–I (Scandate with Re) cathodes is lower than that of standard impregnated or I cathodes (metal matrix: W and metal surface: W or Os or Ir or Re …), at least during the initial 1000 h. Figure 2 of [47] shows that Ba evaporation from the I cathodes is higher than that of the two top-layer 'Sc'-I cathodes. An exponential fit of the data yields activation energy for Ba evaporation $E_{act} = 3.15$ eV for all 4 cathodes, which is due to the same generation mechanism. An explanation for the lower rates for 'Sc'-I cathodes could be that Ba is needed for buildup and replenishment of the Ba–Sc–O surface complex.

In conclusion, one limiting mechanism is the Ba generation and evaporation, which is mainly dependent on the design of the I cathode base. According to Aida et al. [65], the life end is above all determined by the exhaust of the Ba supply reaction of the impregnant with W (pore walls). Hence, it depends on the total amount of impregnant in the porous W matrix, i.e., for 20% porosity, and also on the thickness of the cathode pill. Aida et al. [65] have measured Ba and BaO evaporation over life (see Fig. 6 of [47]). They observed a clear correlation: end of life has been reached when the Ba evaporation (linked to Ba generation) falls below BaO evaporation. A detailed quantitative description of I cathode life-limiting mechanisms has also been given by Roquais et al. [68].

Due to the addition of Re, which is also more persistent during ion bombardment, the base emission is that of the Re–I cathode, which is about 10 A/cm^2 at T_{op} = 965 °C(Mo-Br) or about 1030 °C true operating temperature. This ensures that despite the possible loss of the Ba–Sc–O complex, the saturated emission current density or transition from space charge limited to temperature limited regime remains at this level at least for the guaranteed lifetime of the (W)-I cathode base [66, 67].

An essential mechanism of life limitation of 'Sc'-I cathodes is the loss of Sc not by evaporation, but by ion bombardment. Hence also due to the short diffusion length of Sc, a rather thick reservoir containing Sc of some 100 nm is needed below the outer surface. This is ensured by the LAD top-layer coating containing BaO and ScO_x.

In Fig. 3.15 lifetime data of LAD top-layer scandate cathode type CG1 are depicted, showing pulsed results at 1.7 kV and 200 V and also DC results for 75 V (see [9]). The time of operation was 17,328 h, with a continuous DC load of 4 A/cm^2 (75 V) applied. It has to be noted that due to electron emission cooling, the operating temperature under load is about 25 °C lower than that given above for the no-load condition. This effect will also depend on the design of the I cathode base.

A series of CG1- and BG1-type LAD scandate cathodes have been operated under UHV at operating times between 1400 to 4000 h at DC levels of 2–3 A/cm^2, with I_{dc}(100 V) remaining constant at about 5 A/cm^2. Here the general conclusion

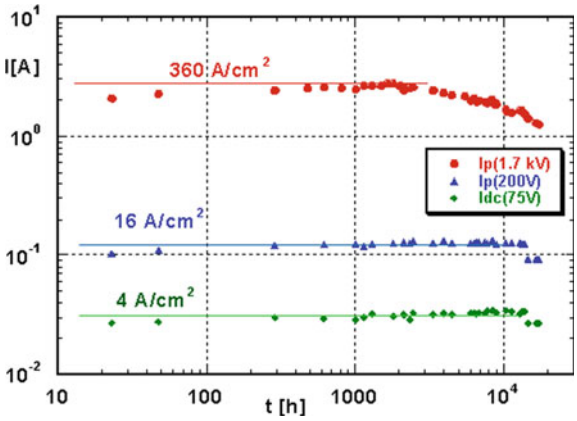

Fig. 3.15 Lifetime data of LAD top-layer scandate cathode type CG1, operated at 940 °C(Mo-Br) and 4 A/cm^2 continuous DC load in planar diode configuration. The graph is based on re-evaluated data of [9] plus additional data

for 'Sc'/Re–I cathodes is that a DC operation base level of 15 A/cm^2 should be maintained for the designed lifetime of the I cathode base, (in our case of 0.65 W Philips I-cathode units of about 20,000 h; pill diameter 1 mm, pill thickness 0.4 mm), due to the persistence of the Re surface. For operation at higher pulse test levels of, e.g., 100–200 A/cm^2, not only the surface adjacent reservoir of Sc (more specifically the amount of the Ba–Sc–O complex) will be decisive, as one can see from the ion bombardment investigations, but also a low UHV pressure level during operation is important.

3.2.3.6 Correlation Between Planar Diode and Electron Gun Emission Measurements

Since the final aim of the project was to apply the LAD scandate cathodes in CRT guns, their behavior in guns needed to be studied and correlated to planar diode results, which were of course much easier to obtain via directly mounting in UHV chambers. Moreover, the real ion bombardment happened in guns via ionization of the rest gas and had to be correlated to bombardment with Ar ions in a diode configuration [28, 44, 49], as we will discuss in the next subchapter.

The main difference between electron gun and planar diode is that in the gun for the electron beam one can only measure roll-off curves (also under-heating curves: electron current versus heater voltage) or activity curves (versus temperature) at a specific grid voltage setting for judging the emission capability of the cathode. It should be noted that there is a direct correlation between heater voltage and temperature via calibration curves (see Fig. 3.12b). In a diode, of course, it is no problem also to measure activity curves besides the *I(U)* characteristics at a set of temperatures. In the operation mode of the electron gun grid 1 usually has the same potential as the cathode (or a slight blocking voltage is applied) and the beam electrons are only extracted from the central region under the grid hole. The other grids have accelerating voltages. Yet there is the possibility to operate also the gun in a diode

mode, where grid 1 serves as the anode and at the other more distant grids higher extraction voltages are applied, so that the electrons from the central part below the hole are still extracted to the other grids. In this diode mode of the gun, the emitting area is now the cathode surface area without the area of the grid opening. Yet it is required, that the correlation is investigated just after activation at the beginning of life, before any damage in the central beam region can happen (see Fig. 3.21a, b). For well-activated cathodes from the same batch, we found good consistency between the *I(U)* characteristics in the planar diode and the diode mode in the gun and also between roll-off curves measured in the planar diode or under so-called half-drive conditions in a gun (see Fig. 3.16a, b).

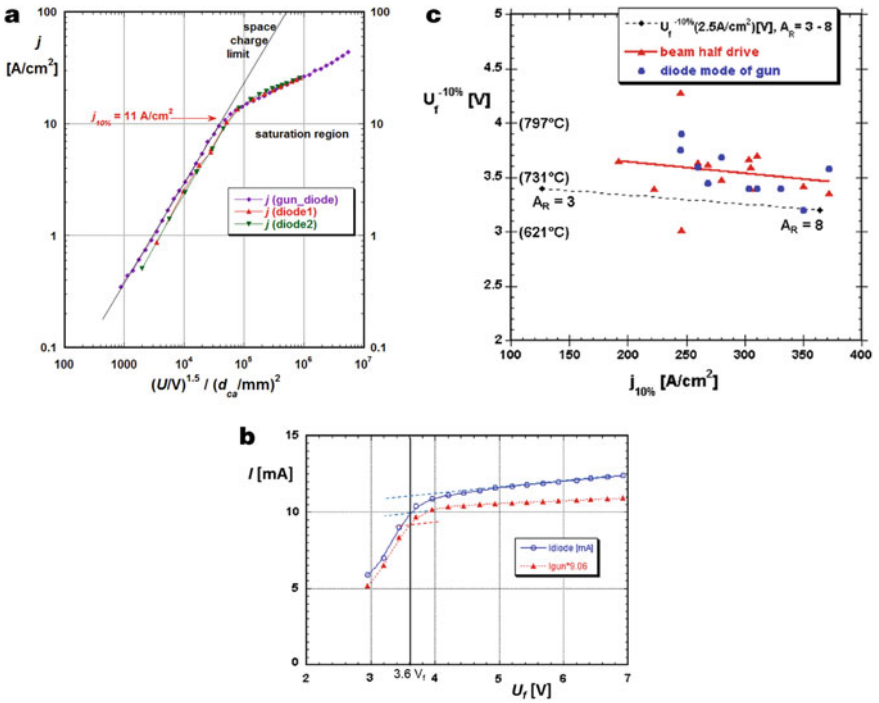

Fig. 3.16 Consistency between gun and diode measurements: **a** Electron emission current density j[A/cm^2] versus dimensionless "reduced space charge voltage coordinates" of $(U/\mathrm{V})^{1.5}/(d_{ca}/\mathrm{mm})^2$ for 3 Philips Os/Ru–I cathodes mounted in 0.65 W cathode units at an operating temperature of 965 °C$_{\text{Mo-br.}}$; based on data from [57, 59, 62]. Copyright of Fig. 3.16a: Georg Gaertner, Aachen, Germany.
b Roll-off measurements of a LAD scandate cathode type DG1 in diode mode (blue circles) and "half"-drive beam mode (red triangles) in 45AX electron gun.
c Roll-off measurements of LAD scandate cathodes type DG$_2$ in "half" drive beam mode (red triangles) and in diode mode (blue circles) in 45AX electron gun versus $j_{10\%}$ measured in the diode mode at 965 °C Mo-br. The temperatures in brackets are the true temperatures for the respective heater voltages. The theoretical values are also given for A_R varying from 3 to 8 A/(cm^{2}K^2) and a work function of 1.15 eV

The good consistency of cathode emission data obtained in a diode or in the diode mode of a gun is shown in Fig. 3.16a. A comparison of emission characteristic measurements in planar diode and in diode mode of a 45AX gun configuration was carried out for different Philips Os/Ru–I cathodes mounted in 0.65 W cathode units at the standard operating temperature of 965 $°C_{Mo\text{-}br}$. The results are shown in a double logarithmic diagram of the electron emission current density j[A/cm^2] versus dimensionless "reduced space charge voltage coordinates" of $(U/V)^{1.5}/(d_{ca}{}^2/\text{mm}^2)$. The cathode to anode distances were 70 μm in case of the diode mode of the gun, 190 μm for diode 1, and 250 μm for diode 2. The I cathodes tested were all standard Os/Ru I cathodes of Philips with 411 impregnants, mounted in 0.65 W cathode units. The agreement between the different Os/Ru I cathodes in the plot with reduced space-charge ordinate in the saturation range is remarkable. The small deviation in the space charge limited range is probably due to the fact that the lowest four data points at 25, 50, 75, and 100 V in the diode case are DC measurements of about 10–20 s duration (with some emission cooling), whereas the gun measurements and the diode saturation data are from pulsed measurements (pulse duration gun: 12 μs, pulse duration diode 5 μs). Also, a better determination of diode distance could result in still better consistency.

Since one can calculate activity curves from *I(U)* characteristics at different temperatures, one may also correlate $j_{10\%}$ at operating temperature and the knee of roll-off curves. The figure of merit is now the knee of the roll-off curve, defined as ${U_f}^{-10\%}$, i.e., the heater voltage value of the 10% deviation from the slightly inclined $I(U_f)$ line (see Fig. 3.16b). Via work function and $j_{10\%}$(T) there exists a correlation between the roll-off knee and the electron emission current density $j_{10\%}$ after IB [28, 49] (compare Fig. 3.16c). The correlation between the roll-off knee and the electron emission current density $j_{10\%}$ exists via the Richardson equation (via work function and Richardson constant), since from the half-drive condition of 1.2 mA or 2.5 A/cm^2 (a criterium used for I cathodes) the knee temperature can be determined or can be read from a plot such as in Fig. 3.12a. For example, ${U_f}^{-10\%} = 4.5$ V_f corresponds to $j_{10\%} = 40$ A/cm^2 at 6.3 V_f. Hence high pulse emission at high temperature is directly correlated with the roll-off knee at very low temperature. If ion bombardment reduces emission at high temperature in the diode, the roll-off measurement in the gun will show an increase of the knee temperature.

Figure 3.16b shows a comparison of roll-off measurements of a LAD scandate cathode type DG1 in the diode mode (blue circles) and in the "half"-drive beam mode (red triangles) in 45AX electron gun for the same ${U_f}^{-10\%} = 3.6$ V_f for both cases The ${U_f}^{-10\%}$ was determined as −10% deviation from the fitted saturation slope as a measure of the knee. The beam measurements have been carried out in the so-called half-drive mode with grid 1 at the ground, grid 2 at +1 kV, and grid 3 at +3 kV, so that the beam current is 1.2 mA at the working point of 6.3 Vf or 965 °C(Mo-br.), which corresponds to 2.5 A/cm^2 peak beam current density according to the electron optical calculations. Based on this density the equivalent current in the diode mode was calculated (I_{gun} times 9.06) and is shown as blue circles in Fig. 3.16b for a direct comparison. In the diode mode, the current density calculated from cathode area minus hole projection is 2.8 A/cm^2. The plot illustrates the good consistency

between half-drive and diode mode measurements. But it can also be used for an estimation of the maximum error, since it could mean that the relevant cathode area is about 12% larger than the geometrical projection. This would imply a diode mode correction in a gun of $j_{10\%}$ by −12%.

In Fig. 3.16c roll-off measurements of a series of LAD scandate cathodes type DG2 in "half"-drive beam mode (red triangles) and in diode mode (blue circles) in 45AX electron gun are depicted as a function of $j_{10\%}$ measured in the diode mode at 965 °C Mo-br. The temperatures in brackets are the true temperatures for the respective heater voltages. The theoretical values are also given for A_R varying from 3 to 8 A/(cm^{2}K^2) and a work function of 1.15 eV. The measurements were all carried out directly after activation ("0 h") and hence further emission increase in the following several hundred hours is not contained in this diagram.

A reliable comparison between gun and diode mode can only be carried out in the beginning, before deterioration in the central beam emitting area starts. Yet also the scatter in the beam mode may be larger, since the beam originates from a much smaller area than the diode part. In conclusion, one can see that the high emission capability of LAD top-layer scandate cathodes in guns at operating temperature is correlated with very low roll-off knee temperature.

3.2.3.7 Ion Bombardment Investigations

In cathode-ray tube applications, an important loss mechanism for Ba is ion bombardment (IB). The ions are generated by the interaction of the electron beam with the residual gas in the tube and are accelerated back to the cathode surface (see Fig. 3.5). The emerging ion beam has a strongly peaked density profile and hence sputter damage is strongly localized [28, 44, 49, 69, 70] in the central emitting area of the cathode (about 6% of the effective emitting beam area of 0.23 × 0.32 mm^2 dimensions of 45AX gun). Most electron gun experiments were done with 45AX guns in UHV chambers with a controlled gas admission valve. In this configuration, the ion life dose (ILD) is proportional to the electron current times the integral of pressure over time (average pressure times lifetime) and was specified as

$$\text{ILD (gun)} = 4.5 \times 10^{-5}\text{mA} \times \text{mbar} \times \text{h} \tag{3.3}$$

for 1.2 mA "half-drive"conditions in a Philips CRT. This corresponds to a leveling off of the initially higher pressure to nearly constant 2×10^{-9} mbar over a tube life of 20,000 h. The effect of ion bombardment in a gun is measured via the "roll-off" curve of the beam current, as we have seen above, starting at 1.2 mA (measured at grid 3) for 6.3 V_f, at given voltage settings (grid 1: 0 V; grid 2: 1 kV; grid 3: 3 kV) as a function of temperature, i.e., heater voltage U_f. The figure of merit is now the knee of the roll-off curve $U_f{}^{-10\%}$ which is correlated to the electron emission current density $j_{10\%}$ after IB [28, 49].

Accelerated ion bombardment experiments conducted in an electron gun configuration (Fig. 3.5) with controlled gas admission were then correlated with experiments in a diode configuration (Fig. 3.6) using an ion gun with a uniform ion density profile. Accelerated life testing of cathodes in the diode configuration has a number of advantageous aspects: the ions are generated externally in an ion gun and the ion current applied to the cathode is measurable, so that the number of ions hitting the surface is really known. The ion current density is constant over the cathode surface, which enables the examination of fundamental behavior and material properties of the cathodes without the influence due to the electron and ion optics in the electron gun, which in case of the gun cause a very sharply peaked ion density profile (hole burning into the emitting electron area, see Fig. 3.23a, b. Since the ion current generated by the electron beam is proportional to electron current and rest gas pressure, the effective ion dose ILD in the electron gun in units of mA*mbar*sec can be scaled to the absolute ion dose (charge) via the relation [28, 49]:

$$\text{mA} * 1\ \text{mbar} * \sec\left[\text{electron gun}\right] \cong 10^4 \mu\text{Asec [diode]} \tag{3.4}$$

This relation was mainly established via correlation of initial decay in gun and diode. In the case of the gun, the real ion dose can be determined from the specific ionization, where gas composition and electron energy need to be known, and from the path length of ionization. Most of the accelerated ion bombardment experiments were done in the diode configuration, using a moveable anode with a circular hole and a differentially pumped Ar ion gun (PerkinElmer Φ 04–303; typical Ar^+ energy 3 keV; see Fig. 3.6). In the first step, the sputter ablation rates of pure and multilayered VSP materials were determined. This gives the correlation between ion dose (ion energy 3 keV) and layer thickness removed (sputter yield Y). For W and Sc_2O_3 VSP-layers, yields of 1.1 and 0.4 atoms/ion were determined. Secondly, IB was applied to the surface of LAD cathodes and the emission recovery was investigated as a function of time, temperature, and ion dose. Qualitative main results were the following: in the W + Sc_2O_3 system emission recovery after IB is inferior and already at low doses (about 10^{17} ions/cm^2), emission falls back to a W–I characteristic. Better IB resistivity is achieved by Re + Sc_2O_3 LAD I cathodes, but the best results were obtained after further addition of the 411x intermediate layer and about 25% of the total life dose of 1700 μAs were achieved for the best variant DG2 + , where additionally the LAD scandate cathodes were not fully activated = under-activated (ua). This is depicted in Fig. 3.17, where the percentage of ILD that survived at a level of 40 A/cm^2 is related to the LAD scandate cathode type. This improvement of scandate cathode types in time scale continued from 1993 to 1997. Since these tests were accelerated tests, the shielding factor related to the dose rate has to be taken into account. With this correction the top value of 25% ILD corresponds to 63% of the reference lifetime dose. In consequence by an improvement of vacuum by a factor of 2 (reduction of average tube pressure by ½ or tube pressure 1×10^{-9} mbar), emission-induced ion bombardment in a CRT during life will be survived at a level of 40 A/cm^2. Figure 3.18 shows the degradation of the *I(U)* characteristic as a function of IB dose: the total emission can be described qualitatively as the superposition of

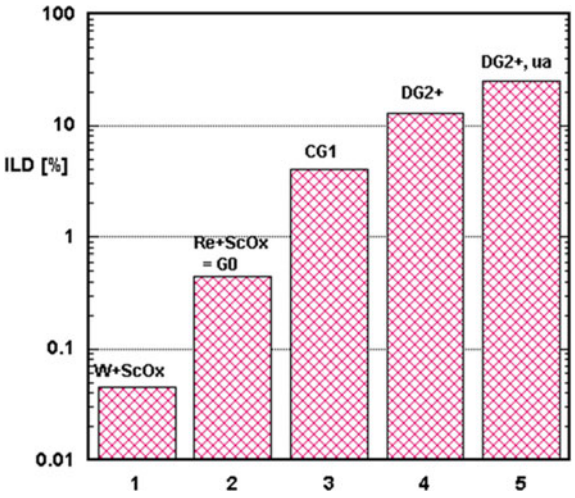

Fig. 3.17 Percentage of ILD survived at a level of 40 A/cm^2 related to the LAD scandate cathode type; compare [30, 31]

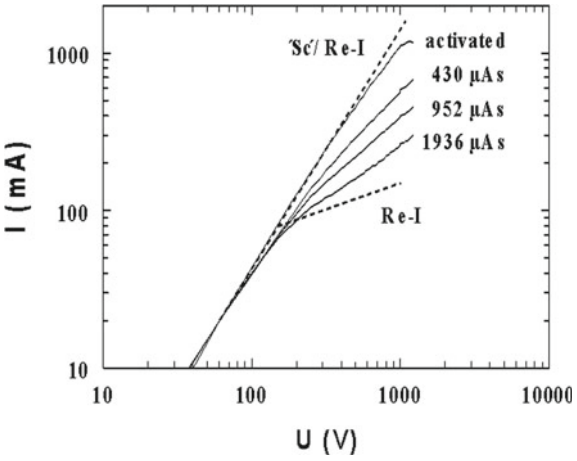

Fig. 3.18 Degradation of *I(U)* characteristic as function of IB dose in diode with Ar ion gun (ILD = 1700 µAs): Dashed lines: perfect 'Sc'/Re–I and Re–I cathodes. Total emission is superposition of area fractions of Scandate (only space charge limited) and Re–I; see [2, 28, 49], G. Gaertner, H. Koops, Chap. 10 of "Vacuum Electronics, Components and Devices", Springer 2008, p. 442

area fractions of Scandate-I (only space charge limited) and Re–I, with some extra space charge leakage into the Re fraction, where the Re–I fraction increases with increasing ion dose [28, 49].

During IB, two processes are competing, namely sputter removal of surface atoms and Ba resupply from the interior. The time change of emission current I

can be formally described [16, 28, 49] by the sum of a destruction term (τ_{IB}) and a regeneration term (τ_{rec}):

$$dI/dt = -I/\tau_{IB} + (I_0 - I)/\tau_{\mathrm{rec}} \tag{3.5}$$

With respect to emission, this initially leads to a fast decline (time constant proportional to inverse ion current) followed by a slow bending to a dynamic equilibrium which is determined by the ratio between destruction and resupply rates. This is illustrated in Fig. 3.19 showing half-drive beam currents of LAD scandate cathodes type DG2 before, during, and after ion bombardment in a 45AX gun for different levels of Ar gas admission. Duration of IB is 15 min for Ar gas admission of 4×10^{-6} mbar (blue circles) and 60 min for 6.7×10^{-6} mbar Ar (red squares). Ar was introduced via a leak valve, since it has no poisoning effect on emission and hence only acts via ionization and ion bombardment of the cathode surface. The longer poisoning interval corresponds to an ion dose of 5.4×10^{-5} mA*mbar*h or 12% of the IB life dose. Similar curves are obtained for ion bombardment in a diode configuration with an Ar ion gun, as shown in Fig. 1 in [28], Fig. 5 of [49] or Fig. 6 of [44], which are not shown here.

Compared to an ILD extrapolation in diode configuration at high IB dose rates (1 μA), the ILD extrapolation at more realistic low dose rates (10 nA) will hence yield an increase in extrapolated IB life of up to a factor of 8 due to the dynamic shielding effect [28, 49].

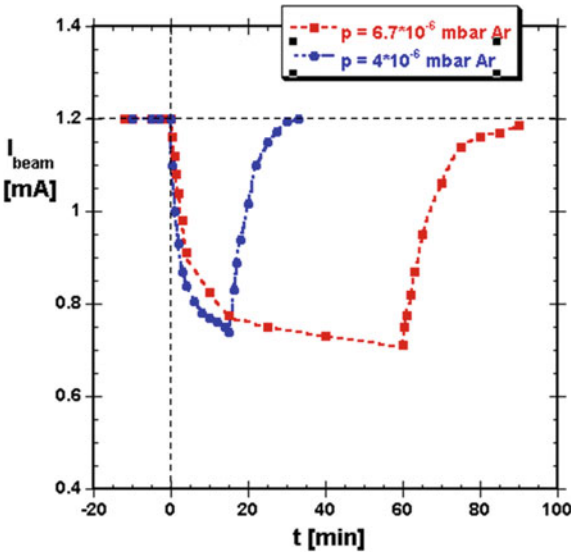

Fig. 3.19 Half-drive beam currents of LAD scandate cathodes type DG2 before, during, and after ion bombardment in a 45AX gun for different levels of Ar gas admission. Duration of IB is 15 min for the blue circles; IB duration is 60 min for the red squares; see [28, 44, 49]

A further requirement is a short recovery time after IB: as specified this should be 1 min. Best time constants achieved for Sc-recovery were 8 min at 965 °C Mo-br. Yet this requirement is only relevant in the initial phase of high tube pressures, which are continuously decreasing, equivalent to an initial dose of 4×10^{-7} mA*mbar*h.

3.2.3.8 Emission Poisoning

From emission poisoning investigations, one can conclude that Ba scandate cathodes are about an order of magnitude less sensitive to poisoning than I cathodes. The figure of merit $p\ (\Delta I = -\ 10\%) = f\ \{\text{gas, cathode type}, T, d_{CA}, i, t\}$ is defined by a 10% current decrease when increasing pressure in the UHV chamber by controlled gas admission through a UHV gas leak. The poisoning threshold $p\ (0.9\ I_0)$ for air admission of 1×10^{-5} mbar for LAD scandate cathodes is about a factor of 10 higher than that of Os/Ru–I, as can be seen from Fig. 3.20. In this case the experiments have been conducted with Re+ScO_x LAD top-layer scandate cathodes (type G0). According to the literature [71–75] and also our own experiments for scandate and I cathodes, the poisoning insensitivity for different gases can be ranked in the sequence (hierarchy): $O_2 < CO_2 <$ air $< CH_4 < CO < H_2$ (most insensitive). For I cathodes water vapor poisoning is less sensitive than O_2 poisoning. Concerning the other parameters, one finds decreasing poisoning sensitivity with increasing temperature and increasing poisoning sensitivity with increased diode spacing (less pumping effect of evaporant!) up to 1.5 mm. The mechanism of emission poisoning is based

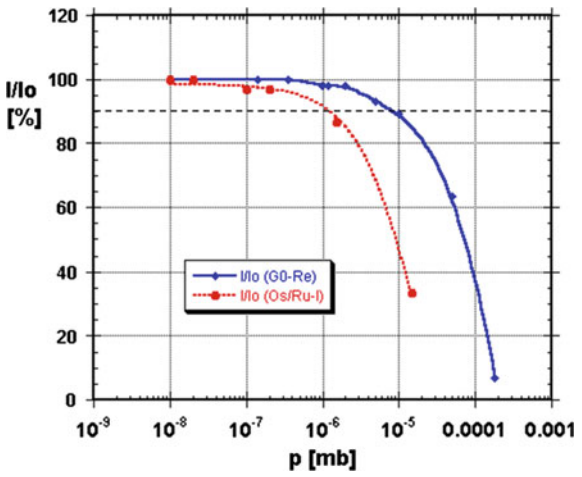

Fig. 3.20 Emission poisoning of LAD scandate cathode of type G0 (Re) and a Os/Ru—I cathode by air introduced at 965 °C Mo-Br. Depicted is the normalized emission (relative emission decline) after 1 min as a function of total pressure increased from UHV by controlled admission of air through a leak valve. The figure of merit is given by $I = 0.9\ I_0$ and is 1×10^{-6} mbar for the Os/Ru–I and 1×10^{-5} mbar for the Ba scandate cathode

on gas molecule adsorption on the cathode surface and hence the change of the work function.

A further important property of these Ba scandate cathodes is that, e.g., after air admission they can be reactivated in vacuum again to $j_{10\%} > 100$ A/cm^2, if they had reached that level before: there is no significant deterioration of emission capability.

3.2.4 High-Resolution Cathode Characterization

High-resolution characterization of LAD top-layer scandate cathodes as prepared and after a certain time of operation was carried out by SEM, EDX, and SAM. Typical SAM analysis conditions and quantification parameters are given in Table 3.4 (sample angle = 0°).

Maps were made at a primary beam voltage of 10 kV, to improve lateral resolution. All spectra were made at a primary beam voltage of 5 kV. For quantification the high energy Auger lines for AI, W, and Re were used. The low energy line for AI interferes with low Ba-lines and the low energy lines of W and Re coincide at 179 eV and cannot be used to discriminate these elements. The same holds for the W-line at 1798 eV and the Re-line at 1799 eV. For that reason, the weaker Re-line on 1858 eV was used for the quantification. The high energy lines are quite insensitive, but there was no alternative for reasonable quantification. The sensitivity data given by Physical Electronics do not give sensitivities for all these Auger lines. Sensitivities for some lines were calculated by using the ratio with other Auger lines. So sensitivities can differ from the elemental sensitivities given by Physical Electronics. So semi-quantitative values of atomic concentrations of the elements present can be obtained. For a quantitative evaluation a correction for the matrix effect and chemical binding effects needs to be carried out and also gauge samples have to be used for the specific elements present. The above conditions are similar to the conditions given by Philips Research in [23, 77].

The information depth in Auger electron spectroscopy (AES) is approximately 2 nm (0.5–5 nm), whereas the lateral resolution depends on the fine-focused electron beam and at best it is about 30 nm, but usually it is averaged over the larger area investigated. A sputter depth profile can be performed to monitor the elemental concentrations as a function of depth. Ar+ ions are used for sputtering, while the sputter conditions have been calibrated using a known SiO_2 layer thickness on Si. The measured sputter rate for SiO_2 was 9.3 nm/min (at raster 1.5 × 1.5 mm^2, 30° tilt angle, 3 keV Ar+, 15.5 nA). This sputter rate may, however, differ for the various

Table 3.4 Typical Auger analysis parameters: V-beam = 10 or 5 kV; I-beam = 20 nA

Element symbol	Sc	O	Ba	AI	W	Re
Peak energy (eV)	340	503	584	1396	1736	1858
Sensitivity	0.200	0.400	0.120	0.070	0.080	0.031

elements and elemental compositions. For Sc_2O_3, a sputter rate of 6 nm/min was calculated under these conditions.

Figure 3.21a shows an SEM micrograph of part of cathode surface SG2 + type after LAD. The surface structures of other cathodes after LAD look similar and will coarsen and shrink on the grains during operation. The result of grain growth and roughening is depicted in the SEM micrograph in Fig. 3.21b for CG1 cathode after gun operation of 750 h. It is a surface area outside the grid hole region, where practically no ion bombardment has taken place, at a magnification of 10,000. Figure 3.21c, d show elemental maps of O(c) and Sc (d) by SAM of the same surface area as in b. The composition here should be similar to the composition after activation, whereas in the sputtered region under the grid hole Sc and Ba concentrations are much lower (not shown here). It is striking that the Sc and O distributions are very similar, indicating that Sc is present as oxide. As can be judged from other elemental maps of LAD cathode surfaces, Ba is more uniformly distributed and usually covers a larger

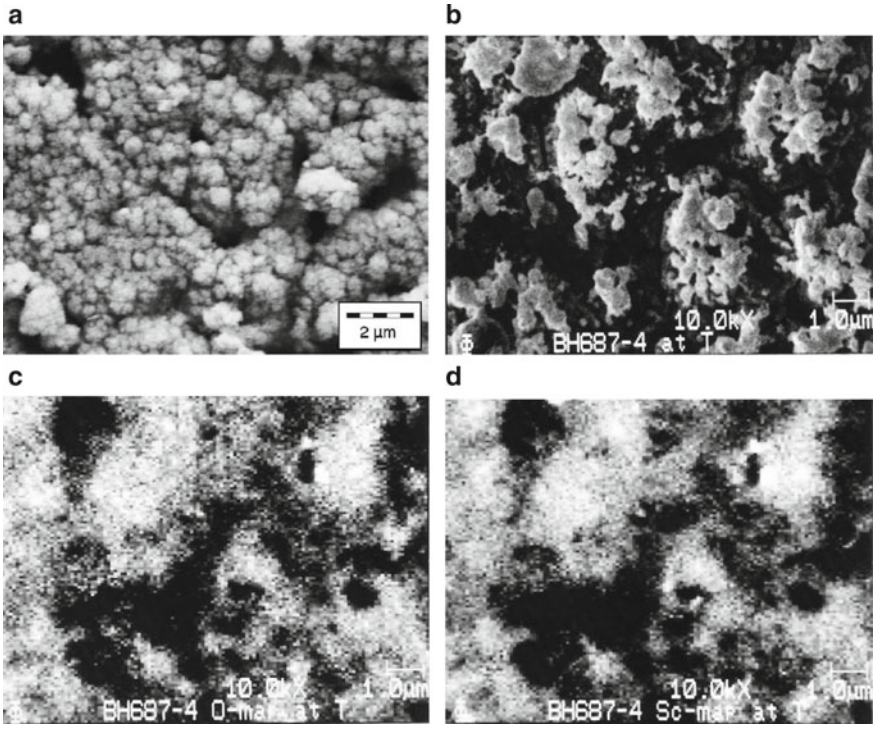

Fig. 3.21 **a** SEM micrograph of surface of SG2 + type cathode after LAD; structures will first coarsen and later on shrink on the grains during operation. **b** SEM micrograph of surface of CG1-type cathode outside grid hole region after gun operation; magnification 10,000x. **c** O elemental map by SAM of cathode surface of CG1-type after gun operation; same area as in 3.21b; magnification 10,000x. **d** Sc elemental map by SAM of cathode surface of CG1-type after gun operation; same area as in 3.21b; magnification 10,000x

surface area than Sc, which partly is concentrated, and is also found outside ScO_x patches. This is due to its resupply from the pores and its longer diffusion lengths. Hence there are two portions of Ba, the one diffusing over the whole cathode surface as a monolayer (including over the complex) and the portion bound in the Ba–Sc–O complex. The elemental composition at room temperature over the surface area at a magnification of 168x was 7% Sc, 15.9% Ba, 24% O, 11.7% Re, and 20.2% W (+4.8% Al). In the area outside the grid of Fig. 3.21b the composition was 8.5% Sc, 14.2% Ba, 20.2% O, and 7.8% W/Re. We can compare this with a similar cathode #CG1_2.1, which also reached a saturated emission current density of 293 A/cm^2 at operating temperature. There we obtain (flocky structure) 7.9% Sc, 17.2% Ba, 20.0% O, 13.5% Re, and 23.9% W (+ 3.1% Al). These results are quite similar.

A sputter depth profile of DG1 cathode (also after gun test) is given in Fig. 3.22a of an area of 200 × 200 μm^2 outside the grid hole region. For comparison the LAD preparation conditions for this cathode were 411_0.35: 8400 pulses, Re: 12,500 pulses, ScO_x: 8300 pulses ($i_{10\%}$ (under-activated) = 230 A/cm^2). Averaging the Ba:Sc:O ratio from 0 to 6 min of sputtering, which corresponds to n Sc sputter depth of 36 nm, one obtains Ba:Sc:O = 1.78: 1: 1.26. Here oxygen associated with W was not taken into account. Figure 3.22b shows another sputter depth profile now of a DG2 + cathode of a surface area of 500 × 500 μm^2. This cathode was mounted in a diode and reached a maximum saturated emission current density of 267 A/cm^2, but with an early deterioration. The LAD preparation conditions for this cathode were 411_0.35: 16,500 pulses, Re: 25,000 pulses, ScO_x: 8400 pulses. Since more Re has been ablated, a higher Re concentration of 55% was reached. Here the averaging over an Sc sputter depth of 36 nm results in Ba:Sc:O = 2.44: 1: 1.4.

The average value from the surface analysis is Ba:Sc:O = 2.04: 1: 2.78. Since Ba as a monolayer on W or Re is independent of the position of the complex, the Ba to Sc ratio of the complex is probably a bit lower.

Figure 3.23a, b show SAM analysis results of a CG1 cathode after life test in a 45AX gun. The Sc elemental map under the rectangular grid opening of 0.7 mm × 0.5 mm illustrates the final removal of Sc by ion bombardment caused by the electron beam, whereas the Ba map is more uniform due to the resupply from the pores.

The micrographs of Fig. 3.21 were first shown by G. Gaertner in a presentation at RWTH Aachen in 2000 and again at South East University Nanjing in 2004; see also [67].

We can compare these data also with the literature. van Veen by XPS [76] and Hasker by AES [77] found a Ba/Sc ratio of 1 for scandate cathodes with emission <100 A/cm^2. According to the investigations of Y. Wang and her coworkers of improved Sc–I cathodes, the emissive surface of the scandate cathodes investigated consists of an active surface multilayer containing (Ba, Sc, O) with a ratio of Ba:Sc:O around 1.9: 1: 2.2 [10]. It is interesting that J. Hasker already presented a depth profile in [15] after activation for a scandate cathode prepared with W and ScH_2 in the top layer, which looks quite similar to Fig. 3.22, Ba and Sc decreasing within the first 6 min of sputtering. The signal ratio Sc/Ba = 2 is consistent with the lower emission capability of this cathode type.

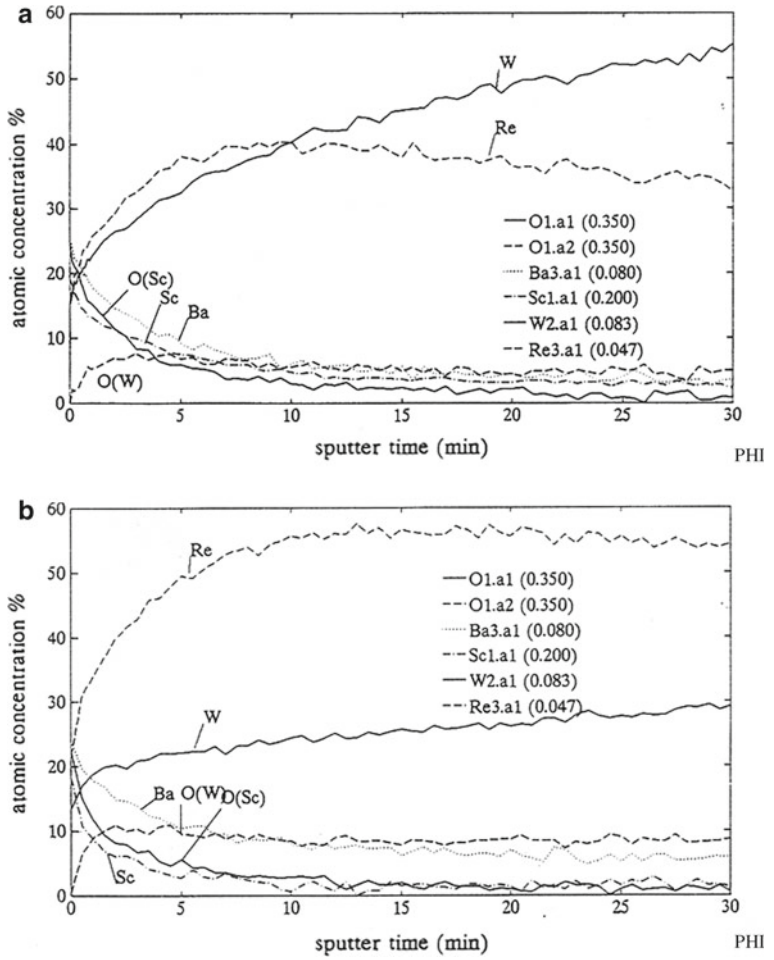

Fig. 3.22 **a** Sputter depth profile of cathode of DG2 type, area of 200 × 200 μm^2 outside grid hole region. **b** Sputter depth profile of cathode DG2 + type, surface area of 500 × 500 μm^2; 5 min sputtering of Sc corresponds to 30 nm depth

All these results would be compatible with a compound containing $Ba_3Sc_2O_6$, which is somewhat in contradiction with the stable compound $Ba_2Sc_2O_5$ in this system. It is interesting that S. Magnus and colleagues have investigated ternary compounds in the $BaO{\cdot}Sc_2O_3{\cdot}WO_3$ system [78]. Together with 10%W and BaO they found increased best emission for the compound $Ba_3Sc_2WO_9$ compared to other Sc containing oxides, yet far from optimized scandate cathode emission. This is consistent with Aachen LAD experiments, where $Ba_2Sc_2O_5$ was used as a target instead of 411x, but without success. However, it has not been discussed before, what happens if W is replaced by Re. Combining the two stable compounds $Ba_2Sc_2O_5$ and $BaReO_4$ one would obtain $Ba_3Sc_2ReO_9$. It would be an alternative route for Ba scandate

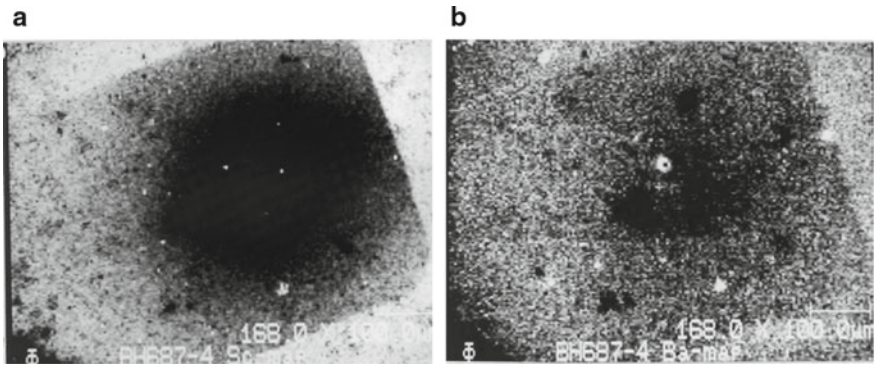

Fig. 3.23 **a** SAM analysis of CG1 cathode after life test in gun; Sc elemental map under the rectangular grid opening of 0.7 mm × 0.5 mm; magnification × 168. **b** SAM analysis CG1 cathode after life test in gun; Ba elemental map under the rectangular grid opening of 0.7 mm × 0.5 mm; magnification × 168

cathode preparation, to start and ablate directly the emissive compound/complex and not to have to rely on a high-temperature synthesis under cathode activation conditions as in our case.

3.2.5 Conclusions on LAD Top-Layer Scandate Cathodes

The outstanding emission capability of LAD top-layer scandate cathodes and their preparation has been discussed in detail. Yet there is some scatter in the emission properties, which can partly be linked to changes of the target surfaces and nanoparticle generation during repeated ablation cycles. The thermomechanical stability of the 411x target still needs to be improved. A further improvement is expected by using more fine-grained I cathode bases similar to SDD cathodes. Alternate and cheaper preparation methods such as sputtering should be investigated for the preparation of similar material layer structures, which anyway will coarsen during activation. In general the formation of the emissive Ba-scandate complex/compound via the high-temperature activation process is a critical step and it would surely help, if this compound could be identified by XRD or other methods and is, for example, prepared via a low (or high) temperature chemical route.

What is now the explanation for the very high pulsed emission capability of the LAD Ba scandate cathode? First one must notice that the high emission capability was just a side effect of achieving high robustness versus ion bombardment at a much lower emission level. In reaching this goal the surface uniformity and Sc reservoir, or better (Ba,Sc,O) reservoir below the surface was increased. The increase in uniformity and emission capability was linked to an increase of the Richardson constant A_R from 3 to 8 A/(cm^{2}K^2), whereas the Richardson work function remained

constant at the low value of about 1.15 eV. The Re base guaranteed at least a higher fall back emission level during and after ion bombardment and also reactions with W could be partly suppressed. Re and the additional 411x reservoir turned out to be essential for high IB robustness. And finally one should notice that oxide cathodes with about the same effective work function can also deliver pulsed emission current densities of 100 A/cm^2 at similar operating temperatures. Hence I am very much in favor of an oxide-semiconductor theory, where the conductivity limitation has been overcome by the conducting base with only a thin but more stable oxide layer on top and good conductivity also here provided by Re at the surface. In such a semiconductor theory, Ba will sit on top of a (Ba,Sc,O) containing oxide with an oxygen deficiency and a high density of these sites will be the aim. In the following part, this will be discussed in more detail.

3.3 Nanosized-Scandia Doped Dispenser Cathodes with W-Base Matrix (Yiman Wang)

3.3.1 Motivation for the Development of the Nanosized-Scandia Doped Dispenser (SDD) Cathodes

In the introduction, the research on different types of Ba scandate dispenser cathodes has been summarized and the LAD top-layer scandate cathode has been discussed in more detail.

In practice, improved impregnated scandate cathodes are the only Ba scandate cathodes which have been utilized in several vacuum microwave electron devices with pulsed current densities between 10 and 30 A/cm^2 at 1000–1050 °C$_b$ [79, 80]; even then they still suffered from poor emission uniformity and reproducibility.

Recently, there are growing interests in the development of the next generation of vacuum electron devices (VEDs) to operate at higher powers and frequencies and in the improvement of electron beam instruments or tubes to reduce the beam size and/or increase the beam brightness.

These make cathodes face a great challenge of providing much higher current densities at lower operating temperatures than that of presently available cathodes.

Therefore, there is strong demand and bright prospects in the application of Ba scandate dispenser cathodes for advanced vacuum electron devices and others after further improvement.

The requirements for cathodes to apply in advanced VEDs are

1. High SCL current densities in both pulsed and DC modes with excellent emission uniformity for good beam quality [48].
2. A long lifetime at reasonable operating temperatures.

3. A low evaporation rate of Ba and other volatile components for minimizing electric and vacuum breakdown.
4. Robustness in fabrication and operation.
5. Reproducibility in manufacturing.

To meet these requirements, a new type of Ba scandate dispenser cathode, the nanosized-scandia doped dispenser (simplify SDD) cathode with Scandia nanoparticles doped W matrix has been developed [10]. The characteristics of this cathode have been investigated comprehensively; high current densities have been routinely demonstrated.

3.3.2 Structure, Features, and Manufacture of Nanosized-Scandia Doped Dispenser Cathodes

3.3.2.1 Basic Ideas on Improvement of Ba Scandate Dispenser Cathodes

Historically, Ba scandate dispenser cathodes have been found capable of providing high emission current densities but suffer from the problem of extremely nonuniform current distribution. It has been commented that a Ba scandate cathode provides poor beam quality when used in electron guns due to the emission nonuniformity, and thus limits the applications of Ba scandate cathodes in VEDs [8].

A Ba scandate dispenser cathode is basically a Ba dispenser cathode with the addition of scandium oxide into the matrix, impregnant, or on its top. It is generally accepted that the electron emission capability and the emission uniformity of Ba scandate dispenser cathodes greatly depend on the distribution uniformity of scandium on the surface of cathodes [16–19]. In view of the well-known fact, that the diffusion rate of scandium is much lower than that of Ba [35, 81], two factors are favorable for the improvement of surface uniformity of Sc. The most important one is a perfect dispersity of small-sized scandium oxide in the matrix. This enables the reactions of scandium oxide with tungsten and other substances to pervade all over the matrix, leading to adequate and well-distributed release of scandium during fabrication and activation. The other is the small average size of the tungsten grains of the matrix, which favors the diffusion and coverage of Sc on the surface.

For a mixed matrix Ba scandate cathode developed by Philips, tungsten powder of 4 μm and Sc_2O_3 powder of 10 μm on average were mixed mechanically [15, 23]. The large sizes of both tungsten and Sc_2O_3 powders and the mixing method result in uneven distribution of Sc on the cathode surface. In the case of a thin-film top-layer Ba scandate cathode, as reported by Sasaki [35], the coated W + Sc-tungstate containing film could be divided into two parts after activation: film-covered impregnated areas A and the tungsten metal areas B (Fig. 3.24), where free Sc was generated in the areas A by reaction with Ba. Since surface diffusion length of scandium is too short to cover the gaps between A areas (i.e., to cover B areas), this physical nonuniformity causes

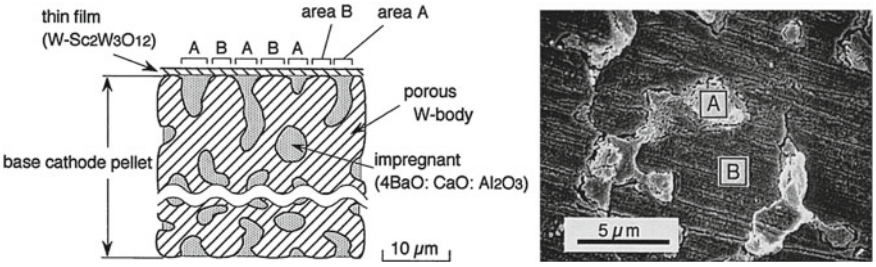

Fig. 3.24 Nonuniformity of Sc coverage on the surface of the thin-film top-layer Ba scandate cathode caused by insufficient diffusion length of scandium to cover the gap B. The graph is based on Fig. 1 of [35]

the emission nonuniformity. Hence a BaO containing layer below the Sc-containing top layer must be further introduced for improvement.

In order to overcome these disadvantages, a doping process has been developed for uniformly adding nanosized scandium oxide to tungsten powder in the manufacturing of a new type of Ba scandate dispenser cathode—nanosized-scandia doped dispenser (SDD) cathode.

3.3.2.2 Structure of SDD Cathodes

There are two types of SDD cathodes, the Scandia Doped Impregnated cathode (SDI cathode) and the Scandia Doped Pressed cathode (SDP cathode). The SDI cathode has a porous matrix fabricated by calcining, reducing, pressing, and sintering the precursor powder containing tungsten and (3–5) wt% scandium oxide. This porous matrix is then impregnated with Ba–Ca aluminate, which is traditionally used for Ba dispenser cathodes, mostly with mole ratios of BaO: CaO: Al_2O_3 of 4:1:1, at 1600–1700 °C for a short period to ensure a weight gain of (8–10) wt% is realized. After that, the surface residual impregnants are thoroughly removed by ultrasonic water cleaning [10]. The SDP cathode is made in a simpler process flow of pressing and sintering tungsten powder that already contains Sc_2O_3 and BaO, CaO, Al_2O_3 in similar mole fractions to that of 411 Ba, Ca aluminate [82].

In both cases, doping processes are used for adding scandium oxide and other compounds into tungsten.

Materials and cathodes for either type above have the following characteristics:

1. Precursor powders are tungsten, uniformly doped with nanosized scandium oxide (for SDI cathode), or compounds containing Sc, Ba, Ca, Al, and O (for SDP cathode). The powder size is several hundred nanometers to 1–2 μm.
2. Matrices of SDI cathodes, that are made from scandia doped tungsten powder and sintered at proper temperatures, have porosities of 24–28% similar to that of Ba dispenser cathodes but exhibit tungsten grains of submicron to 1–2 μ size and uniformly distributed nanosized scandia particles [43].

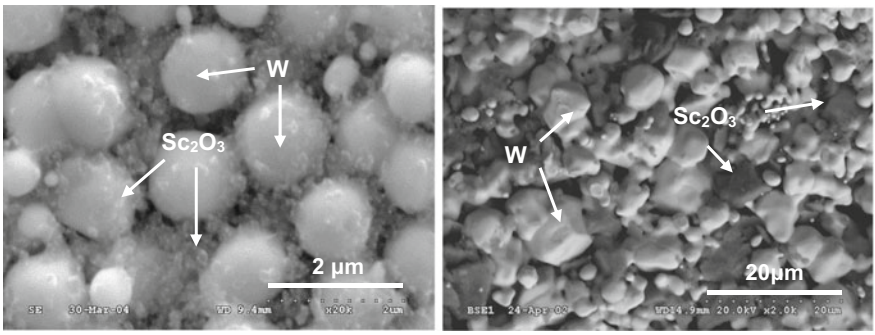

Fig. 3.25 **a** Scanning Electron Microscopy (SEM) image of a matrix composed with nanosized-scandia doped tungsten powder. **b** Back Scattered Electron (BSE) image of a matrix produced by mechanical mixing of Sc_2O_3 and W

3. Cathodes produced from the abovementioned matrices (for SDI cathodes) or the doped precursor powders (for SDP cathodes) consist of tungsten grains of submicron to 1–2 μ and uniformly distributed powder particles containing Sc, Ba, Ca, Al, and O [10, 82].

For simplicity sake, scandia-doped impregnated cathode is considered as a representative for SDD cathode in most cases below.

It has been noticed that the microstructures of matrices composed of the scandia doped tungsten powder are strongly different from that of the mechanically mixed scandium oxide with tungsten, shown in Fig. 3.25a, b, respectively. In contrast to the case of the mechanically mixed matrix where Sc_2O_3 lumps insert locally to W grains, the nanosized scandium oxide particles are evenly dispersed among and on the W grains in the scandia doped matrix. X-Ray Diffraction (XRD) analysis reveals that the Sc_2O_3 is the sole form of scandium in the W matrix [83].

Since the SDD cathode is based on above scandia-dispersed and fine-grained matrix, more efficient and extensively distributed reactions of scandium oxide with tungsten and Ba, Ca aluminates can be expected at processes of impregnation and activation as compared to other types of Ba scandate dispenser cathodes, allowing for a sufficient release and uniform spread of free scandium in the body and onto the surface of the cathode.

It has been further found that the uniformly distributed Sc_2O_3 in the matrix of Fig. 3.25a had mostly disappeared from the surface of cathode after impregnation and ultrasonic water cleaning, as shown in Fig. 3.26a. There are only small amounts of Ba, Sc, Ca, Al, and O to be observed in Fig. 3.26b within the detection depth of Energy Dispersive X-Ray Spectroscopy (EDS) analysis. This reflects that the aforementioned full reactions between Sc_2O_3 and others actually took place and the resultant reaction products were then dissolved and removed by water cleaning. The details will be discussed later.

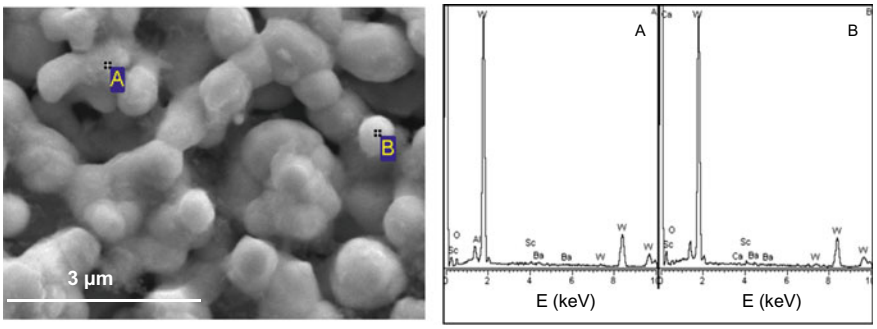

Fig. 3.26 **a** SEM image of an SDD cathode after impregnation and ultrasonic water cleaning. **b** EDS analysis at point A and B

As presented in SEM image of Fig. 3.26a, the cathode contains uniform pores with short pore distances. Such a structure is advantageous for the diffusion of active substances, including Sc, from the body of the emitter to its surface and over the tungsten grains during activation. As a result, a uniform surface layer containing Ba, Sc (and O) is formed on W substrate after activation. This has been proven by Scanning Auger Mapping (SAM) of Ba and Sc done in an activated cathode in Fig. 3.27a. The SAM maps of Sc and Ba of Fig. 3.27c, d show that Sc distributes over the surface of W grains and coincides perfectly with Ba while the latter exhibits a more even distribution.

In addition, compared with the top-layer scandate cathodes by thin-film techniques, the SDD cathodes have the advantage of being controllable in manufacturing, providing excellent resistance to possible surface abrasions in fabrication and assembling, and therefore are suited for practical applications.

3.3.2.3 Doping Processes

Several doping processes have been developed for adding scandium oxide into tungsten powder, replacing mechanical mixing technology, for scandia-doped impregnated dispenser cathodes.

The first doping technology applied to powder preparation is Liquid–Solid (L–S) doping method. In L–S doping, scandia is added to the tungsten oxide in the form of a scandium nitride aqueous solution. By reduction in a hydrogen atmosphere, the Sc-doped tungsten oxide is converted into scandia-doped metallic W powder. Compared with the powder produced by mechanical mixing, the size of scandia is obviously reduced while its distribution among W grains remains unsatisfactory.

As a major improvement, Liquid–Liquid (L–L) doping technologies were introduced. Two methods have been utilized. The technology which has been mainly adopted is a sol–gel process [84]. In the process, scandium nitride and ammonium

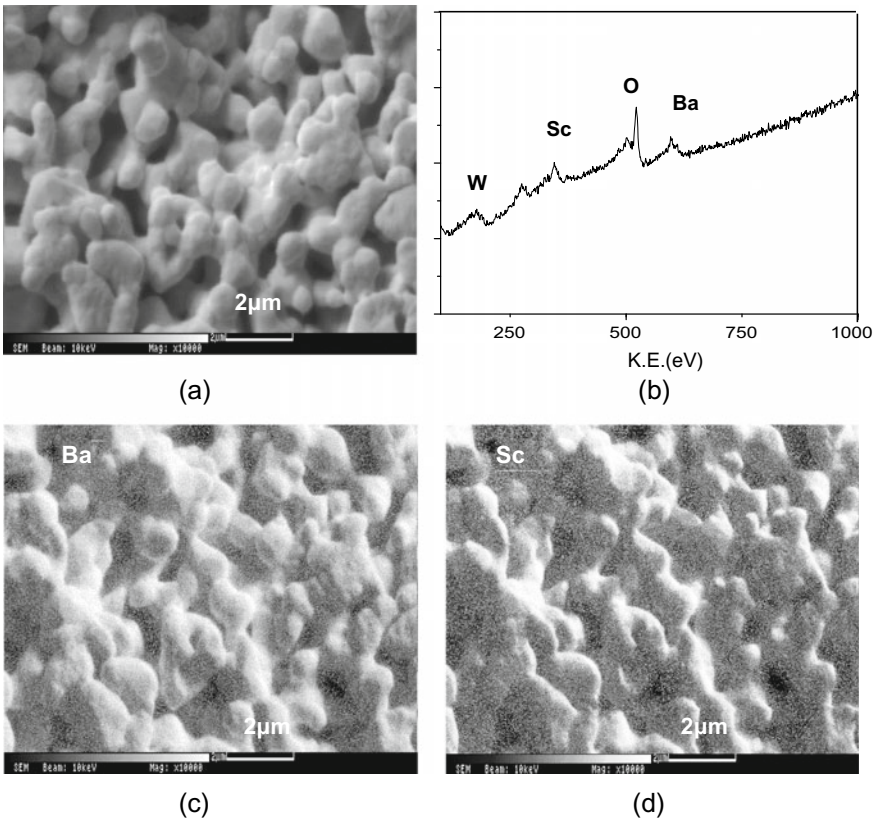

Fig. 3.27 Coverage of Ba and Sc on the surface of an SDD cathode after activation. (**a**) SEM image. (**b**) Auger Electron Spectrum taken from area shown on the SEM image. (**c**) SAM mapping of Ba. (**d**) SAM mapping of Sc

metatungstate (AMT) are used as the raw materials. The above materials were mixed in aqueous solutions to form sol and then converted into gel by bake-out. After calcining in air to remove the organics containing N and C, the Sc_2O_3 doped tungsten oxide powder was reduced into scandia-doped tungsten powder in hydrogen atmosphere. Since the raw materials are mixed in their aqueous solutions, the admixture is exceedingly uniform.

To illustrate the improvement, SEM images of the powders produced by L–S doping and sol–gel process are compared in Fig. 3.28a and the left side of Fig. 3.28b. On the right side of Fig. 3.28b a Transmission Electron Microscopy (TEM) image of a grain of the sol–gel doping powder is displayed, which indicates that tiny scandium oxide particulates are well dispersed over the surface of a tungsten grain.

By controlling the parameters of the processes, the resultant doped-tungsten grain sizes from submicron to about 2 μm can be normally produced.

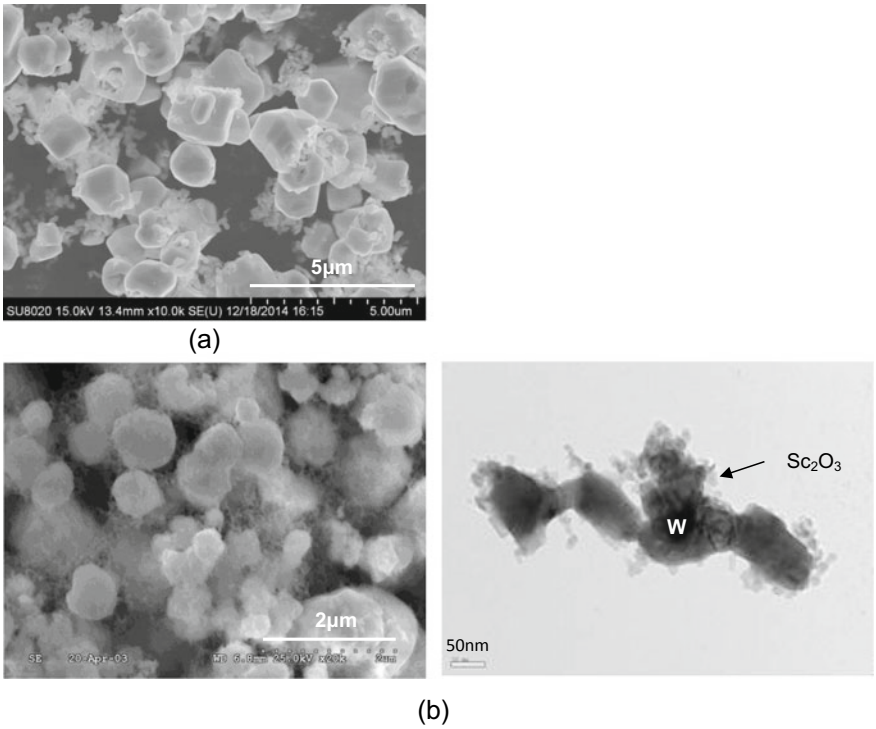

Fig. 3.28 Images of scandia doped tungsten powders. **a** SEM image of powder by L–S doping. **b** SEM image of powder by sol–gel doping process (left) and TEM image of one of the grains (right)

Another technology, spray drying, has also been developed for nanosized-scandia doped tungsten powder preparation. In the process the raw materials are mixed by spray drying method with Spray Dryer [85] and then followed by the same procedures as that of the sol–gel process above. Powders with a quasi-Gaussian distribution and mean size of around 1 or 2 μm, shown in Fig. 3.29a, can be routinely produced. The mixing uniformity of Sc_2O_3 with W, which is analyzed by Energy Dispersive X-Ray Spectroscopy (EDS) at different grains and illustrated in Fig. 3.29b, is similar to that of the sol–gel process.

In general, while the sol–gel technology results in the most homogeneous mixing of Sc_2O_3 with W, the spray drying process has the advantages that the morphology, size, and size distribution of the produced powder are more controllable based on the spraying conditions [86].

Both sol–gel and spray-drying are acceptable for the manufacture of Scandia Doped Pressed cathodes (SDP). In the doping process, ammonium metatungstate (AMT) and nitrides of scandium, barium, calcium, and aluminum are used as the raw materials.

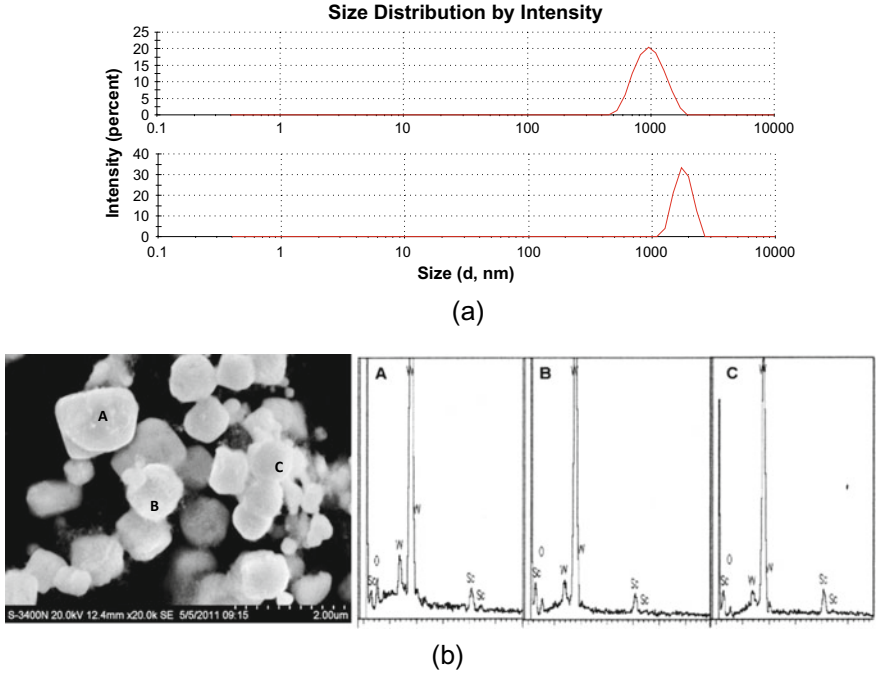

Fig. 3.29 Sizes **a** and elemental distributions **b** of scandia doped tungsten powders by spray-drying doping

3.3.3 Emission Characteristics of SDD Cathodes

3.3.3.1 Emission Evaluation Methods

The ways of emission characterization for dispenser cathodes used in VEDs have been summarized in detail by Shroff [87] in the later 90s and Gilmour [48] recently. Two types of test vehicles have been used: the close-spaced planar diode structure and the electron gun-type structure.

In close-spaced diodes, the zero-field saturated current density which is based on the Schottky equation is normally used to characterize the emission of Ba dispenser cathodes [87].

Owing to the peculiarities of Ba scandate cathodes that their saturation characteristic is not Schottky-like [8], which will be discussed later, it becomes problematic to adopt this approach in emission evaluation. Several alternatives have been proposed to approximate the saturation current density. Maloney [50] suggested the 73% slope method and Manenschijn of Philips used $I_{10\%}$ instead [39]. The latter has been discussed in detail in Sect. 3.2 of this chapter and also used for the emission evaluation of LAD scandate cathodes.

As cathode emission is required to maintain Space Charge Limited (SCL) when working in most VEDs [48], determination of SCL emission region becomes important. From the relation between current and voltage in a parallel-plane diode configuration, SCL region can be found according to the Child-Langmuir law by plotting current density as a function of voltage in log J-log U format. The plot is nearly a straight line for space charge limited operation. A critical SCL current density is then defined as the point where the deviation from the linear part of the tested log J-log U plots becomes noticeable. Though the theoretical slope of the linear part in this type of plots should be 1.5 according to the Child law, the slopes are actually affected by many factors in experiments, such as the differences between the structures of real test vehicles and the ideal parallel-plane diode, the characters of the tested cathodes themselves, and so on. It has been found that the slopes range from 1.33–1.46 for Ba scandate cathodes [9, 10, 39, 88] at operating temperatures in a diode configuration. Under comparable test conditions, the slope will reflect the emission uniformity to a certain extent.

This critical SCL current density provides a good reference for VEDs application and is adopted for the evaluation of SDD cathodes in most cases.

It should be noticed that the critical SCL current density is lower than the "saturated" current density determined by the $I_{10\%}$ for the same emission level.

Apart from testing in a diode, emission of SDD cathode is also characterized in a Pierce gun structure where a proper electrode arrangement leads to a parallel electron flow passing though the cathode–anode space. The Child-Langmuir law can be written as $I = \mathrm{P}\, U^{3/2,}$ where $I = J\mathrm{A}_{\mathrm{cath}}$ with $\mathrm{A}_{\mathrm{cath}}$ being the cathode surface area and P is known as perveance [48] (I is the emission current and U is the voltage applied between cathode and anode measured in Volt). Since the perveance is a function of geometry only, it can be designed and actualized by the electrode geometric structures. At a designed perveance, the current which meets the above law will be in the full space charge regime.

Another method, which is widely used for evaluation of Ba dispenser cathodes, is the well-known roll-off curve (or activity plot) and its normalized version—Miram curve [89]. For a certain current density, the knee temperature from SCL to Temperature Limited (TL) regions in a roll-off or Miram curve and the sharpness of the knee reflects the emission capability and emission uniformity of the cathode, respectively: the lower the knee temperature the higher the emission capability; the sharper the knee the better the emission uniformity. Among the different ways in determining the knee temperature, the intersection of linear extrapolation of the TL and SCL lines is applied.

By superposition of Miram curve against a family of normalized theoretical temperature-limited emission current curves based on Richardson–Dushman equation that have been constructed over a range of electron work function values, the Practical Work Function Distribution (PWFD) analysis method was derived [89]. Both roll-off curve and PWFD plot have been utilized as a useful tool to make emission comparison for different types of cathodes and to diagnose the characteristics of the cathodes in real applications [90]. They are applied in SDD cathode study for emission, work function evaluation, and for fundamental research.

The traditional Richardson plot is used for the estimation of the Richardson work function.

The tested data are treated and analyzed by a dedicatedly developed software.

The cathode temperatures described below are measured by an intensity comparison pyrometer with a minimum target diameter of 0.1 mm at the sleeves near the top of the cathode pellets through a quartz glass viewing window. Molybdenum brightness temperatures (°C_b) are normally utilized in emission characteristics expression. The brightness temperatures are also converted into true temperatures (°C or K), where an effective wavelength of 0.65 μm and an emissivity of 0.4 for Mo are adopted, in the determination of work functions, evaporation rates, and so on. In this conversion, a brightness temperature of 950 °C_b is related to a true temperature of 1015 °C or 1288 K, and 850 °C_b for 905 °C or 1178 K.

3.3.3.2 Cathode Emission Characteristics

(a) Cathode Activation

Cathode activation is an essential procedure for most of the thermionic cathodes. For Ba dispenser cathode, the activation is normally completed at 1200–1250 °C_b in less than one hour, because a forced diffusion of barium at 1160 °C is necessary for starting full and patchless emission by continuous barium dispensation until the entire surface is covered by barium layer at 1240 °C [91]. Unlike the Ba dispenser cathode, a relatively long time at a lower temperature of 1150 °C_b is necessary to activate Ba scandate cathodes properly. This fact has been reported for various types of Ba scandate cathodes [16, 19] as well as for SDD cathode. For the latter, the emission continuously increases with the activation time up to 2 h or longer related to different preparation processes and W grain sizes. The reason for that will be discussed in the following sections.

(b) Emission Capability

Emission capability of SDD cathode is evaluated mainly by the critical SCL current density, and tested in either parallel-plane diode configuration or Pierce-type electron gun structure.

In close-spaced diodes, cathodes mostly in diameters (D) of 2–3 mm are tested in a dynamic UHV system with a water-cooled copper anode. The distance (d) between anode and cathode is adjustable and set at about 0.3–0.4 mm, within the range of d/D = 0.1–0.2 [87], to minimize the effect of edge emission. Pulsed emission was normally measured with pulses of 5–10 μs in width and 50–100 Hz repetition frequency in an automatically graduated-raising manner.

Critical SCL current densities of over 30 A/cm^2 at 850 °C_b and over 100 A/cm^2 at 950 °C_b, Mo-brightness temperature, have been routinely measured for either SDI or SDP cathodes since their development [10, 43, 88]. This emission capability remains unchanged when operating at high duty cycles and long pulse widths. As an example, a set of experimental Log J-Log U plots measured for a cathode 2 mm

in diameter is shown in Fig. 3.30a. The relative waveforms of current and voltage with pulse widths of 50 μs–250 μs, at a same repetition frequency of 100 Hz, are displayed in Fig. 3.30b. While SCL current density of over 120 A/cm^2 is achieved at 950 °C$_b$, a total current of 3.1 A which corresponds to a current density of 100 A/cm^2 is identical for each duty cycle, indicating that the SDD cathodes are able to provide high current densities at a variety of pulse conditions.

From the I-U characteristics above, the well-known unsaturated emission behavior or abnormal Schottky effect of Ba scandate cathodes are clearly displayed, especially

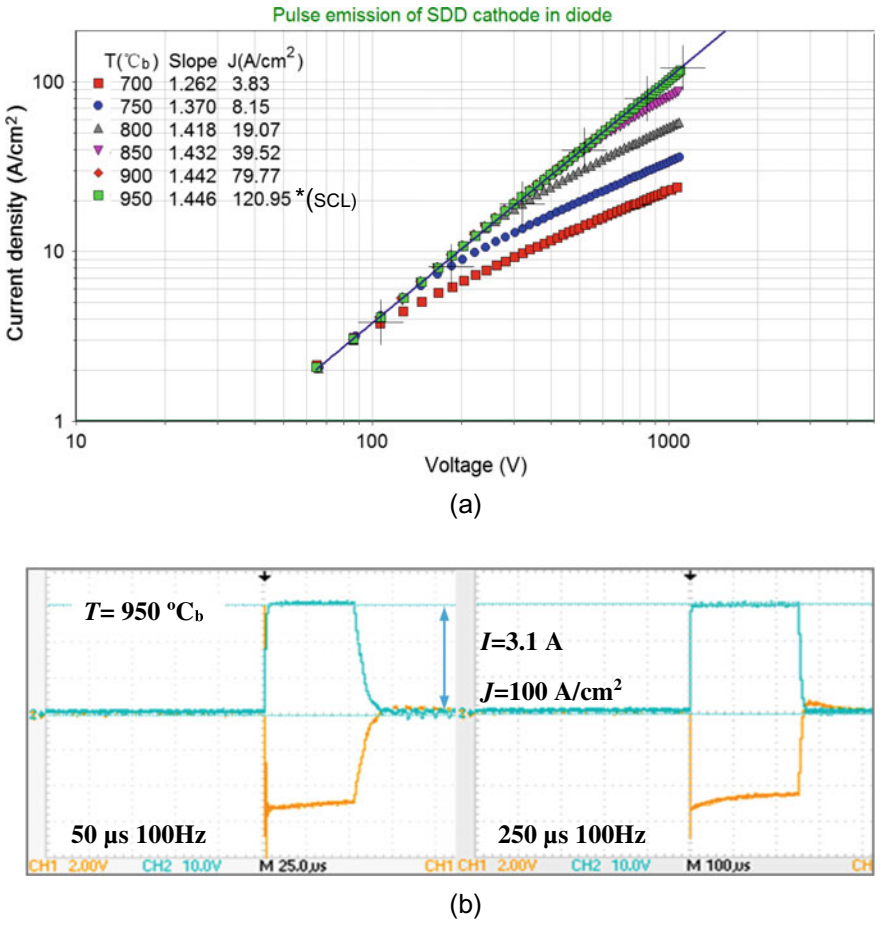

Fig. 3.30 Pulsed emission characteristics of SDD cathode tested in close-spaced diode. **a** Log *J*-Log *U* plots at different operating temperatures. Critical current densities and slopes of the linear part of the plots are shown on left corner. **b** Pulsed waveforms of I and U with pulse widths of 50 μs (left) and 250 μs (right) at a repetition frequency of 100 Hz, tested from an SDD cathode of 2 mm in diameter at cathode temperature of 950 °C$_b$. A total current of 3.1 A corresponds to 100 A/cm^2 current density

at high temperatures. This feature brings about problems in the determination of zero field emission J_0 by extrapolating a plot of ln(J) versus $\sqrt{E}$ to E = 0 at normal operating temperatures, causing inaccuracy in the Richardson work function and Richardson constant. This problem may be mitigated by only taking J_0 at relatively low temperatures. In this manner, the Richardson work function ϕ_R of around (1.13–1.15) eV and Richardson constant A_R of (2–4) $A{\cdot}cm^{-2}\cdot K^{-1}$ have been estimated and denoted in Fig. 3.31 as an example for reference. The temperature coefficient α introduced in [87], then, is about 3×10^{-4} $eV{\cdot}K^{-1}$.

In DC operating mode, the electron cooling effect begins to emerge, leading to a drop in cathode temperature. This effect becomes obvious when high DC current is emitted.

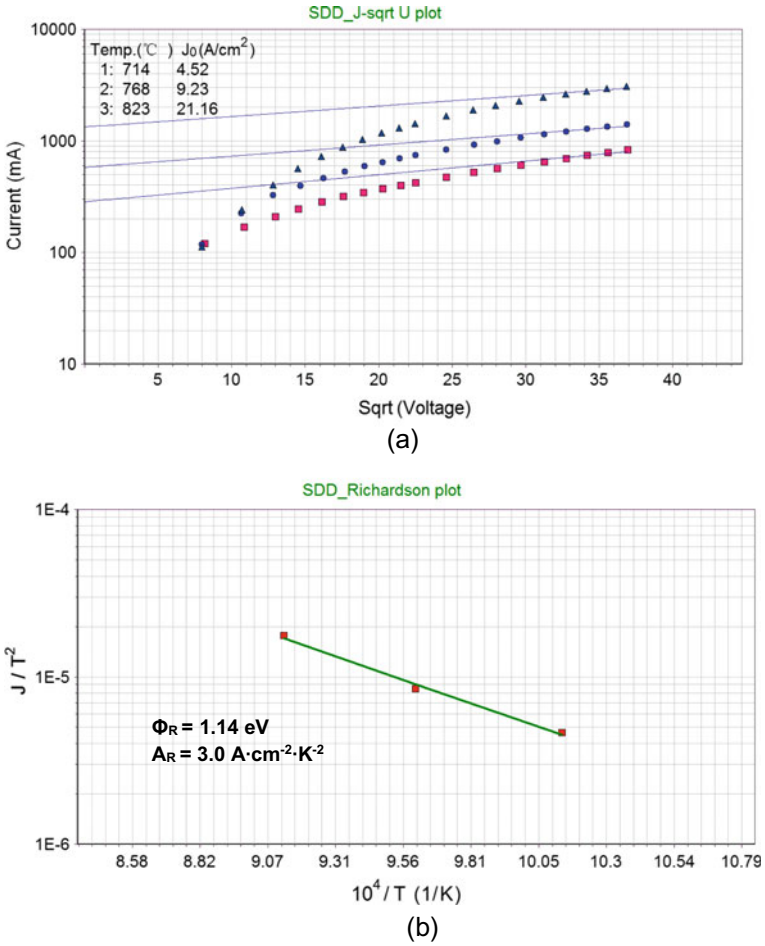

Fig. 3.31 **a** Zero field emission taken from low operating temperatures. **b** Richardson plot derived by the data from (**a**)

In order to evaluate the DC emission capability, the temperature drop needs to be corrected by heating power compensation [92]. DC characters measured at an initial temperature of 850 °C_b, with and without temperature compensation, are shown in Fig. 3.32a.

For cathodes with a reduced diameter of 1 mm in the diode configuration with d_{a-c} of 0.15–0.2 mm, DC current densities of 60–70 A/cm^2 were repeatedly measured at 950 °C_b after compensation for electron cooling. A group of Log *J*-Log *U* plots is shown in Fig. 3.32b together with a pulsed emission plot measured at 950 °C_b for comparison. The DC emission coincides with the pulsed emission until its measurement limitation is imposed by the overloading of the anode.

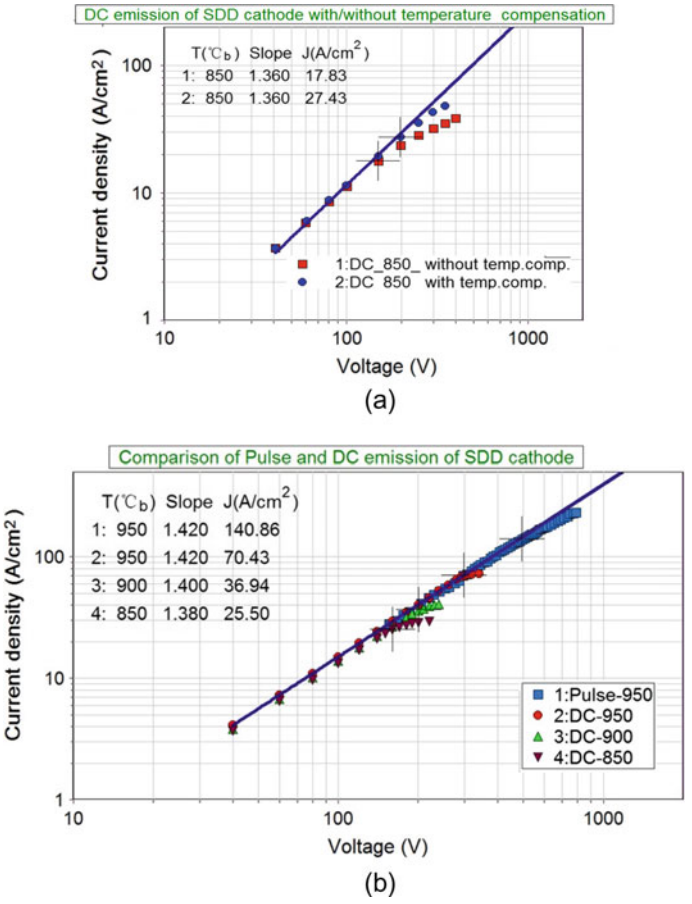

Fig. 3.32 DC emission of SDD cathode. **a** DC emission with and without temperature compensation, indicating the effect of electron cooling. **b** Comparison of pulse and DC emission with temperature compensation. The graph is based on re-evaluation of data presented in [92]

SDI cathodes have been further tested in Pierce-type electron gun tubes. This test structure allows for high current loadings without the drawbacks happening in diodes, such as cathode edge emission, barium or contaminants backscattering from the anode, and plasma formation. Furthermore, the test results are a useful reference for cathodes application in real VEDs.

A schematic diagram of a Pierce electron gun consisting of an anode and two depressed collectors with its basic electron trajectory are shown in Fig. 3.33a. The cathode disk is with a planar surface in diameter of 2 mm. The designed perveance of the electron gun is 0.6 μp [93]. Hence, a total current of 3.14 A or a current

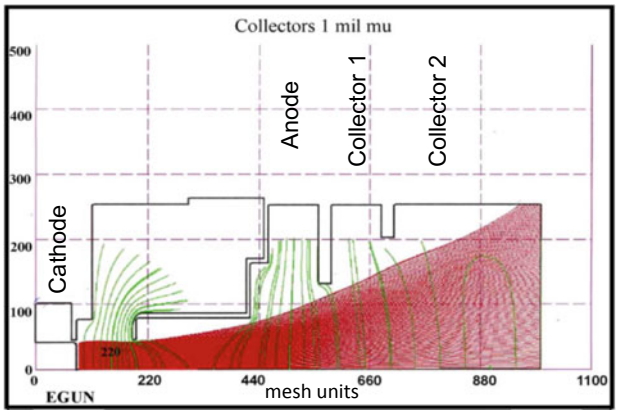

(a)

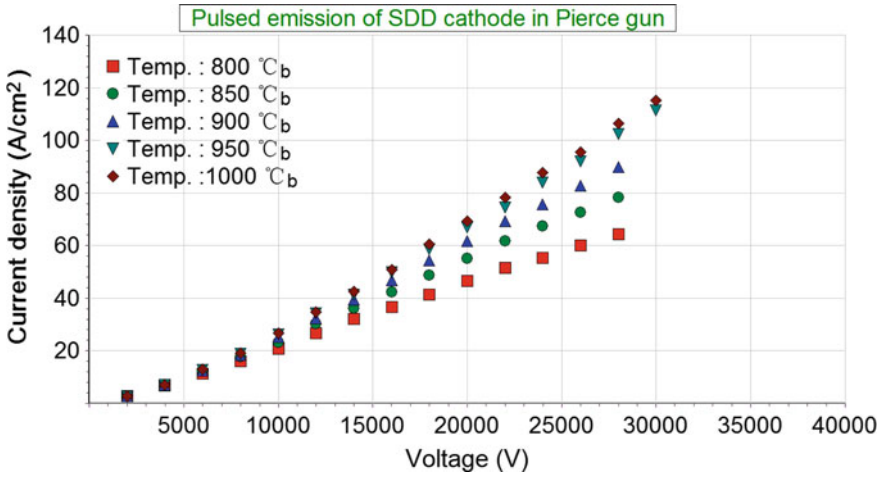

(b)

Fig. 3.33 **a** Schematic diagram of a Pierce electron gun with its basic electron trajectory. **b** Tested pulsed emission of an SDD cathode in the Pierce gun

density of 100 A/cm^2 should be obtained at an anode voltage of 30 kV if the cathode operates in full space charge limited regime. The J-U plots tested in above Pierce electron gun structure, operating in pulse mode with a pulse width of 3 μs and a repetition frequency of 5 Hz, are shown in Fig. 3.33b. At temperatures of 950 °C$_b$ and 1000 °C$_b$, the two J-U plots are almost overlapping and nearly identical current densities of 110 A/cm^2 and 115 A/cm^2, a bit higher than the expected value of 100 A/cm^2, are reached at the nominal anode voltage of 30 kV. Given the possibly of slight errors in practical perveance, the test results distinctly demonstrate that a full space charge limited current density of 100 A/cm^2 has been reliably achieved at brightness temperature 950 °C$_b$ or true temperature 1015 °C.

As pointed out by Gilmour [48], there is a practical limit to the current density that can be drawn from a cathode when applying in linear beam VEDs, regardless of its emission capability. This upper limit results from the electrical breakdown between cathode or focus electrode and anode in vacuum and appears to be about 100 A/cm^2 for DC currents.

Well-conducting cathodes with smooth surfaces will be a benefit for reducing the risk of local field enhancement. Hence, SDD cathodes seem most suitable for these applications.

(c) Emission Uniformity

Emission nonuniformity is one of the major problems for Ba scandate cathodes. An evidence of the nonuniformity is that blurry knees on roll-off or Miram curves together with a broad PWFD appear in the early Ba scandate cathodes. Figure 3.34a shows a Miram curve and the related PWFD plot taken from an impregnated scandate cathode [48, 94]. It takes a wide range of over 300 °C, from ~750 °C to ~1100 °C, for the emission to transit from TL to SCL region. The work function of f(ϕ) $\geq$ 0.1 spreads over 0.34 eV, from 1.52 eV to 1.86 eV. This is an indication of the emission nonuniformity of the early Ba scandate cathode. With the recently developed doping technologies described above, the emission uniformity has been improved greatly. Sharp knees have been repeatedly observed on the SDD cathodes by L–L doping processes [93, 95] after a full activation. A normalized roll-off curve (Miram curve) measured in a Pierce gun structure for initial current densities of 48 A/cm^2 is exhibited in Fig. 3.34b. While the knee temperature is as low as about 880 °C true temperature, much narrower transition ranges of about 150 °C with flat SCL region appear in the curve. The peak work function is about 1.41 eV with a PWFD of only 0.14 eV, from 1.40 eV to 1.54 eV above f(ϕ) of 0.1.

It was once supposed that a Ba scandate cathode provides poor beam quality when used in an electron gun due to emission nonuniformity [8]. To inspect the actual situation, an SDD cathode with a cylindrical diameter of 2.88 mm and an emitting surface curvature radius of 3.26 mm was tested in an electron gun with perveance of 1.0–1.1 μp. After an SCL current density of 80 A/cm^2 was reached at a rated voltage of 30 kV [93], beam profiles were measured by a 3D movement apparatus at positions of 2–8 mm from the exit of the anode aperture along the beam

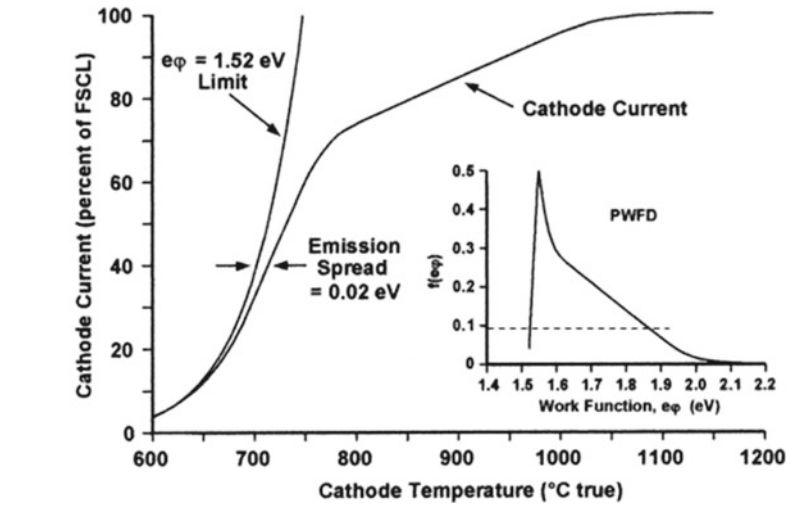

(a)

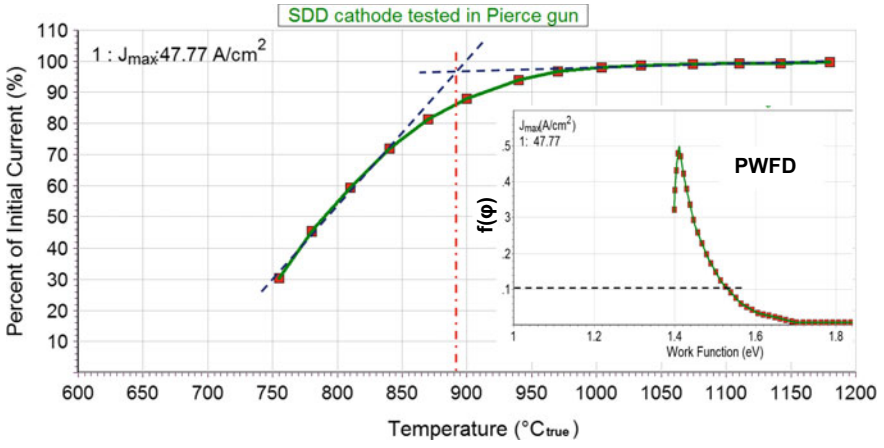

(b)

Fig. 3.34 Miram curves and PWFD plots of **a** an early scandate cathode. The graph is based on Fig. 5.33, [48]. **b** An SDD cathode

axis. Current distributions at related positions were also simulated by the EGUN 2 code. When an anode voltage of 10 kV is applied and at the position of 2 mm beyond the anode exit, indicated in Fig. 3.35a, the simulated current distribution is well coincident with both the tested cross-section of the electron beam and the 2D current distribution profile measured from the above electron gun at the same position, illustrated in upper, middle, and lower of Fig. 3.35b, respectively.

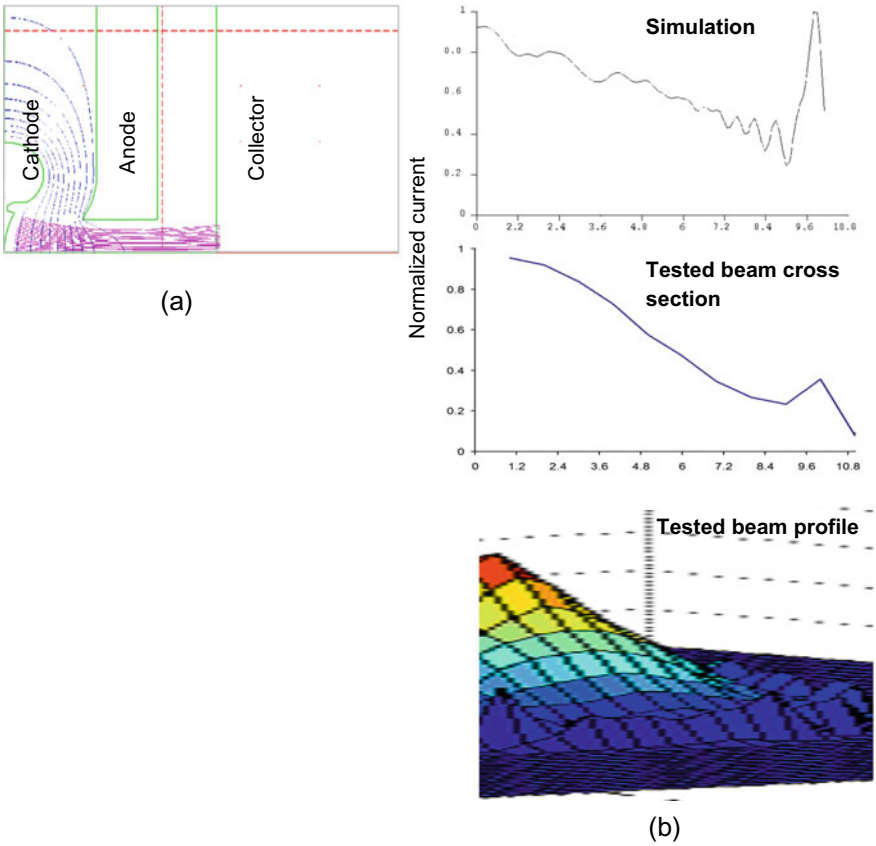

Fig. 3.35 Beam analysis in an electron gun with SDD cathode. **a** Simulated electron trajectory when collector sets at 2 mm beyond the anode exit. **b** Comparison of the simulated current distribution at collecting position (upper) with the tested cross-section of the electron beam (middle) and beam profile (lower) at the same condition. The graph is based on Fig. 8 of [93] with additional data

Since the simulation is based on uniform emission, the results prove that beam quality in an electron gun with this kind of cathode is acceptable.

The above investigations clarified that the nonuniform emission in early Ba scandate cathodes can be distinctly ameliorated in SDD cathodes with the nanosized-scandia doping technologies, optimal control of tungsten grain sizes, and proper activation procedures.

Deriving from Miram curves of SDD cathodes, peak work functions of about 1.40–1.45 eV can be established.

With the improvement for Ba Scandate cathode, the well-known "Quality of Thermionic Cathodes 'Best of Class' PWFD" [89, 96] is updated and given in Fig. 3.36.

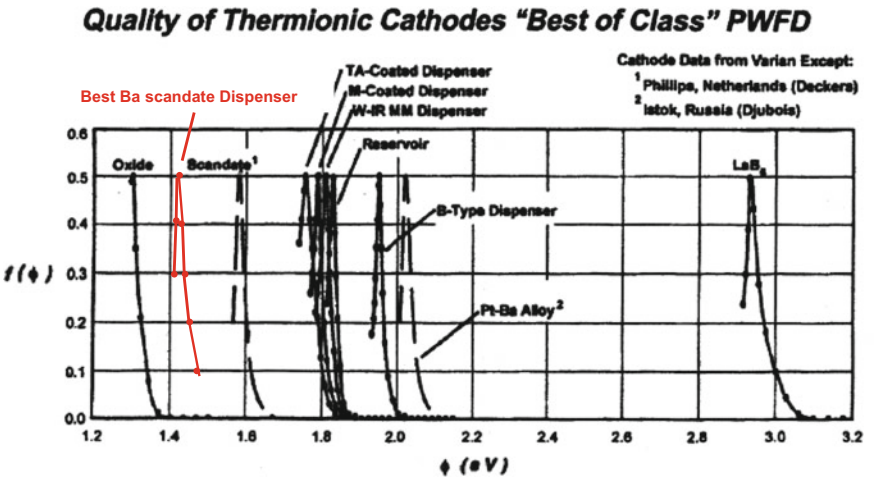

Fig. 3.36 Updated thermionic cathodes "Best of Class" PWFD, see [89, 96]

(d) Life Evaluation

Lifetimes for SDD cathodes with different doping procedures have been evaluated in both diode and Pierce-type electron gun configurations at normal operating temperatures.

In a diode with a water-cooled copper anode, a sol–gel doping SDD cathode had been operated with a continuous DC load of 2 A/cm^2 at 950 °C$_b$ while pulsed critical SCL current density at 850 °C$_b$ was measured periodically to monitor the change of the emission capability with time. The critical current density, shown in Fig. 3.37a, increased in the first two thousand hours of life and then remained stable for more than 10,000 h [10]. The stability of the current density at a critical level, at least higher than 35 A/cm^2 at 850 °C$_b$ or 1178 K, reveals that the high emission capability of SDD cathode can be well maintained for more than ten thousand hours.

With DC load of 30–40 A/cm^2, which is the highest DC load on life test for all kinds of thermionic cathodes, the SDD cathode has been working smoothly at 970 °C$_b$ for up to 5000 h, as shown in Fig. 3.37b [92]. Both the DC current load at fixed anode voltage and the critical SCL DC current densities have improved during the first ~1000 h.

In summary, by using doping processes to mix well-distributed nanosized scandium oxide into tungsten powder of proper sizes, the scandia doped dispenser cathodes provide uniform emission with critical space charge limited current density of greater than 100 A/cm^2 at 950 °C$_b$, Mo-brightness temperature, or 1015 °C true temperature. There is little difference between pulsed and DC emission. Lifetimes of $\geq$10,000 h can be achieved.

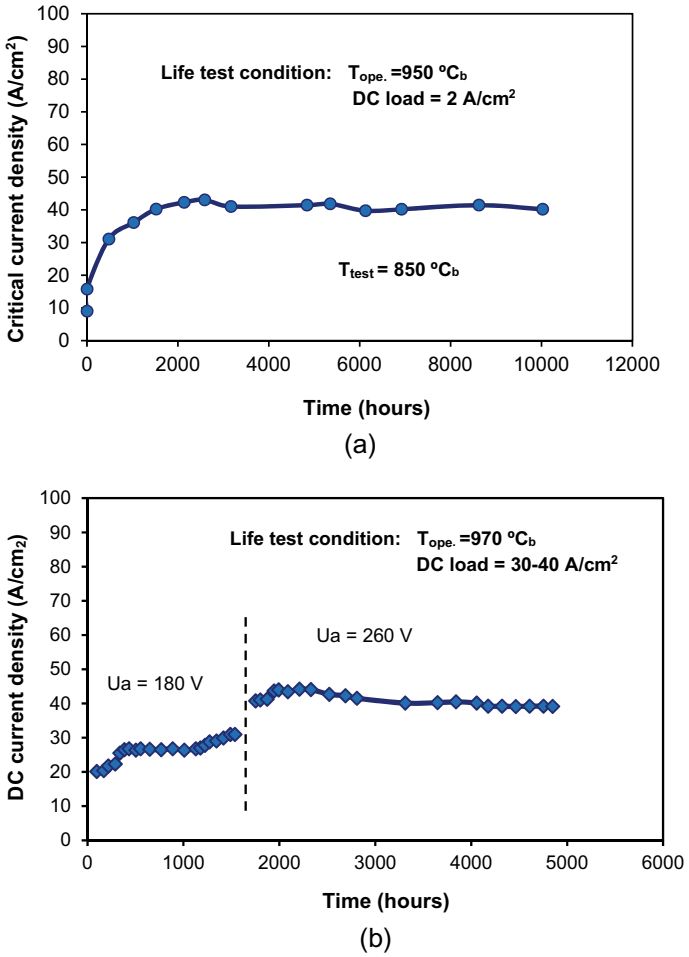

Fig. 3.37 Emission performance of SDD cathodes during life test. **a** Change of critical pulse SCL emission at 850 °C_b, checked intermittently during life test carried out at 950 °C_b with a continuous DC load of 2 A/cm^2. **b** Change of DC emission during life test at 970 °C_b with DC loads of 30–40 A/cm^2

3.3.4 Generation of Miniature Electron Beams

The advanced VEDs like millimeter wave and Terahertz vacuum electron devices demand high cathode emission capability because the required beam current density is proportional to the operating frequency squared. With the need for miniaturization, a variety of very serious challenges are posed for cathode performance. The challenges are to confine the electron beam to an increasingly small cross-section and generate and realize in the interaction space the extremely high current densities [3, 97].

Miniature electron beams can be obtained from normal cylindrical cathodes by means of specially designed compression systems [98]. However, direct generation of the miniature beams from cathodes has the advantages of simplifying the focus optics which makes the devices more compact and facilitates the formation of high-quality, high-aspect-ratio electron beams. To form the required beams, the cathodes itself must be able to provide emission current densities in the order of 100 A/cm^2 at reasonable operating temperatures. The SDD cathode described above, thus, becomes one of the most promising candidates for this application.

Before the 3D print technology could be applied to thermionic cathode manufacture, one of the approaches to obtain a miniature beam from a cathode is to cover the cylindrical cathode with an anti-emission mask, leaving a defined opening for electron emission. In this way, standard construction methods can be employed without much modification for fabricating the underlying thermionic cathode. The anti-emission mask can be a solid metal mask made from refractory metals or a thin film of emission-suppressing materials such as Ti, Hf, and Zr. An opening in the required shape and dimension is constructed on the mask by micromachining technologies [88].

A rectangular sheet beam realized by a masked cathode assembly and measured in an emission distribution testing system is shown in Fig. 3.38a. The beam has an aspect ratio of 6:1 and a current density of over 50 A/cm^2 at 950 °C$_b$ [99]. Design of a sheet-beam electron gun schematized in Fig. 3.38b is based on the above cathode. It uses one-dimensional three-fold beam cross-sectional area compression to meet the specific requirement of a beam to be formed of height 30 μm and width 600 μm at the beam–waist position with over 100 A/cm^2 uniform current density and 0.068 π-mm-mrad emittance. The electron gun is typically for 0.5 THz devices [100].

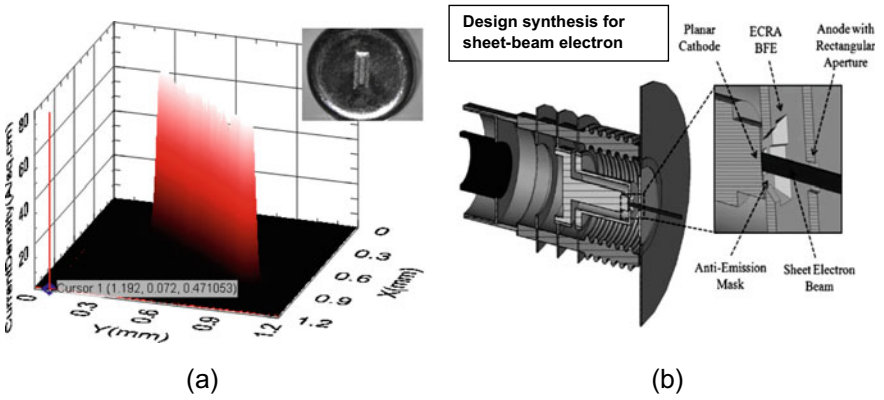

Fig. 3.38 High current density sheet-beam generated directly from an SDD cathode. **a** Beam profile of 600 μm × 100 μm with over 50 A/cm^2 SCL current density. Photo of cathode assembly is shown in the inset. **b** Schematic of half-sectioned sheet-beam electron gun. The figure is based on Fig. 1 of [100]

3.3.5 Fundamentals of Ba Scandate Dispenser Cathodes

3.3.5.1 A Brief Review of Previous Studies on Ba Scandate Dispenser Cathode Fundamentals

R. E. Thomas and his coworkers stated incisively in the later 90s [8] that "with the advent of modern surface analytical capabilities that enable one to better understand the physics and chemistry of emitter surfaces significant improvements have been made in thermionic electron sources". Based mainly on surface studies during the 70s–80s, the fundamentals of Ba dispenser cathodes have been investigated intensively and a model of Ba–O dipole monolayer on W has been deduced and widely accepted [101–103]. However, the emission mechanism of the Ba scandate cathodes is still controversial and study results tend to differ from one another.

Before a further discussion on the matter is made, the proposed emission models for Ba scandate cathode are reviewed in brief.

The different types of Ba scandate cathodes introduced in part Sect. 3.1 of this chapter can eventually be divided into three groups by the ways of adding scandium oxide: adding into the tungsten matrix or powder [10, 14, 16], adding into the impregnant [13, 79, 80], and coating on a Ba dispenser cathode as thin films [9, 17, 21, 22, 35]. Although these types of Ba scandate cathodes have different structures, they feature similar emission characteristics, i.e., (i) distinctly higher emission capability than that of Ba dispenser cathodes, though in varying degrees; (ii) obvious non-saturated emission character, though the physical distribution uniformity of scandium oxide has been increased from type to type through persistent improvements on processing technologies [95]. Therefore, it is believed that the emission mechanism for various types of Ba scandate cathode should be basically identical.

It must be pointed out that, in most of these Ba scandate cathodes, the traditional tungsten powders or matrices which are composed of Ba dispenser cathodes and even Ba dispenser cathodes themselves are constituted as part of the Ba scandate cathodes. The facts above argue strongly on a proposal presented by some researchers [25], in which it is suggested that particular crystallographic facets, like {112} facets, of the W grains may be critical to the enhanced emission performance of Ba scandate cathodes. Though facets of tungsten grains do impact the emission of thermionic cathodes, it is unlikely that this is the reason for emission enhancement of Ba scandate cathodes over Ba dispenser cathodes.

Several emission models have been suggested in the history of the development of Ba scandate cathode; they are redisplayed in Fig. 3.39a–c: a BaO layer covering on bulk Sc_2O_3 assumed by Forman [104], a Ba–Sc–O monolayer by Yamamoto [105], and a semiconductor layer by Raju and Maloney [50]. Among them special attention has been fixed on the latter two. One is the Ba–Sc–O monolayer model, which was first proposed by S. Yamamoto, based on the observation that a surface layer composed of Ba, Sc, and O on a mixed matrix Ba scandate cathode which is easily removed by Ar ion sputtering [14]. Lately, when Yamamoto investigated a top-layer Ba scandate cathode sputter-coated with a W + Sc_2O_3 thin film to improve

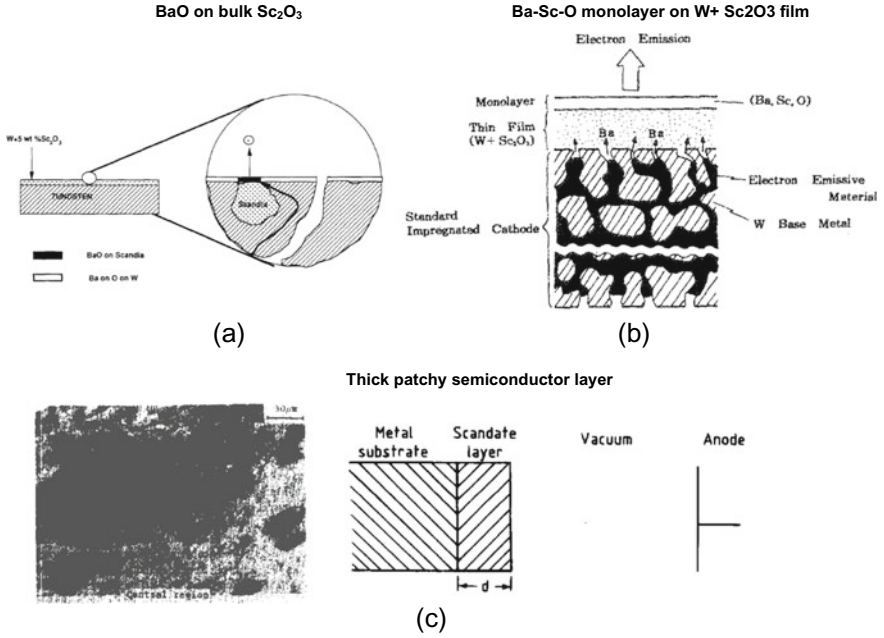

Fig. 3.39 Proposed emission models for Ba scandate cathode, based on **a** BaO on bulk Sc_2O_3, Fig. 16 of [104]; **b** Ba–Sc–O monolayer on W-Sc_2O_3 film, Fig. 1 of [105]; **c** Thick patchy semiconductor layer: Left: SEM image of the layer, Fig. 12a of [50]; Right: proposed sandate cathode in diode, Fig. 5a of [50]

the mixed matrix one, he pointed that electron emission enhancement is achieved when a surface layer consisting of Ba, Sc, and O is formed with uniform thicknesses of a monolayer on top of the W-Sc_2O_3 coating film of 50–400 nm, see Fig. 3.39b, and the work function reaches its minimum when an ordered phase of Ba, Sc, and O is formed out of a disordered phase which contains extra amounts of Ba and Sc [105]. It should be noted that the suggested monolayer above, in fact, is located on a thick Sc-containing film but not on the tungsten substrate as the conventional monolayer of Ba-O dipole on W for Ba dispenser cathode. No more details about the layer were reported. The other model is the semiconductor model presented by Raju and Maloney [50]. In their model, the cathode surface is composed of a substantially thick patchy semiconductor layer of some scandium compounds like scandium tungstate, shown in Fig. 3.39c.

Shih and Yater highlighted in their study [106] that the thick layer of semiconducting material required by Raju and Maloney's model is possible to form from the simultaneous presence of BaO, Sc_2O_3 on W. In their study, Temperature-Programmed Desorption (TPD) and Auger electron spectroscopy (AES) were used to characterize Ba and BaO on a W substrate and on a Sc_2O_3-coated W substrate to simulate the surface layer of the conventional Ba dispenser cathode and the Ba scandate cathode.

They found that a partial layer of BaO forms on W, which is similar to the Ba-O surface layer that forms on a Ba dispenser cathode. However on the Sc_2O_3-coated W substrate, there are no longer partial surface layers of BaO coverage. Instead, a stable BaO-containing compound forms and continues to accumulate to form a bulk-like layer. In addition, a high heating temperature could cause a tight binding BaO partial layer to form on the coated surface. They suggested that the layer may serve to reduce the electron affinity of the compound formed underneath, causing the Ba scandate cathode to behave like an oxide cathode.

The thick layer or multilayer proposal has been further supported by A. P. Makarov in a simulation study on jointly adsorbed atoms of barium, scandium, and oxygen on the facet (100) of a tungsten crystal [107]. The study discovered that the work function of a monolayer complex Ba–Sc–O consisting of 1 barium monolayer and 0.5 scandium monolayer with an optimal doze of adsorbed oxygen on the surface of the facet (100) W amounts to 2.1 eV, while the complex Ba–Sc–O consisting of 1 Ba monolayer and 1 Sc monolayer even comes to 2.15 eV, both are higher than the work function of 1.9–2.1 eV for Ba-O on W (100) systems. On the other hand, the work function of a multilayer film of jointly adsorbed atoms of Ba, Sc, and O on the facet (100) of tungsten crystal, consisting of 2–3 Ba monolayers and 2–3 Sc monolayers with an optimal doze of adsorbed oxygen when heated at temperature 1400–1500 K and then activated by monolayer of barium atoms, drops down to 1.70–1.75 eV, which is a bit nearer to the work function value of Ba scandate cathodes.

Based upon the above proposals, investigations have been made for understanding the fundamentals of SDD cathodes [95, 108, 109] and are summarized below.

3.3.5.2 Behavior of Surface Active Layer on Nanosized-Scandia Doped Dispenser Cathodes

To characterize the outer surface of the cathode as to explain its electron emission performance, techniques probing the first atomic layers are most adequate.

The behavior of the surface active layer on SDD cathodes has, then, been diagnosed in detail by modern surface analysis techniques, including Auger Electron Spectroscopy (AES) and X-Ray Photoelectron Spectroscopy (XPS). Atomic Force Microscopy (AFM) as a direct surface nanostructure detecting technology has also been used for topography observation.

The importance of in situ analysis has been emphasized since the surface analysis was applied in thermionic cathode research [101–103]. Thus, in situ surface analysis has been carried out during heating, activation, operation, and life test of the SDD cathodes.

(a) Surface Layer Composition

The in situ XPS studies, in which a large or even whole area of the cathode surface can be analyzed by X-ray excitation, have first been used for surface composition diagnosis. Survey spectra taken from the activated cathodes are shown in Fig. 3.40a.

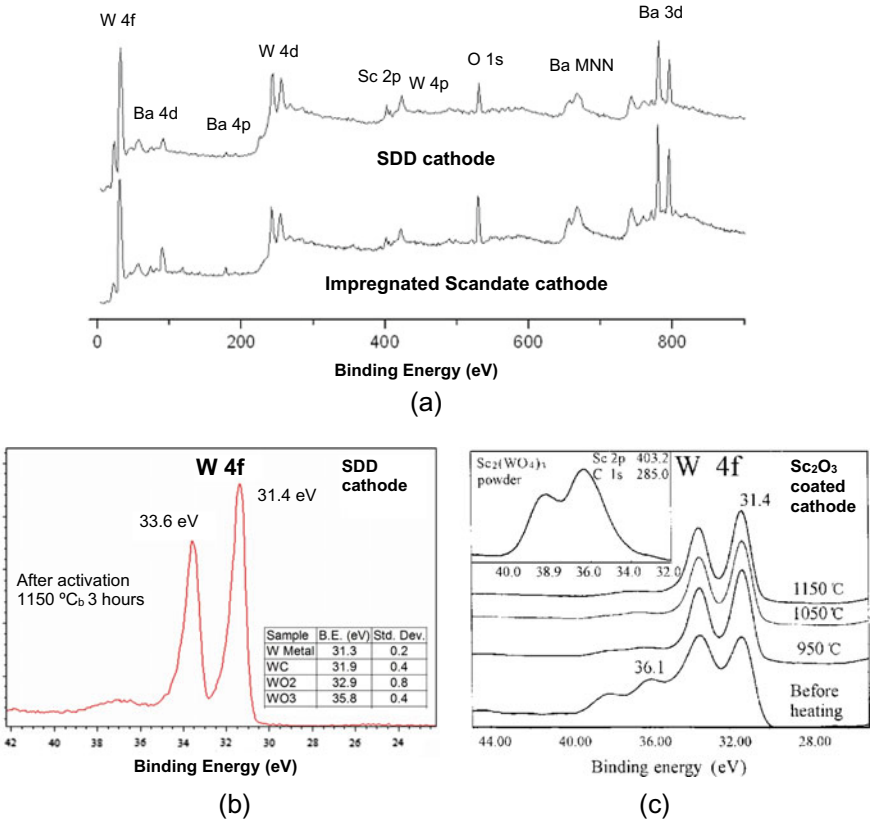

Fig. 3.40 Surface composition of a fully activated Ba scandate cathodes analyzed by in situ XPS analysis. **a** Survey spectra of SDD cathode and impregnated scandate cathode. **b** W4f spectrum of SDD cathode after activation (inset: list of BE of W4f$_{7/2}$). **c** W4f spectra of a Sc_2O_3 coated thin film cathode (insert: W4f of $Sc_2W_3O_{12}$ powder), based on Fig. 6 of [21]

Similar to that of Ba dispenser cathode, Al and Ca disappear from the surface after activation though they are the components of the impregnant [110]. There is no element other than Ba, Sc, O, and W to appear on the surface of a fully activated SDD cathode. This is also true for other Ba scandate cathode like impregnated scandate cathode, though the Sc signal is relatively weaker.

Moreover, it is noticed that the W4f$_{7/2}$ XPS peak is with binding energy (BE) of 31.4 eV for an SDD cathode after activation and it is the same for laser-deposited thin film scandate cathode [21], shown in Fig. 3.40b, c, respectively. This peak position corresponds to metallic W, denoted in the inserted list of Fig. 3.40b and much lower than the BE of a tungstate illustrated in the inset of Fig. 3.40c. The results ruled out the hypotheses that scandium tungstate such as Sc_6WO_{12} [50] or barium scandium tungstate such as $Ba_3Sc_2WO_9$ [77, 78] constitutes the surface layer of Ba scandate cathodes.

(b) Features of the Surface Layer

It is distinctly important to figure out the presentation of the suggested monolayer or the possibly thick layer described in the previous researches on the surface of Ba scandate cathodes.

In the studies of Ba dispenser cathode, the surface model was investigated through synthesizing the surface conditions existing on an impregnated tungsten cathode by depositing barium or oxidized barium on a tungsten surface with depth varied from many monolayers to partial monolayer coverage. In situ Auger analysis and effective work functions measurement were used to compare synthesized surface with the activated impregnated cathode surface [101]. Auger peak-to-peak height (APPH) ratios of surface-covering constituents to the substrate are used for surface layer thickness and coverage estimation. Based upon the above investigations, it reached a consensus that for a conventional Ba impregnated tungsten cathode there exists a monolayer or partial monolayer of barium and oxygen on a tungsten surface [101, 103, 111]. Consequently, if the monolayer assumption is suitable for Ba scandate cathodes, then similar surface features must appear. Table 3.5 summarizes the APPH ratios of surface active elements Ba, O (and Sc) to substrate W, which are taken from AES spectra of modeling systems and real cathodes. In the table, Auger peaks of Ba (584 eV), O (512 eV), Sc (334 eV), and W (179 eV) are chosen for analysis as they have similar escape depths.

Besides, Auger spectra taken from the synthesized barium and oxidized barium monolayer on a tungsten surface, an activated impregnated tungsten cathode, and an SDD cathode are compared in Fig. 3.41a, upper, middle, and lower.

From the data in the table and the figures, the APPH ratios of Ba/W of about 0.2–0.4 and O/W of 0.5–1.0 are for the Ba impregnated cathodes, agreeing with the data for monolayer. In contrast, the Auger spectra taken from the activated SDD cathodes exhibit a completely different fashion. The APPH ratio of Ba to W goes up to 1.6, almost five times higher than that of Ba dispenser cathodes. Similarly, the

Table 3.5 Auger Peak-to-Peak Height ratios for different surface configurations containing Ba, O and in some cases Sc

Surface configuration	APPH ratios			References
	Ba/W	O/W	Sc/W	
One monolayer of oxidized Ba	0.37	1.3		Figure 5 in [101]
Activated impregnated Ba tungsten cathode	0.21	0.5		Figure 2 in [112]
S-type cathode at lowest Φ	0.30	1.02		Figure 31 in [87]
Monolayer of Sc on W (100) after oxidation		1.14	0.85	Figure 6 in [113]
Ba-W dispenser cathode after activation	0.31	0.72		Under the same test condition as for SDD cathode
SDD cathode after full activation	1.6	5.2	3.3	Average of in situ analyses

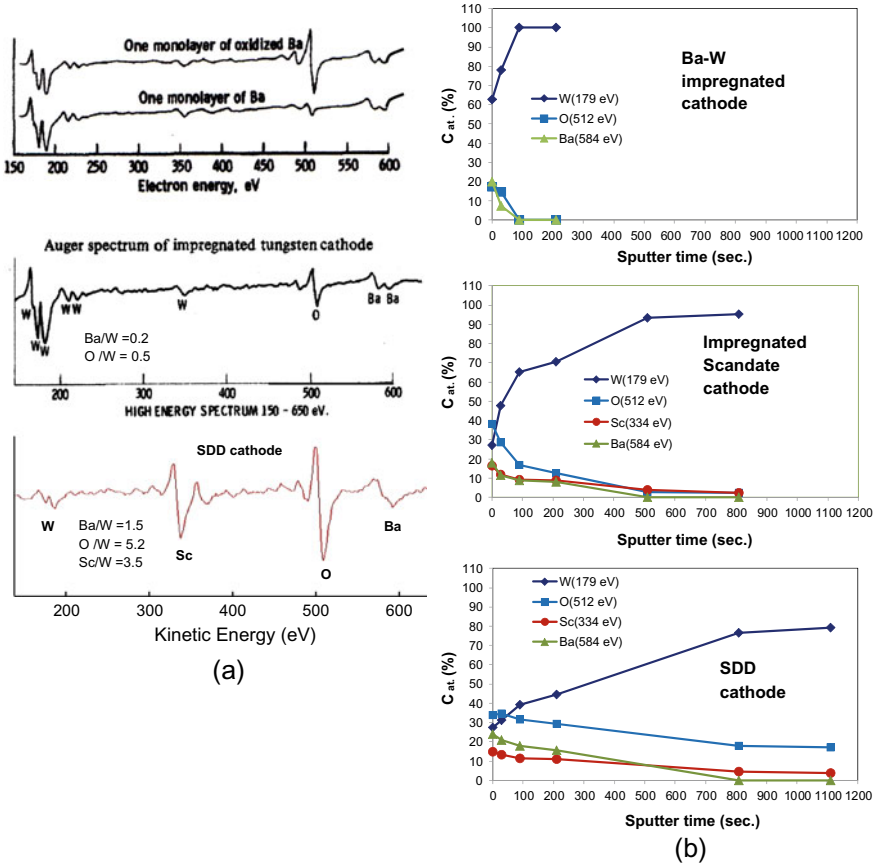

Fig. 3.41 In situ AES analysis on surface layers of thermionic cathodes. **a** Auger spectra from simulated surface layers and activated cathodes tested at operation states. Upper: Auger spectra of barium and oxidized barium monolayer on tungsten surface, based on Fig. 5 of [101]; Middle: Auger spectrum of an activated impregnated tungsten cathode, based on Fig. 2 of [112]; Bottom: Auger spectrum of an activated SDD cathode. **b** AES depth profiles of cathodes after activation, taken at room temperature. Sputtering condition: Ar^+ ions of 4 keV, 300 nA. Upper: Ba-W impregnated dispenser cathode; Middle: Impregnated scandate cathode; Bottom: SDD cathode

Sc/W of SDD cathode is about 3–4 times of that from a monolayer of oxidized Sc [113], while O/W goes even higher.

The data imply that the layer of Ba, Sc, and O on the surface of SDD cathode is far beyond a monolayer.

The above conclusion has been further verified through the in situ Auger depth profiles investigation, in a VG MICROLAB MK II surface analysis instrument, by comparing Ba-W impregnated dispenser cathode, impregnated scandate cathode, and SDD cathode. The profiles are shown in Fig. 3.41b, upper, middle, and bottom,

respectively. All the cathodes were fully activated in situ, then sputtered step by step by Ar^+ ions of 4 keV, 300 nA and analyzed at room temperature in an area of 100 μm × 100 μm to get average signal of the elements [83]. By referring to VG's technical documents on estimating sputter rates for VG ion gun, a sputter rate of about 6–8 nm/min has been estimated.

While stoichiometric Ba and O were removed simultaneously in around one minute for Ba-W impregnated cathode, a high concentration of Ba with O and Sc is slowly reduced in a period of several times longer for SDD cathode than the situation for Ba-W impregnated cathode. Moreover, O and Sc stay with little change at low levels to the end of the test.

The observations strongly suggest that Ba and O are bound with Sc, tighter than that with W, to form a Ba–Sc–O layer much thicker than a monolayer on Ba-W impregnated cathode.

A similar situation was also found for other Ba scandate cathode, such as the impregnated scandate cathode as shown in the middle of Fig. 3.41b. A Ba–Sc–O layer can be observed there, but it is thinner and with less Ba compared to that on SDD cathode.

On the other hand, the surface feature of SDD cathode significantly differs from a thick patchy layer proposed by Raju and Maloney (Fig. 3.39c).

The Ba, Sc, and O actually distribute uniformly over a single W grain and on different W grains. This has been confirmed by repeatable observation results during a decade of SDD cathode development [95, 114]. As an example, a set of AES spectra measured by an AES system (PHI700, ULVAC-PHI) with spatial resolution of 40 nm at nine different points on surface of an activated SDD cathode is presented in Fig. 3.42a. It clearly indicates the nearly identical surface composition at each point.

Furthermore, it is also demonstrated that the Ba, Sc, and O are evenly distributed along certain depth on W grains at different sites. As checked by the same AES instrument above and shown in Fig. 3.42b, where the surface active elements and substrate W versus sputter time at three points marked on the SEM image are displayed, the Ba, Sc, and O are distributed in similar depths over the whole substrate of W grain. By referring to the sputter rates calibrated with thermally oxidized SiO_2/Si, the distribution depths of up to tens of nanometers are reckoned.

The special surface feature of SDD cathode should bring visible spectacle on its topography. The obvious disparity of surface topographies between Ba dispenser cathode and SDD cathode has been observed by Atomic Force Microscopy (AFM), illustrated in Fig. 3.43. Both Ba-W impregnated cathode and SDD cathode used for diagnosis were fully activated and aged to enable stable surface structures to be established. As expected, the phase image of Ba-W cathode on the left side of Fig. 3.43a exhibits a smoothly metal-like surface. On the other hand, significantly different from the metal-like surface, a layer-like structure appears on W grain of the activated SDD cathode, shown in the middle of Fig. 3.43a. Since this structure does not present on the surface of the scandia doped matrix, as indicated on the right

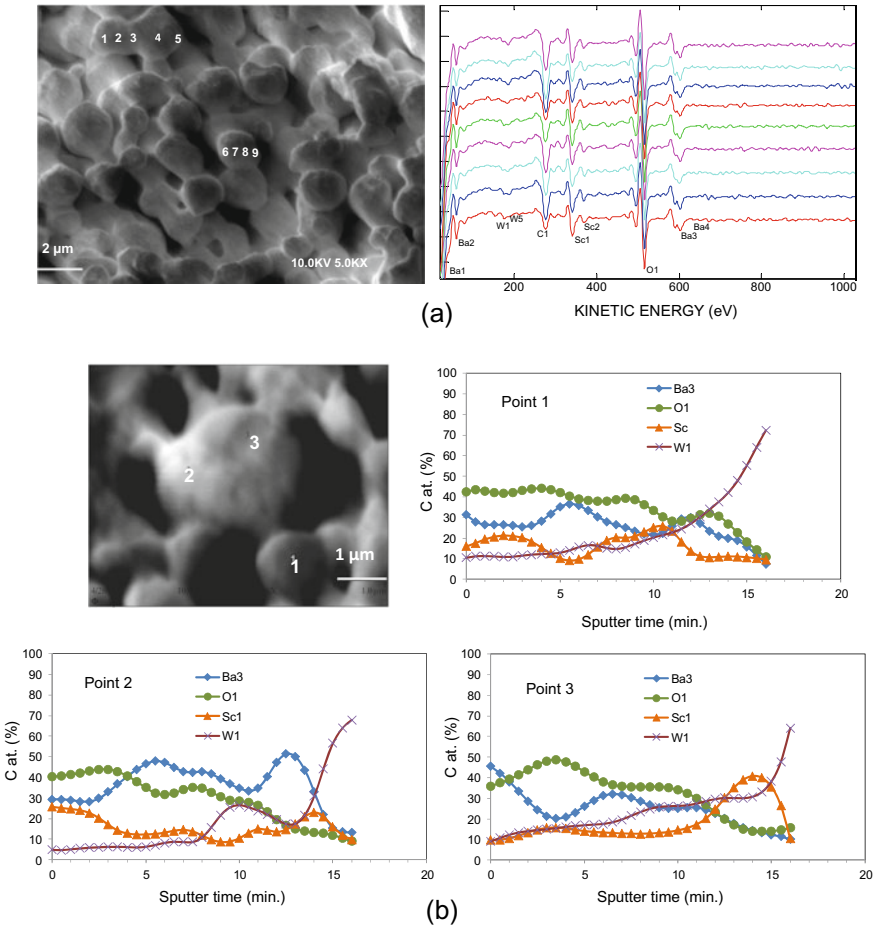

Fig. 3.42 Surface and depth distributions of Ba, Sc, and O on surface of activated SDD cathodes. **a** AES spectra (right) from nine points on the SEM image (left). **b** Depth profiles of three points on SEM image. Sputtering rate: 2 nm/min for (1–9) min and 13 nm/min. For the rest, calibrated for thermally oxidized SiO_2/Si

side of Fig. 3.43a, it is proved that the layer is formed after SDD cathode activation. From the height sensor image of an activated SDD cathode, the layer has a thickness essentially in agreement with the AES depth analysis results.

In summary, Ba, Sc, and O on the surface of SDD cathodes present neither as a monolayer as in the case of Ba dispenser cathodes, nor as a thick patchy layer. Rather, a multilayer of Sc with Ba and O, which are of higher amounts than that on Ba dispenser cathode surface, is consistent with the surface feature of a real SDD cathode. The layer is uniformly distributed on the surface of SDD cathodes in a thickness of about tens of nanometers.

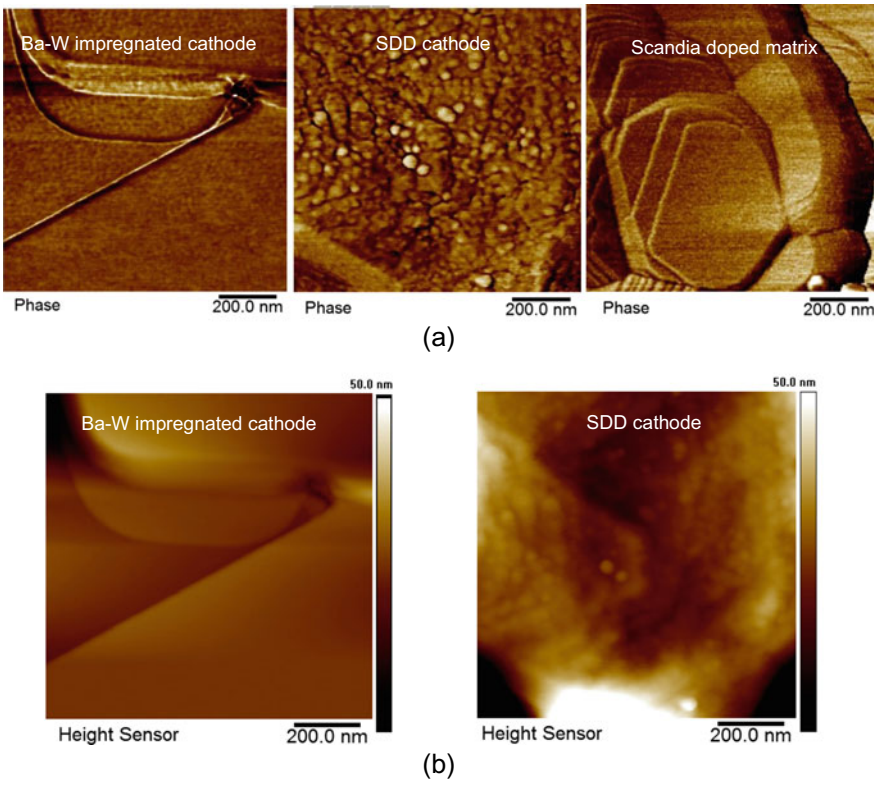

Fig. 3.43 Comparison of surface topographies of fully activated Ba-W impregnated cathode, SDD cathode and Scandia doped matrix. **a** AFM phase images. Left: activated Ba-W impregnated cathode; Middle: activated SDD cathode; Right: Scandia doped matrix. **b** AFM Height sensor images. Left: activated Ba-W cathode; Right: activated SDD cathode

(c) Correlation Between Surface Layer Parameters and Emission of SDD Cathode

A strong correlation between surface layer parameters and emission properties of SDD cathodes has been found from the summarized data of emission measurement and in situ analysis in cathode activation, operation, air exposure, and the life tests carried out in AES system.

The thickness of the layer and the atomic ratios of surface active elements are closely correlated with the emission properties of the SDD cathode [108]. A summary of the relationship between surface features and the emission is given in Table 3.6. In the table, the APPH ratio of Ba/W reflects the layer thickness, and the constituents of the active components are expressed by atomic concentration ratios of Ba:Sc and O:Sc. The layer normally has optimum atomic concentration ratios of Ba:Sc:O of about (1.5–2):1:(2–3) at operation condition after the cathodes were fully activated [95]. Improper producing processes, insufficient activation, or overheating will cause

deviations from the optimum atomic ratios and/or layer thickness, resulting in unfavorable emission. Both thickness and the surface active elements ratios remain almost the same during life test at normal operating temperature of 1000 °C_b for about ten thousand hours [115], which are demonstrated in Fig. 3.44. But all the three ratios deviate from their optimum levels when working at an elevated temperature of over 1150 °C_b for thousand hours with a coincident degradation in emission.

It was thus concluded that the copious electron emission of Ba scandate cathodes is due to a Ba–Sc–O multilayer described above and the emission capability stays unchanged as long as the multilayer remains.

This multilayer structure minimizes the influences of substrate components on the work function of the cathode, which is the case for M-type cathodes. Hence, other additives to W substrate such as Re, Os, or Ru have limited contribution to emission capability of Ba scandate cathodes.

Table 3.6 Correlation of emission of SDD cathodes with surface behavior

Cathode status	Surface behavior				Emission J(A/cm^2) at 850 °C_b
	Atomic concentration ratios			APPH ratio	
	Ba	Sc	O	Ba/W	
After full activation Average range	1.5–2.0	1	2.0–3.0	1.4–1.9	30–40
Operating at 1000 °C_b 7000 h	2.0	1	2.0	1.4	Stable
Operating at 1150 °C_b 3000 h	6.1	1	7.8	0.3	Low

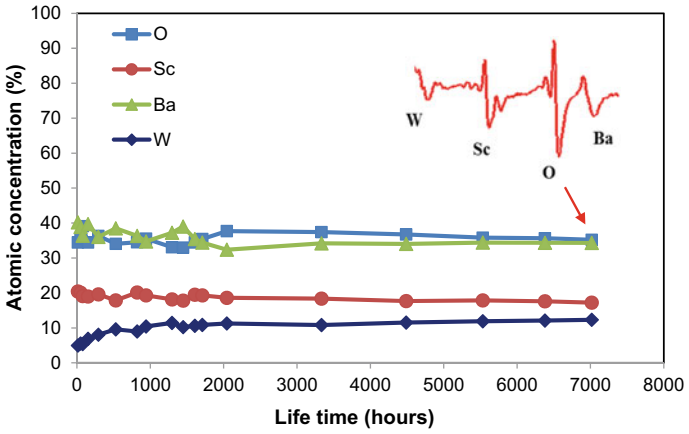

Fig. 3.44 Change of surface composition of an SDD cathode during operation at 1000 °C_b after activation, analyzed at 800 °C_b by in situ AES

3.3.5.3 Function of the Surface Layer

As a well-known fact, anomalous Schottky effect has been observed for all types of Ba scandate cathodes. It was once assumed that a patch work function is responsible for this non-saturated emission characteristic if a dipole monolayer emission model is adopted. However, as previously described, a uniform Ba–Sc–O multilayer of tens of nanometers in thickness actually exists on the surface of SDD cathodes and the emission uniformity is generally similar to that of Ba dispenser cathode. Therefore, a new interpretation is required. A. Shih has pointed out based on the thick Ba, Sc, O-containing compound layer they found in their study [106] that, if a semiconductor model is considered for Ba scandate cathodes, the emission should be basically uniform but not patchy. In the semiconductor model suggested by Maloney [50], the anomalous Schottky effect observed in the emission versus voltage measurements is thought to be the result of penetration of the external electric field into the surface layer and lowering the work function, causing a continuous increase in emission current with increased anode voltage, like that proposed by Wright for oxide-coated cathodes [116].

In a recent study, a special emission feature has been noticed in a PWFD-type analysis for SDD cathodes, and also for other kinds of Ba scandate cathodes. This feature is contrary to the typical behavior of Ba dispenser cathode, which is based on a Ba-O dipole emission model. The special feature is

1. When the actual Miram curves from Ba scandate cathodes are superimposed on a group of theoretical J_0-T curves derived only using the Richardson–Dushman equation, i.e.:

$$J_0 = 120\,T^2 \exp(-\phi/kT) \tag{3.6}$$

   to form PWFD plots, the peak work function (WF) values of the PWFD plots that result from Miram curves with different initial SCL current densities do not overlap as in the case of Ba dispenser cathodes [90].
2. The peak work function values decrease sequentially as the initial SCL current densities increase, so that the lowest peak WF always corresponds to the highest initial SCL current density. This is also the case when the Schottky effect is taken into account in determining the PWFD plots [95]. Because the initial SCL current densities are directly related to the applied electric field, the special feature implies that the lowest peak work function is subjected to the highest external electric field in the normal PWFD analysis. As an example, a comparison of PWFD plots from an SDD cathode and a Re-W base M cathode, tested in close-spaced diodes under the same conditions, is illustrated in Fig. 3.45.

To explain this special emission feature quantitatively, the influence of external electric fields on the emission properties when semiconductor models for thermionic emission are taken into account, which was proposed by Wright [116], has been

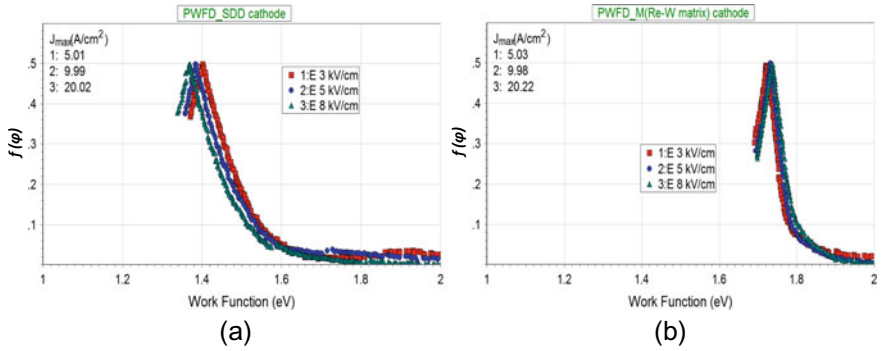

Fig. 3.45 PWFD plots at different initial SCL current densities, corresponding to different external electric fields, for **a** SDD cathode and **b** M (Re-W matrix) cathode. The peak work functions shift with the increase of the electric fields only for SDD cathode

introduced. According to Wright's model, the applied external field penetrates the surface of the semiconductor due to the low concentration of free electrons in its conduction band, forming a layer of space charge. The energy levels are then tilted in the semiconductor layer, producing a reduction $\delta\chi$ of the work function ϕ, so that

$$\phi' = \phi - \delta\chi \tag{3.7}$$

$\delta\chi$ is determined as

$$\delta\chi = 2kT\sinh^{-1}\frac{E}{4(2K\pi n_0 kT)^{1/2}} \tag{3.8}$$

where E is the electric field at the surface of the cathode produced by the applied anode potential, n_0 is the concentration of electrons in the conduction band of the semiconductor at T, and K is related to the dielectric constant of the semiconductor. By combining Schottky effect and above semiconductor modification, the Temperature Limited (TL) emission $J_{TL\text{-}S}$ is then described as

$$J_{TL-S} = J_0 e^{\frac{\delta\chi}{kT}} e^{\frac{4.4\sqrt{E}}{T}} \tag{3.9}$$

While the tested Miram curves of an SDD cathode with different initial SCL current densities, which are related to different anode voltages at a fixed anode–cathode distance, i.e., electric fields E, are superimposed to (i) a family of J_0-T curves calculated according to the Richardson–Dushman equation and (ii) the $J_{TL-S} - T$ curves calculated by taking both Wright's semiconductor model and the Schottky effect into account, two groups of PWFD plots are derived and illustrated in Fig. 3.46a, b, respectively.

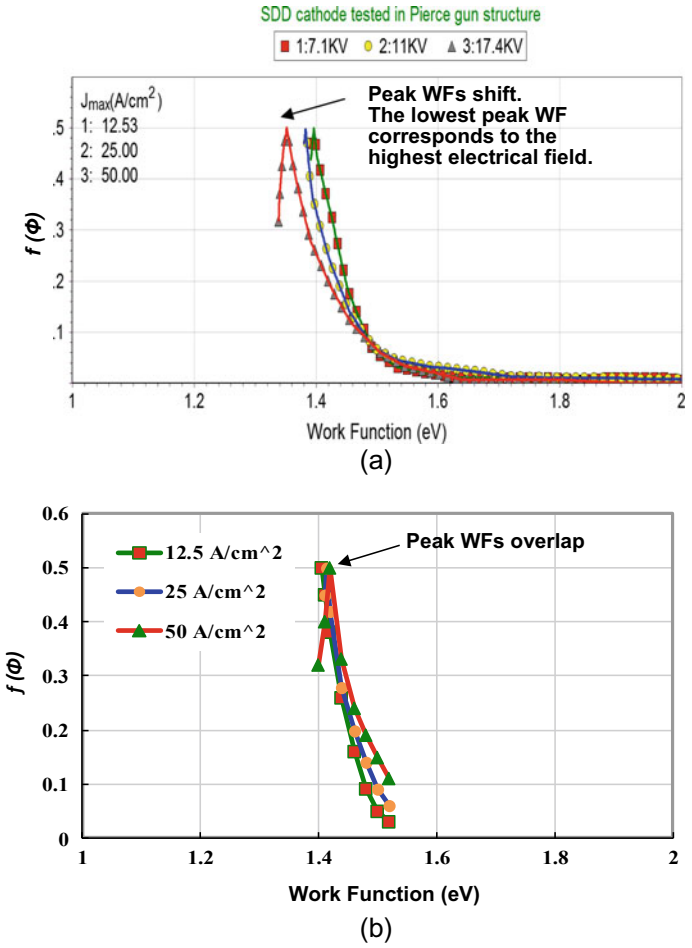

Fig. 3.46 PWFD curves of an SDD cathode resulted from superimposing of tested Miram curves at different initial SCL current densities (external electric fields) with **a** a family of J_0-T curves calculated according to the Richardson–Dushman equation. **b** The $J_{TL\text{-}S}$ -T curves calculated by taking both the Schottky effect and the Wright's semiconductor model into account

The peak work function values for the three initial SCL current densities shift obviously in the case of (i) and the lowest WF is related to the highest anode voltage. However, in the case (ii), where the influence of extra electric fields on emission from the semiconductor model has been involved, the peak WFs tend to normally overlap with an average WF of around 1.41 eV. The analyses results denote that the emission from SDD cathode (and other Ba scandate cathodes) is more related to a semiconductor structure rather than a dipole monolayer model.

This proposal could be substantiated after applying the Longo–Vaughan (L–V) relations of thermionic cathodes to the SDD cathodes. In L–V relation, the cathode current density J can be expressed with the following equation [117],

$$1/J^{\alpha} = 1/J_{SCL}^{\alpha} + 1/J_{TL}^{\alpha} \tag{3.10}$$

where J_{SCL} is given by Child-Langmuir's law, J_{TL} is determined by Richardson's equation with Schottky correction, and α is called the shape factor. By fitting the tested J with the equation, the work function can be estimated. This approach has been successfully applied for Ba dispenser cathode performance evaluation [118].

However, similar to the case of PWFD analysis, when fitting the experimental data from SDD cathodes to the equation, the obtained WFs from different initial SCL current densities are inconsistent with each other and the lowest WF-value is always corresponding to the highest initial SCL loading.

Nevertheless, by taking into account Wright's modification on the emission and choosing the concentration of electrons, n_0, from 10^{14} to 10^{16} electrons per cm^3, it is found that WFs are almost identical with values of around 1.41 eV if n_0 is in the region of 10^{15} electrons per cm^3, indicated in Fig. 3.47.

From the above analyses, it can be concluded that the extraordinary emission properties of Ba scandate cathodes are mainly attributed to the influence of external electric field on the semiconductor layer on the cathode surface rather than the patch effect. In other words, the Ba–Sc–O multilayer on the surface of Ba scandate cathode functions as a semiconductor layer.

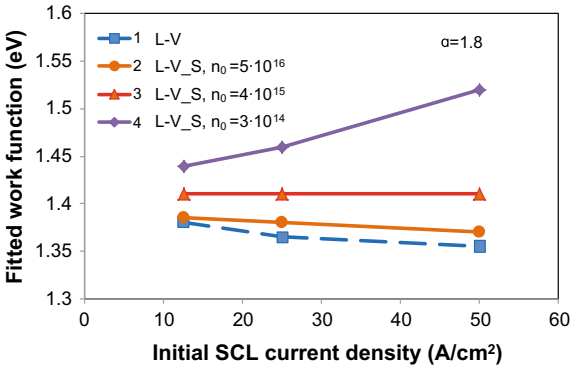

Fig. 3.47 Variation trend of the fitted work functions related to initial SCL current densities. The dashed line noted as "L–V" indicates the resultant work functions by fitting the tested data with Longo–Vaughan relation. The solid lines noted as "L–V_S" indicate the fitted work functions when Wright's modification for semiconductor is included and with different concentrations of electrons per cm^3 (n_0) in conduction band of the semiconductor layer. A shape factor of 1.8 is adopted for fitting

3.3.5.4 Formation of the Surface Layer

Owing to the essentiality of the surface layer to emission performance of Ba scandate cathodes, a deep understanding of the formation process of the layer is propitious for operation mechanism investigation and manufacturing technology development.

Though the Ba scandate cathode is basically constituted by adding scandium oxide to Ba dispenser cathode, whatever to matrix, impregnants, or on top of the cathode, the original added scandium oxide itself does not, in fact, join the surface layer directly.

In the case of SDD cathode, as pointed out in cathode structures description, the scandium oxide dispersed in the matrix no longer exists after impregnating with Ba, Ca aluminate. Compounds such as scandium tungstates, barium scandates, Ba, Sc-tungstates and Ba, Sc-aluminates, as well as Ba, Ca-aluminates like that in conventional Ba dispenser cathodes are produced and have been detected by X-Ray Diffraction (XRD) in thermochemical experiments [108]. The generation of these compounds is coincident with the previously reported possible reactions by the thermochemistry investigation for $BaO{\cdot}Sc_2O_3{\cdot}WO_3$ ternary system [78] and real cathodes [119]. These water-soluble compounds are then removed from the surface area of cathodes after ultrasonic water cleaning as displayed on the left side of Fig. 3.48a.

The formation of the surface Ba–Sc–O layer is, therefore, a re-accumulating of Sc with Ba and O, by diffusing from the body to the surface with increase of temperatures, during activation in vacuum. It is observed in an in situ AES analysis exhibited on the right side of Fig. 3.48a, that on the surface of an SDD cathode which was firstly ion etched to remove the residual impregnants, the surface atomic concentration ratios of Sc, Ba, and O to substrate W, i.e., Sc/W, Ba/W, and O/W, increase obviously with temperature and time, indicating the diffusion process of Sc with Ba and O during heating and activation. Furthermore, the identical migration patterns of Sc/W and Ba/W from the pole area to W grains on a 2 μm thick W film deposited on SDD cathode surface, shown in Fig. 3.48b, reveal that a lateral co-diffusion of Sc with Ba, O occurs over the surface.

In contrast, when heating the Sc_2O_3 doped W matrix up to activation temperature, the concentrations of Sc and O remain unchanged [83]. This implies that little diffusion of scandium oxide takes place in the mentioned temperature region. The same conclusion has also been drawn from observations made on the thin film Ba/BaO on Sc/Sc_2O_3 model cathodes by in situ Photoelectron Emission Microscopy (PEEM)/Thermionic Emission Microscopy (ThEEM). The observation confirms that scandium as a metal diffuses on tungsten but Sc_2O_3 does not diffuse at operating temperatures [120].

To sum up, free or ionic Sc is released by reactions of Sc-containing compounds, which are produced from originally added Sc_2O_3, with other compounds or oxides during processes of impregnation and activation. The free Sc diffuses to the W surface with Ba and O to form the Ba–Sc–O layer during activation. The above processes are time consuming; that could explain the aforementioned longtime activation for Ba scandate cathodes.

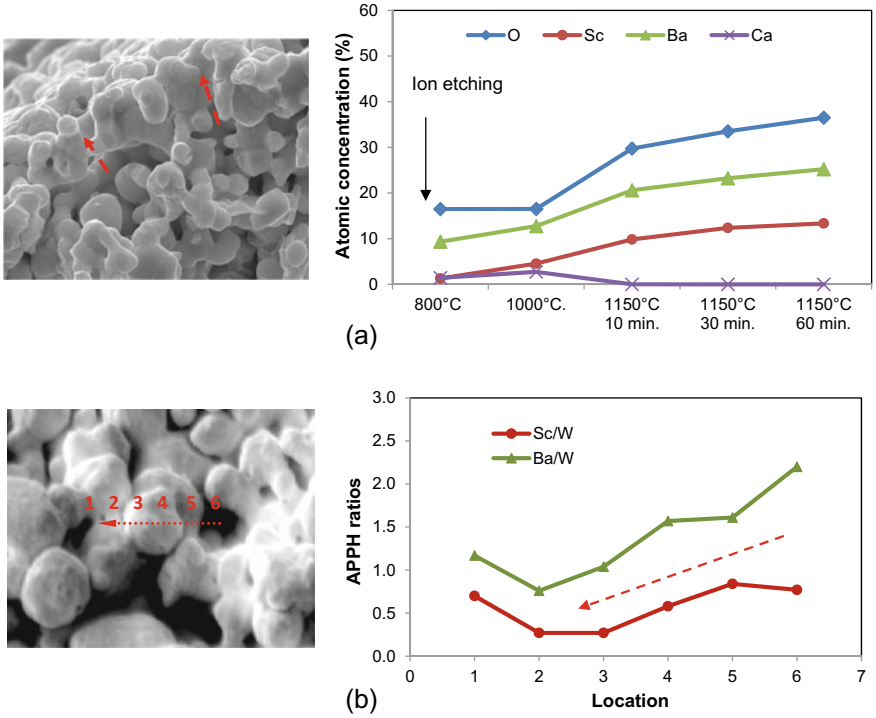

Fig. 3.48 Diffusion of Sc with Ba, O during activation and surface migration of Ba, Sc along a W grain. **a** Changes of AES atomic concentration ratios of Sc/W, Ba/W, and O/W during activation with temperature (°C_b) and time (right); analyzed at the surface of cathode after impregnating and surface cleaning shown in SEM image (left). **b** Variation of Auger Peak–Peak Height APPH ratios of Ba/W and Sc/W (right); from pore to a W grain shown in SEM image (left)

On the other hand, a different picture is valid for the cathode after air exposure. The Ba–Sc–O layer formed during a long initial activation, by removing residual impregnants such as Ca-containing compounds and gradually diffusing Sc, Ba, and O, is soon established after air exposure, just when the surface adsorbed carbon-containing contamination is eliminated, see Fig. 3.49a. Accordantly, the emission rises up to the original or even better level in a period much shorter than that at initial activation, illustrated in Fig. 3.49b. The simultaneous change of all surface elements at the beginning of re-activation indicates the surface layer is already in existence and the Ba, Sc, and O has a close chemical association. Once the layer forms at initial activation, it is basically stable during air exposure.

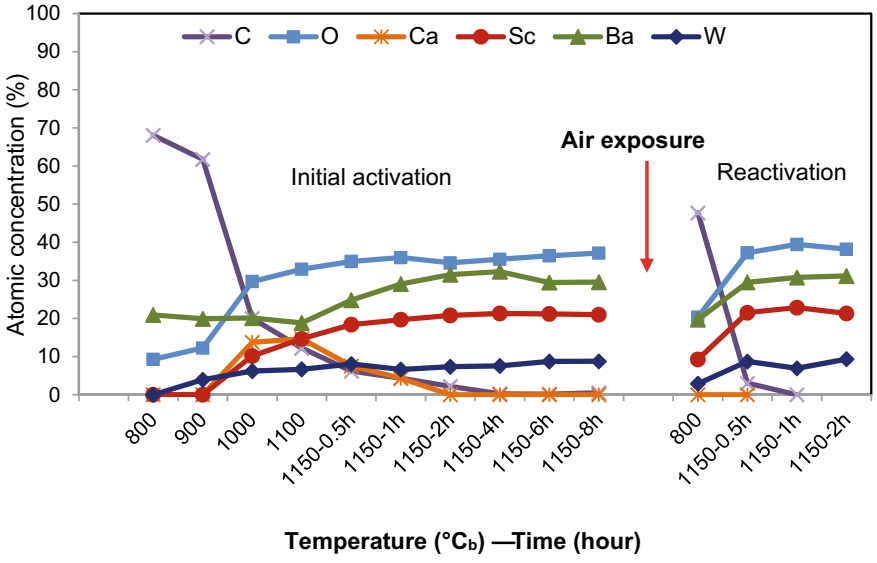

(a)

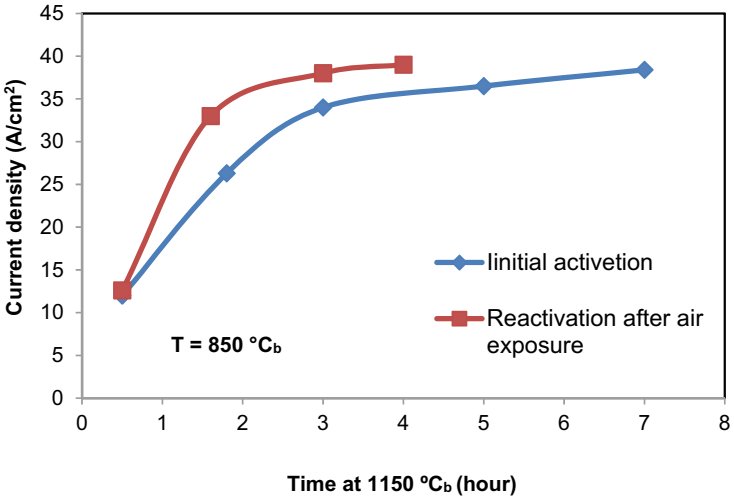

(b)

Fig. 3.49 Performances of an SDD cathode at initial activation and reactivation after air exposure. **a** Change of surface elements at different status by in situ Auger analysis. **b** Critical SCL current density at 850 °C_b with activation time

3.3.5.5 Properties Related to the Surface Layer

The Ba–Sc–O multilayer surface feature of Ba scandate cathode, which differs from a monolayer Ba-O dipole on Ba dispenser cathode, brings about distinctions in several properties.

Lower Evaporation Rates

Evaporation properties of SDD cathode have been investigated and compared with that of traditional Ba dispenser cathodes by using of a vapor-collection apparatus equipped with a quartz crystal oscillator and a Time-of-Flight Mass Spectrometer (ToFMS) [108].

The total evaporation rate of SDD cathodes measured by the quartz crystal oscillator is listed in Table 3.7. At an operating temperature of 1050 °C_b or a true temperature of 1400 K, the average evaporation rate is about 1.15×10^{-9} g·cm^{-2}·s^{-1} for SDD cathode. It is almost one magnitude lower than the evaporation rate of 1.48×10^{-8} g·cm^{-2}·s^{-1} for the ordinary Ba dispenser cathode at its normal operating temperature of 1100 °C_b or 1457 K. Moreover, the intensities of ionic Ba peaks on ToFMS mass spectra for SDD cathodes are much lower than those of the Ba dispenser cathodes and with higher activation energy. A comparison of ionic current for Ba^{++} (69), from 1000 °C_b to 1150 °C_b, measured from traditional Ba-W impregnated cathode, M-type cathode, and SDD cathode, is shown in Fig. 3.50.

The lower Ba evaporation rate is consistent with the surface analysis results and the inference described before: barium as well as oxygen binds much stronger to the surface of SDD cathode, by forming a Ba–Sc–O layer, when compared to the Ba on W for Ba dispenser cathode.

In practical applications, the low evaporation of SDD cathodes is beneficial to reduce the possibilities of vacuum electrical breakdown or arcing, secondary emission, and fogging of the output windows when applying the cathodes into VEDs.

Higher Robustness to Residual Gas Poisoning

The Ba–Sc–O semiconductor layer on the surface of Ba scandate cathode also exhibits less sensitivity to residual gas poisoning [121].

Poisoning by oxygen and air for SDD cathodes and M cathode has been compared under the same test conditions and the results are listed in Table 3.8, where partial pressure corresponding to the emission drop to 90% of its initial value is defined as the critical poisoning pressure. The comparison reveals that the critical pressures for SDD cathodes are about half to one order of magnitude higher than that of M

Table 3.7 Average evaporation rates of M-type and SDD cathodes

Cathode type	Average evaporation rate (g·cm^{-2}·s^{-1}) at true temperature (K)		
	1400	1457	1513
M	6.23×10^{-9}	1.48×10^{-8}	5.68×10^{-8}
SDD	1.15×10^{-9}	3.38×10^{-9}	1.02×10^{-8}

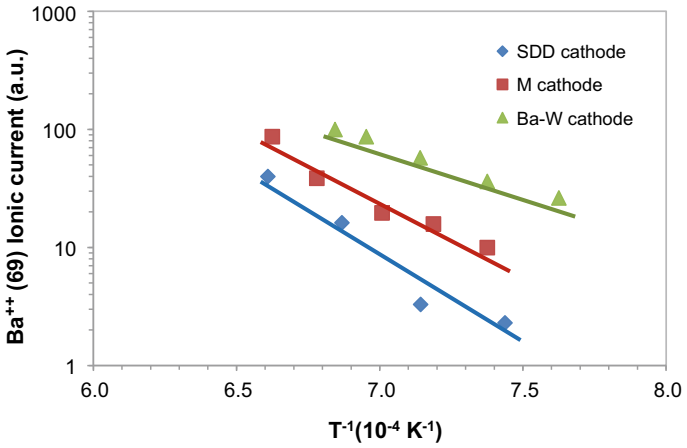

Fig. 3.50 Comparison of Ba evaporation rates of the SDD cathode and Ba dispenser cathodes

cathode at the same temperature, at which the SDD cathode is capable of providing much higher current density than M cathode.

In addition, a full emission recovery is visible for SDD cathode after the poisoning gases are pumped off. The recovery character of SDD cathode is also better than that of M cathode, as indicated in Fig. 3.51. For either cathode, the poisoning-recover test started with an initial current density of 20 A/cm^2 at an operational temperature of 1000 °C$_b$. However, owing to the difference in their poisoning critical pressures, the O_2 partial pressure was 5×10^{-5} Pa for M cathode but 5×10^{-4} Pa for SDD cathode in the testing. A faster emission drop with time and a relatively long recovery was observed for M cathode while the SDD cathode exhibits moderate emission degradation and completes recovery after the termination of the oxygen admission.

The high poisoning pressures and the reversible character for Ba scandate cathodes imply that the Ba–Sc–O layer is more tolerant of a gas poisoning than the Ba-O dipole layer. A physical adsorption of gases rather than a chemical reaction may dominate the poisoning process for this kind of cathode.

Table 3.8 Critical poisoning pressures of air and oxygen for SDD and M cathode

Operating temperature (°C$_b$)	Critical pressure (Pa)			
	Air		O_2	
	SDD	M	SDD	M
900	6.5×10^{-4}	1.1×10^{-4}	2.1×10^{-4}	3.6×10^{-5}
1000	1.4×10^{-3}	2.1×10^{-4}	5.4×10^{-4}	4.9×10^{-5}
1100	6.5×10^{-3}	5.8×10^{-4}	1.1×10^{-3}	2.2×10^{-4}

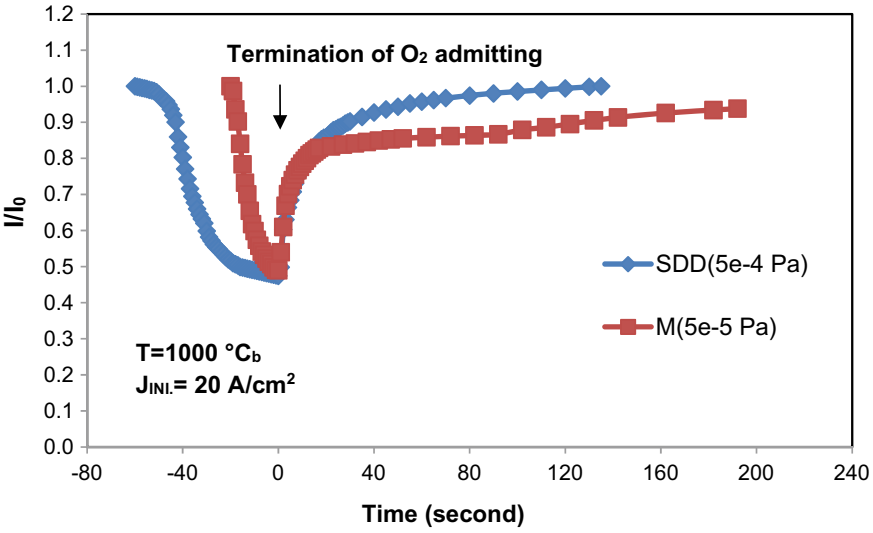

Fig. 3.51 Emission poisoning by O_2 and recovering on SDD cathode and M cathode

Uniqueness of the Contribution of Scandium Oxide to Emission Improvement
Since the addition of scandium oxide to Ba dispenser cathode leads to great enhancement in thermionic emission, other rare-earth oxides such as yttrium and europium oxides were once assumed to evoke equal effects as scandia. To verify the assumption, the W powders have been doped with single Y_2O_3, and with 50/50 mixtures of Sc_2O_3–Eu_2O_3 or Sc_2O_3–Y_2O_3 in a similar manner as doping of Sc_2O_3. These precursor powders were then fabricated into matrices and cathodes in the standard ways. The added contents (in wt%) of Sc_2O_3, Eu_2O_3, and Y_2O_3 in precursor powders and the atomic percentage concentrations (at. %) of elements on the surface of matrices and cathodes after heating or activating are listed, respectively, in Table 3.9. The emission performance of each sample is also indicated for comparison.

It is interesting to find that among the added rare-earth elements, only Sc has been detected on the surface of these cathodes though other elements do exist on the surface of their relative matrices. As a result, for the single Y_2O_3 added cathode (Y6), no active elements other than Ba and O present on W substrate and its emission is just similar to that of the normal Ba dispenser cathode. For the cathodes co-doped of Sc_2O_3–Eu_2O_3 (E3) or Sc_2O_3–Y_2O_3 (Y3), the emission is close to, but not excess, the level of a single Sc_2O_3 doped cathode (S5), resulting only from the appearance of Sc (with Ba and O) on the surface of these cathodes.

Consequently, it is believed that rare-earth oxides other than scandium oxide have little contribution to electron emission though they may have similar chemical and physical properties. The innate character of this interesting phenomenon is expected to trigger/stimulate further investigations.

Table 3.9 Original doped contents of rare-earth oxides in precursor powders and atomic concentrations of Sc/other rare-earth elements on surface of matrices and cathodes with the relevant emission properties of the cathodes

Sample	Doped content (wt%) in precursor powder			Content on matrix surface at 1150 °C_b (at.%)				Content on cathode surface after activation at 1150 °C_b (at.%)					Emission J (A/cm^2)	
	Sc_2O_3	Eu_2O_3	Y_2O_3	Sc	Eu	Y	O	Sc	Eu	Y	Ba	O	850 (°C_b)	1000 (°C_b)
S5	5			33			39	17			25	41	35.7	
E3	3	3		20	18		36	9	0		20	20	20.6	
Y3	3		3	15		7	41	15		0	30	34	34.7	
Y6			6			20	40			0	28	22		3.4

3.3.6 Summary and Discussion

3.3.6.1 Summary

The nanosized-scandia doped dispenser cathode, as a new kind of Ba scandate cathode, exhibits the characteristics as follows:

(1) The cathode has the ability to provide a critical Space Charge Limited (SCL) current density of over 100 A/cm^2 at Mo-brightness temperature of 950 °C$_{B\text{-}Mo}$ or true temperature of 1015 °C. There is little difference between pulsed and DC emission with temperature compensation for electron cooling in DC operation.
(2) The lifetime, during which the high critical SCL emission level can be stably maintained, is longer than ten thousand hours.
(3) The peak work functions determined from Practical Work Function Distribution(PWFD) plots are about 1.40–1.45 eV. The Richardson work functions estimated from zero field emission at low temperatures are around 1.13–1.15 eV with Richardson constants of (2–4) A·cm^{-2}·K^{-2}.
(4) The emission uniformity is greatly improved and becomes similar to that of Ba dispenser cathode. The beam quality is acceptable for application in VEDs.
(5) A Ba–Sc–O semiconductor layer of tens of nanometers thick with certain atomic concentration ratios on W substrate is the source for the copious electron emission.
(6) The high emission property of the cathode remains stable as long as the Ba–Sc–O layer maintains.
(7) The layer has lower evaporation rate, higher tolerance to gas poisoning than that of Ba-O dipole monolayer.
(8) Nanosized Scandia particles doped W matrix in grain size of submicron to 1–2 micron promotes a uniform distribution of Ba–Sc–O layer on W, leading to improvements on both emission capability and uniformity. The more uniform the layer on W substrate, the higher the emission and the better the emission uniformity.

3.3.6.2 Discussion

(a) The Constituents of the Ba–Sc–O Layer

Owing to the difficulty in determining the exact composition and structure of the surface layer on a real Ba scandate cathode by experimental approaches, hypotheses to describe the physics behind the enhanced emission of Ba–Sc–O systems presented recently are mostly based on the investigation of model systems or theoretical analysis [122–124]. These investigations provided interesting results and promoted an understanding of the possible emission mechanism. However, so far no consensus is achieved.

As described before, the surface layer is formed by diffusion of free Sc (with Ba and O) during activation for a real Ba scandate cathode like SDD cathode. But Sc_2O_3

may possibly form on the surface again from the out-diffused free Sc, by a reaction proposed by Hasker [15]:

$$3BaO + 2Sc = Sc_2O_3 + 3Ba \tag{3.11}$$

$$\Delta G^0 = -26 \text{ kcal/(mol. Ba) at } 1200\,K \tag{3.12}$$

In addition, it has been verified by investigations of thermochemistry on the ternary system [78] and practical cathode materials [108, 119] that a reaction of BaO with Sc_2O_3 occurs at 950 °C to produce ternary compound $Ba_2Sc_2O_5$ and decompose into $Ba_3Sc_4O_9$ above 1100 °C.

$$2BaO + Sc_2O_3 = Ba_2Sc_2O_5 \text{ at } 950\,^{\circ}C \tag{3.13}$$

$$2Ba_2Sc_2O_5 = Ba_3Sc_4O_9 + BaO \text{ at } 1100\,^{\circ}C \tag{3.14}$$

As these reactions are possible to take place during cathode activation, a proposal is then drawn up. That is a Ba adsorbed or doped barium scandate, such as $Ba_3Sc_4O_9$, thin layer may represent the Ba–Sc–O layer on the surface of Ba scandate cathode. The proposal is supported by the atomic ratios measured on real cathodes, shown in Table 3.10.

Further investigation is expected to explore the exact constitution of the surface layer. That is important not only for emission mechanism understanding, but also for guiding the improvement of cathode technologies.

(b) The Essential Processes in Forming of Free or Ionic Scandium

Emission degradation by ion bombardment in practical applications is sometimes unavoidable. This problem is especially serious while cathodes work in a relatively poor vacuum environment, such as in CRTs, and consequently caused a particular concern in the early development stage of the Ba scandate cathode [9, 16, 19, 22]. The VEDs usually operate with excellent vacuum conditions and in SCL regime, reducing the influence of ion bombardment. However, this is still a great challenge for all kinds of Ba scandate cathodes.

Ultimately, the recovery of emission after ion bombardment is related to the restoration of the surface layer. It has been noticed that when the surface elements are removed by strong ion beam etching, reactivating arouses a full recovery of Ba

Table 3.10 Atomic ratios of barium scandates and Ba–Sc–O layer on SDD cathode

	Atomic ratio		
	Ba	Sc	O
$Ba_2Sc_2O_5$	1	1	2.5
$Ba_3Sc_4O_9$	0.75	1	2.25
Ba–Sc–O layer	1.5–2	1	2–3

in a short time while the re-diffusion of Sc only provides a partial recovery in a time depending on the W grain size. This process brings about a big confusion that why the obvious liberation of free or ionic Scandium taken place at initial activation can only be partially performed during reactivation after ion etching.

Till now the reactions to release the free or ionic Sc are still unclear. Two possible reactions have been suggested.

The one is proposed by Yamamoto [18]:

$$Sc_2W_3O_{12} + 3Ba = 2Sc + 3BaWO_4 \tag{3.15}$$

and the other is by Magnus and Hill [78]:

$$Ba_3Sc_4O_9 + W = Ba_3Sc_2WO_9 + 2Sc \tag{3.16}$$

However, no thermodynamic data were ascertained.

Although the microstructure of SDD cathode is beneficial to liberation and diffusion of free Sc, it, nevertheless, needs an essential improvement on the recovery property of scandium. To achieve this, a full understanding of the fundamental generation mechanism of free Sc is one of the major expectations.

(c) The Nature of the Surface Nanoparticles

In the context of the above discussion, it is interesting to observe that, apart from uniformly spread Ba–Sc–O multilayer, a multitude of nanoparticles have been observed on the surface of the layer, especially along the visible growth boundaries of the underlying W grains [10].

The particles, which can be clearly seen from the AFM amplitude image shown on the left-hand side of Fig. 3.52a, appear only for SDD cathodes after full activation and operation [10]. Neither such particles have been found for the activated Ba dispenser cathodes as shown on the right-hand side of Fig. 3.52a, nor are they present in SDD cathodes before activation.

No other elements except Ba, Sc, and O have been detected at the nanoparticle areas by AES with 40 nm spatial resolution. Because the sizes of the particles are below the resolution, it is not clear if the analyzed results correspond well to the actual constituent of the particles.

The potential effects of these nanoparticles on emission have been evaluated by assessing the local electric field enhancement around the particles. Referring to Edgcombe and Valdre's report [125], for a cylindrical shank in parallel-plane electrode geometry with tip-to anode distance of 0.1 mm or more, the field enhancement factor γ can be expressed as

$$\gamma \approx 1.2(L/R + 2.15)^{0.9} \tag{3.17}$$

where L is the tip length and R is the tip radius.

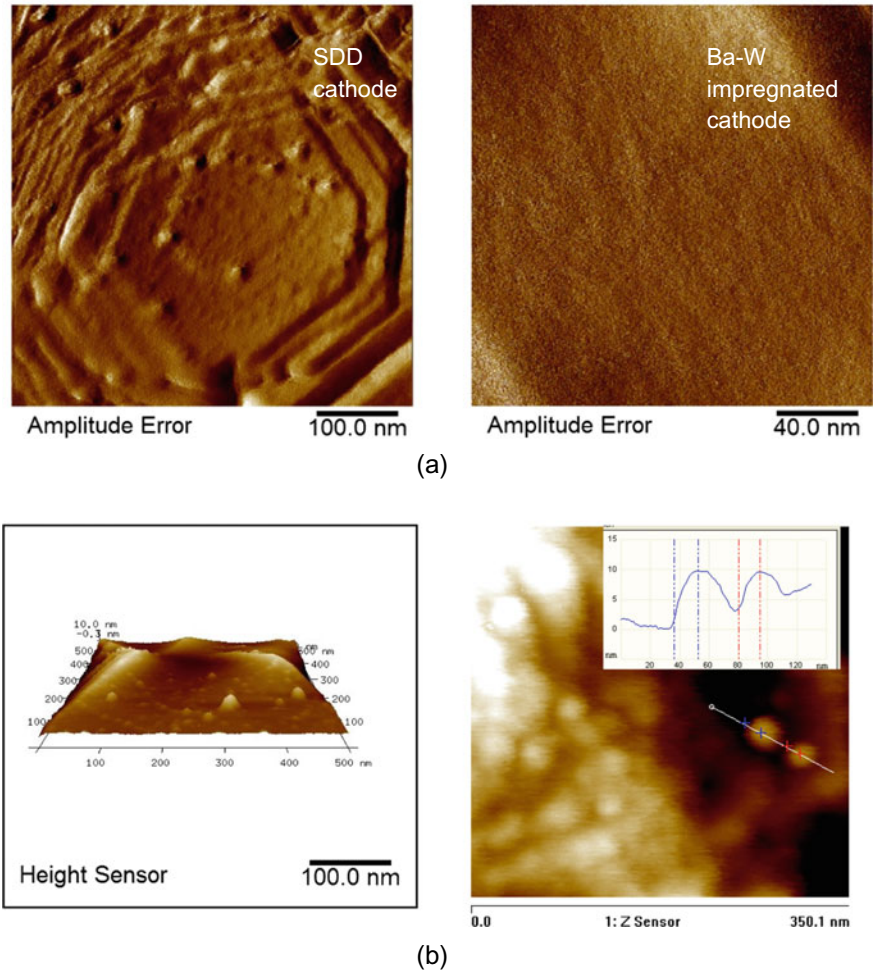

Fig. 3.52 **a** AFM amplitude images of activated SDD cathode (left) and activated Ba-W impregnated cathode (right). **b** Shapes (left) and dimension estimation (right) of the nanoparticles in AFM height sensor images

By considering a nanoparticle as a projection with a length of 10 nm and radius of 5 nm, like that shown by AFM in Fig. 3.52b, the field enhancement factor will roughly equal to 4.3.

Thus, at an average field strength of about 40 kV/cm between cathode and anode, which is related to the field that an SCL critical current density of 100 A/cm^2 can be reached under normal experimental conditions such as the cases of Figs. 3.30 and 3.32, the electric field near the nanoparticles will be around 170 kV/cm, i.e., about 1.7×10^7 V/m. This field strength is still much lower than 10^8–10^9 V/m for the

starting of field emission unless the L/R of the particle reaches an unrealistic value of about 30.

However, the influences of this electric field on electron emission can be exerted by Schottky effect on thermionic emission and, especially, by field penetration when a semiconductor model is considered for Ba scandate dispenser cathodes to heighten the emission. If that is the case, the appearance of nanoparticles on SDD or other Ba scandate cathodes will not only strengthen the emission, but also cause emission nonuniformity while the cathodes operate at low temperatures in TL regime, but will have limited effects in SCL regime.

It must be pointed out that the SEM and AFM observations were not obtained at cathode operating temperatures. The activated or operated cathodes were cooled down to room temperature before analysis. The exact shapes and dimensions of these nanoparticles at operation conditions are not clearly figured out yet.

The nature of these surface particles, their formation process and existence status, behavior, and effects on emission are interesting subjects for a deeper study.

Ba scandate cathodes with their proven outstanding emission capability have attracted continuous attention for almost half a century. However, as described above, many phenomena are still unclear and/or controversial. The comment for the old oxide-coated cathode made by Gilmour [48] should be also suitable for this kind of cathodes: "It is clear that as far as science goes, the state of the oxide coated cathode is confused indeed. Not only does theory fail to help us make good cathodes; it seems not to fit all the evidence. Maybe cathodes work sometimes one way and sometimes another, which isn't as ridiculous as it may sound. At any rate, while some physicists are uninterested and others confused, cathode making continues to be an art practiced, it seems, by artists with a good deal of witch doctor in their make-up. When something goes wrong, this or that demon is exorcised, and eventually things go right again. And, unlikely as it seems, cathodes continue to improve".

3.4 General Conclusions and Outlook

In the preceding sections, two successful versions of Ba scandate-type cathodes have been described in detail, namely the LAD top-layer Ba scandate + Re dispenser cathodes on W–I base as pioneered by Philips Research [9] and nanosized-scandia doped dispenser cathodes with W-base matrix (SDD) as introduced first by Beijing University of Technology (BJUT) and Beijing Vacuum Electronics Research Institute (BVERI) and continued by BJUT in China [10]. A common feature of all Ba scandate-type cathodes is that they exhibit a low Richardson work function of about 1.15 eV and Richardson constants varying from 2 to 8 A/(cm^2K^2), with increasing uniformity and electron emission capability. This feature is connected with a second characteristic property that Ba scandate cathodes show anomalous behavior in the saturation range which does not follow the Schottky effect as for Ba dispenser cathodes, but is similar to oxide cathodes. This results in only a small gradual deviation from the space charge limit in the current-voltage characteristics at higher temperatures. From emission

characterization of LAD and SDD scandate cathodes, it was found that one can describe saturation by a power law with power x_s (slope x_s in double logarithmic *I(U)* plot), which is smaller than the space charge limit (slope x_{scl}). In LAD and SDD scandate cathode experiments, it was observed as a rule that higher uniformity (higher A_R in the case of LAD cathodes) caused steeper slopes x_s. A convincing model and a theory of the saturation behavior is still needed, but there are a lot of indications that basically an oxide-type model can explain most of the properties, but eventually linked to an increasing area fraction of a surface compound containing (Ba, Sc, O) and, possibly, a Ba monolayer on top. In this context it would be helpful, to prepare very flat polished surfaces of Ba scandate cathodes for high-resolution work function mappings as, for example, described by Eng [126] or Back et al. [127] and correlate it with Auger elemental mappings.

On average, the AES depth profile results for LAD scandate cathodes gave a ratio of Ba:Sc:O = 2.04: 1: 2.78 to a depth of about 36 nm. This is in line with the results for SDD cathodes of Ba:Sc:O = (1.5–2): 1: (2–3). W or Re do not play a direct role and just serve as the conducting base. The Ba:Sc:O ratios are consistent with a surface compound composition of $2BaO{\cdot}Sc_2O_3$ with a surface coverage of 2 Ba (about a monolayer). It is not clear if there exist 2 phases or maybe an unknown high-temperature phase only formed after activation.

The success of the LAD scandate cathode and SDD cathode is linked to higher emission capability and higher uniformity of emission. This is due to finer surface structures and more homogeneous distribution of Sc, in case of LAD cathodes due to surface coating with nanoparticles of initially uniform distribution (but on a coarser base) and in case of SDD cathodes due to the fine-grained structuring of porous tungsten base uniformly doped with scandia nanoparticles. The advantage of the SDD cathode is that it is prepared by a much cheaper and practical method than the top-layer preparation by LAD, which only can get competitive for high volume production of cathodes as in the high noon of CRT production. Nowadays scandate cathodes are still needed for high-end applications such as THz imaging devices, but in smaller numbers. Therefore SDD cathodes especially with high DC emission are the cathodes of choice. Yet there are good prospects that one can also use the less-expensive sputtering instead of LAD, but with targets of the same composition as used for LAD to realize the high-performance cathode. In view of the great demands on applications of high current density cathodes, the doors for new ideas and technologies are always open for further improvement of the currently existing Ba scandate cathodes.

References

1. G. Gaertner, Historical development and future trends of vacuum electronics, J. Vac. Sci. Technol. B **30/6**, 060801 (2012)
2. G. Gaertner, H.W.P. Koops, Vacuum electron sources and their materials and technologies, chapter 10 of *Vacuum Electronics, Components and Devices*, Ed. J. Eichmeier, M. Thumm, Springer (2008)

3. R. Barker, Miniature Electron Sources for Tomorrow's Vacuum THz Devices, Report No. AFRL SR-AR-TR-06-0330, Institute for Research in Electronics and Applied Physics, Univ. of Maryland, July 2006
4. M.J. Rosker, Vacuum electronics and the world above 100 GHz, in Proceedings IVEC 2008, Monterey, CA, p. 5–7 (2008)
5. M.C. Green, Cathode technology overview—Current status and future Directions, in Proceedings IVEC 2008, Monterey, CA, p. 3–4 (2008)
6. B.C. Djubua, A.P. Makarov, A.A. Negirev, S.E. Rozhkov, E.M. Zemchikhin, Metal alloy cathodes for very high emission- density applications, in Proceedings IVEC 2010, Monterey, CA, p. 155 (2010)
7. B.C. Djubua, Research and development of dispenser, metal alloy and oxide thermionic Cathodes, 1994 TRI-Service/NASA Cathode Workshop, Cleveland/Ohio, Conference Record, p. 3–6 (1994); based on older results from 1967/1979
8. R.E. Thomas, J.W. Gibson, G.A. Haas, R.H. Abrams, Thermionic sources for high-brightness electron beams. IEEE Trans. Electron. Dev. **37**(3), 850–861 (1990)
9. G. Gaertner, P. Geittner, H. Lydtin, A. Ritz, Emission properties of top-layer Scandate cathodes prepared by LAD. Appl. Surf. Sci. **111**, 11–17 (1997)
10. Y. Wang, J. Wang, W. Liu, K. Zhang, J. Li, Development of high current-density cathodes with scandia-doped tungsten powders. IEEE Transact. ED **54**(5), 1061–1070 (2007)
11. A. Figner, A. Soloveichik, I. Judinskaya, Metal Porous Body Having Pores Filled with Barium Scandate, US Patent 3 358 178, filed 27.10.1964, granted 12.12.1967
12. A. van Oostrom, L. Augustus, Activation and early life of a pressed barium scandate cathode. Appl. Surf. Sci. **2**(2), 173–186 (1979)
13. A. van Stratum, J. van Os, J.R. Blatter, P. Zalm, Barium-Aluminum-Scandate Dispenser Cathode, US-Patent 4007393, granted 8-2-1977, priority 21-2-1975
14. S. Taguchi, T. Aida, S. Yamamoto, I.E.E.E. Trans, Electron Dev. **31**(7), 900–903 (1984)
15. J. Hasker, J. van Esdonk, J.E. Crombeen, Properties and manufacture of top-layer scandate cathodes. Appl. Surf. Sci. **26**, 173–195 (1986)
16. J.E. Crombeen, J. Hasker, Some experiments on the role of oxygen and surface reactions for tungsten and scandate thermionic emitters. IEEE Trans. Electron Dev. **37**(12), 2589–2594 (1990)
17. S. Yamamoto, S. Sasaki, S. Taguchi, I. Watanabe, N. Koganezawa, Application of an impregnated cathode coated with W-Sc_2O_3 to a high current density electron gun. Appl. Surf. **33–34**, 1200–1207 (1988)
18. S. Yamamoto, S. Taguchi, T. Aida, S. Kawase, Study of metal film coating on Sc_2O_3 mixed matrix impregnated cathodes. Appl. Surf. Sci. **17**, 517–529 (1984)
19. S. Yamamoto, I. Watanabe, S. Taguchi, S. Sasaki, T. Yaguchi, Formation mechanism of a monoatomic order surface layer on a Sc-type cathode. Jpn. J. Appl. Phys. **28**, 490–494 (1989)
20. R. Longo, D. Dibb, Dispenser scandate cathode: a progress report, Conf. Record, 1992, TRI Cathode Workshop, Greenbelt/Md, 51–56
21. Y. Wang, T. Pan, Investigation of pulsed laser depositing Sc-coated cathode, Appl. Surf. Sci. **146**, 62–68 (1999) and Vac. Sci. and Technology (in Chinese), vol. **16/1**, p. 10, 1996
22. G. Gaertner, P. Janiel, J.E. Crombeen, J. Hasker, Top-layer scandate cathodes by plasma-activated CVD, *Vacuum Microelectronics 1989*, Institute of Physics Conf. Series No. **99**, Bristol and New York, Ed. R. E. Turner, 25–28 (1989)
23. U. van Slooten, P. Duine, Scanning Auger measurements of activated and sputter cleaned Re-coated scandate cathodes. Appl. Surf. Sci. **111**, 24–29 (1997)
24. SMI Spectra-Mat Inc., Dispenser Cathode Products, PB-100-A- 04/14 (2014); Emission Characteristics for Scandium Type Dispenser Cathodes, TB 119 (2001) and "Notes on Dispenser and Oxide Cathodes", TB 128 (1999), Watsonville (USA) and b) S. Fukuda et al.,Appl. Surf. Sci. **146**, 84–88 (1999)
25. D. Kirkwood, J. Balk et al., Frontiers in thermionic research. IEEE Trans. ED **65**, 2061–2071 (2018)

26. G. Gaertner, P. Janiel, H. Lydtin, L. Rehder, Generation of very small particles by laser ablation in a carrier-gas, deposition and characterization, in Synthesis and Measurement of Ultrafine Particles, Delft University Press 1993, pp. 41–50
27. G. Gaertner, H. Lydtin, Review of ultrafine particle generation by laser ablation from solid targets in gas flows. NanoStruct. Mater. **4/5**, 559–568 (1994)
28. G. Gaertner, P. Geittner, D. Raasch, A. Ritz, D. Wiechert, Dynamic Shielding during ion bombardment of Ba dispenser cathodes. Appl. Surf. Sci. **146**, 12–16 (1999)
29. G. Gaertner, P. Geittner, E. Klein, "Elektrische Entladungsröhre oder Entladungslampe und Scandat-Vorratskathode", priority 31.7.1995 DE, Europ. Patent EP 0757370 granted 5.7.2000 and US-Patent 6 348 756 B1, "Electric discharge tube or discharge lamp and Scandate dispenser cathode", granted 19.2.2002
30. G. Gaertner, P. Geittner, H. Lydtin, "Scandat-Vorratskathode mit Re und Barium-Calcium-Aluminat-Beschichtung", German Patent application 19828729, filed 29.6.1998
31. G. Gaertner, P. Geittner, D. Raasch, D.U. Wiechert, "Scandat-Vorratskathode", German Patent 19961672B4, filed 20.12.1999, granted 9.4.2009
32. G. Gaertner, E. Klein, Scandate Dispenser Cathode, European patent application EP 04106783.6, filed 21.12.2004, and WO 2006/067670 A2, publ. 29.6.2006
33. G. Gaertner, W. Keur, "Target material for Barium Scandate Dispenser Cathode or Material", US-Patent application 3.8.2011, 2011P00729US_110803, 31.7.2012 patent filed WO2013/018027A1, "Target for Barium Scandate Dispenser Cathode", published 7.2.2013
34. C. Makovicka, G. Gaertner, A. Hardt, W. Hermann, D.U. Wiechert, Impregnated cathode investigations by SFM/STM and SEM/EDX. Appl. Surf. Sci. **111**, 70–75 (1997)
35. S. Sasaki, T. Yaguchi, N. Mori, S. Taguchi, M. Shibata, Non-uniform emission distribution on a scandate impregnated cathode. Appl. Surf. Sci. **146**, 17–21 (1999)
36. P. van der Heide, "Os/Ru coated Impregnated Cathode for Use in Cathode Ray Tubes", 1992 TRI-Service/NASA Cathode Workshop, Conf. Record, 155–159 (1992)
37. J. B. Scott, "Extension of Langmuir space-charge theory into the accelerating field range". J. Appl. Phys. **52**(7), 4406–4410 (1981)
38. J. Hasker, P. van Dorst, Pitfalls in the evaluation of cathode properties from I-V characteristics. IEEE Trans. ED **36**, 201–208 (1989) and J. Hasker, J.E. Crombeen, P. van Dorst, Comment on progress in Scandate cathodes. IEEE Transact. Electr. Dev. **36**, 215–219 (1989)
39. A. Manenschijn, S. Deckers, T. Weekers, P. van der Heide, *"Emission characterization of impregnated cathodes and Scandate cathodes", Conference record of 1992 TRI-Service/NASA Cathode Workshop* (Greenbelt/Md, USA, 1992), pp. 67–71
40. J. Hasker, Calculation of diode characteristics and proposed characterization of cathode emission probability. Appl. Surf. Sci. **16**, 220–237 (1983)
41. J. Hasker, Beam current characteristic and cathode loading of electron guns with rotational symmetry: some important properties and method of calculation. Philips Res. Reports **27**, 513–538 (1972)
42. T.G. Spanjer, A.A. van Gorkum, W.M. van Alphen, Electron guns for projection television. Philips Tech. Rev. **44**, 348–356 (1989)
43. H. Yuan, X. Gu, K. Pan, Y. Wang, W. Liu, K. Zhang, J. Wang, M. Zhou, J. Li, Characteristics of scandate-impregnated cathodes with sub-micron scandia-doped matrices. Appl. Surf. Sci. **251**, 106–113 (2005)
44. X. Zhang, G. Gaertner, Ion bombardment investigations of impregnated cathodes. Appl. Surf. Sci. **215**, 25–32 (2003)
45. G. Gaertner, P. Geittner, J. Crombeen, "Aktivierung von thermionischen Kathoden", German patent application P 199 32 564.2, filed 20.12.1999, disclosed 28.6.2001
46. G. Gaertner, S. Ording, T. Bisschops, "Comparison of Ba evaporation from different Ba-dispenser cathode types", ITG-Fachber. **150**, *Displays and Vacuum Electronics*, VDE-Verl., 489–494 (1998)
47. G. Gaertner, P. Geittner, D. Raasch, D.U. Wiechert, Supply and loss mechanisms of Ba dispenser cathodes. Appl. Surf. Sci. **146**, 22–30 (1999)

48. A.S. Gilmour, Jr., Chapter 5, "Thermionic Cathodes" in *Klystrons, Traveling Wave Tubes, Magnetrons, Crossed-Field Amplifiers and Gyrotrons*, ARTECH HOUSE (2011)
49. G. Gaertner, P. Geittner, D. Raasch, A. Ritz, D.U. Wiechert, Investigation of the shielding-effect during ion bombardment of ba-dispenser-cathodes, ITG-Fachbericht **150**, *Displays and Vacuum Electronic*s, VDE-Verlag, 483–487 (1998)
50. R.S. Raju, C.E. Maloney, Characterization of an impregnated scandate cathode using a semiconductor model. IEEE Trans. Electron Dev. ED **41**(12), 2460–2467 (1994)
51. R. Cortenraad, A.W. Denier van der Gon, H.H. Brongersma, G. Gaertner, A. Manenschijn, Thermionic cathodes studied by low-energy ion scattering, ITG-Fachbericht **150**, *Displays and Vacuum Electronics*, VDE-Verlag, 477–482 (1998)
52. R. Cortenraad, A. van der Gon, H. Brongersma, G. Gaertner, A. Manenschijn, Quantitative LEIS analysis of thermionic dispenser cathodes. Appl. Surf. Sci. **146**, 69–74 (1999)
53. R. Cortenraad, A. van der Gon, H. Brongersma, G. Gaertner, A. Manenschijn, Surface analysis of thermionic dispenser cathodes. Appl. Surf. Sci. **191**, 153–165 (2002)
54. S. Yamamoto, T. Yaguchi, S. Sasaki, I. Watanabe, Work function measurement of (W-$Sc_2W_3O_{12}$)-coated impregnated cathode by Retarding Potential method utilizing titaniated W(100) field emitter. Jpn. J. Appl. Phys. **28**, L865f (1989)
55. P. Zagwijn, J. Frenken, U. van Slooten, P.A. Duine, A model system for scandate cathodes. Appl. Surf. Sci. **111**, 35–41 (1997)
56. J. Eichmeyer, *Moderne Vakuumelektronik*, Springer 1981, pp. 208–210
57. G. Gaertner, D. Barratt, New developments and life aspects of oxide and Ba dispenser cathodes, ITG-Fachbericht **183**, *Displays and Vacuum Electronics*, VDE-Verlag, 111–116 (2004)
58. G. Gaertner, P. Geittner, H. Lydtin, Emissionseigenschaften von Top -Layer Scandat Kathoden, ITG Fachbericht **132**, "Vakuumelektronik und Displays", VDE Verlag, 35–40 (1995)
59. G. Gaertner, P. Geittner, D. Raasch, Low temperature and cold emission of Scandate cathodes. Appl. Surf. Sci. **201**, 61–68 (2002)
60. G. Gaertner, P. Geittner, H. Lydtin, Low-temperature cathode having an emissive nanostructure, US-Patent 5 866 975, granted 2.2.1999, priority 5.5.1995 DE
61. P. Geittner, G. Gaertner, D. Raasch, "Low temperature properties of Ba-dispenser cathodes", Technical Digest 05.19p, 12th Int. Vacuum Microelectronics Conf. 1999, Darmstadt, 190–191 and J. Vac. Sci. Techn. B **18**, 997–999 (2000)
62. D. Raasch, P. Geittner, G. Gaertner, "Ba losses due to oxygen adsorption on Ba-dispenser cathodes", Technical Digest 05.20p, 12th Int. Vacuum Microelectronics Conf. 1999, Darmstadt, 192–193, and J. Vac. Sci. Techn. B **18**, 1000–1002 (2000)
63. G. Gaertner, P. Geittner, D. Raasch, U. Schiebel, Low Temperature Thermionic Cathodes for CRTs and FPDs, Eurodisplay '99, 283–287 (1999)
64. A. Shroff et al., Performance and life tests of various types of impregnated cathodes. Applic. Surf. Sci. **8**, 36–49 (1981)
65. T. Aida, H. Tanuma, S. Sasaki, T. Yaguchi, Emission life and surface analysis of barium impregnated thermionic cathodes. J. Appl. Phys. **74**, 6482–6487 (1993)
66. G. Gaertner, P.A.M. van der Heide, New developments in CRT cathodes, in Proceedings of IDW 2000, Kobe, Japan, CRT4-1 (invited), 513–516 (2000)
67. G. Gaertner, D. Barratt, Life-limiting mechanisms in Ba-oxide, Ba dispenser and Ba Scandate cathodes. Appl. Surf. Sci. **251**, 73–79 (2005)
68. J.-M. Roquais, F. Poret, R. le Doze, J.L. Ricaud, A. Monterrin, A. Steinbrunn, Appl. Surf. Sci. **215**, 5–17 (2003)
69. T. Higuchi et al., Modeling of life deterioration by ion bombardment of a dispenser cathode coated with W/Ir film. Appl. Surf. Sci. **200**, 125–137 (2002)
70. T. Higuchi et al., Modeling of emission slump by ion bombardment of a dispenser cathode in an electron tube, Ext. Abstracts IVEC-IVESC 2012, Paper 07
71. C. Marrian, A. Shih, The operation of coated tungsten based dispenser cathodes in nonideal vacuum. IEEE Transact. Electr. Dev. **36**(1), 173–179 (1989)
72. A. Sharma, A. Chopra, R. Mathew, Emission poisoning studies on impregnated tungsten dispenser cathodes under O_2 and CO_2 environment, Appl. Surf. Sci. **40**, 97–101 (1989)

73. S. Kimura, D. Miyazaki, M. Hara, M. Fujiwara, Emission characteristics and surface composition of dispenser cathodes in realistic vacuum. Vacuum **41**, 1763–1765 (1990)
74. H. Gallagher, Gas poisoning of cathodes, IEEE Conf. Record, 9th Conf. on Tube Technology New York 1968, 15–22
75. R.O. Jenkins, W. Trodden, The poisoning of impregnated cathodes. J. Electron. Control **7**, 393–415 (1959)
76. N. van Veen, XPS on impregnated cathodes: surface concentrations and thermal stability. Appl. Surf. Sci. **29**, 113–126 (1987)
77. J. Hasker, H. van Stoffelen, "Alternative" Auger analysis reveals important properties of M type and scandate cathodes. Appl. Surf. Sci. **24**, 330–339 (1985)
78. S. Magnus, D. Hill, W. Ohlinger, Emission properties of compounds in the $BaO{\cdot}Sc_2O_3{\cdot}WO_3$ ternary system, Appl. Surf. Sci**. 111**, 42–49 (1997); Thermochemistry in the $BaO{\cdot}Sc_2O_3{\cdot}WO_3$ ternary system, Appl. Surf. Sci. **111**, 50–55 (1997)
79. J. Li, S. Yua, W. Shao, Q. Chen, M. Zhu, Investigation and application of impregnated scandate cathodes. Appl. Surf. Sci. **215**, 49–53 (2003)
80. T. Shintake, N. Akasaka, H. Matsumoto, Y. Ohkubo, H. Yonezawa, Development of C-band 50 MW pulse klystron for e^+ e^- linear collider, Proc. Particle Accelerator Conference, 1997, Vancouver, Canada, p. 533 (1997), https://doi.org/10.1109/pac.1997.749748
81. E. Uda, O. Nakamura, S. Matsumoto et al., Emission and life characteristics of thin film top-scandate cathode and diffusion of Sc_2O_3 and W. Appl. Surf. Sci. **146**, 31–38 (1999)
82. J. Wang, W. Liu, L. Li, Y.C. Wang, Y. Wang, M. Zhou, A study of scandia-doped pressed cathodes. IEEE Trans. Electron Dev. ED **56**, 799 (2009)
83. W. Liu, K. Zhang, Y. Wang, K. Pen, X. Gu, J. Wang, J. Li, M. Zhou, Operating model for scandia doped matrix scandate cathodes. Appl. Surf. Sci. **251**, 80–88 (2005)
84. J. Wang, M. Zhou, Y. Wang, W. Liu, Manufacturing method of precursor powder for Sc-containing dispenser cathode, China Patent ZL 200510053831.6 (2005)
85. J. Wang, Y. Cui, W. Liu, Y. Wang, F. Yang, F. Zhou, M. Zhou, A study of scandia-doped impregnated cathode fabricated by spray drying method. IEEE Trans. Electron Dev. ED **62**, 1635–1640 (2015)
86. Y. Cui, J. Wang, W. Liu, Preparation and characterization of scandia-doped tungsten powders prepared by a spray-drying method, Res. Chem. Intermed., published on line, https://doi.org/10.1007/s11164-011-0248-4
87. A.M. Shroff, Review of dispenser cathodes. Revue Technique, Thomson-CSF **23**, 948–1026 (1991)
88. L. Li, J. Wang, Y. Wang, Generation of high-current-density sheet electron beams. IEEE Electron Device Lett. **30**, 228–230 (2009)
89. M.J. Cattelino, G. Miram, Predicting cathode life expectancy and emission quality from PWFD measurements. Appl. Surf. Sci. **111**, 90–95 (1997)
90. T. J. Grant, A powerful quality assurance technique for dispenser cathodes and electron guns, in IEDM Tech. Dig., 1984, p. 334–337
91. A. Sandor, Activation Process of Impregnated Dispenser Cathode Viewed in the Large-screen Emission Microscope. Int. J. Electron. **13**(5), 401–416 (1962). https://doi.org/10.1080/00207216208937447
92. W. Liang, Y. Wang, J. Wang, W. Liu, F. Yang, DC emission characteristic of nanosized-scandia-doped impregnated dispenser cathodes. IEEE Trans. Electron Dev. ED **61**, 1749–1753 (2014)
93. W. Liu, Y. Wang, J. Wang, Y.C. Wang, B. Vancil, Emission characteristics of nanosized scandia-doped dispenser cathodes in open electron-gun structures. IEEE Trans. Electron Dev. ED **58**, 1241–1246 (2011)
94. G. Miram, L. Ives, M. Read, R. Wilcox, *Emission Spread in Thermionic Cathodes* (Technical Digest, Fifth IEEE IVEC, 2004), pp. 303–304
95. Y. Wang, J. Wang, W. Liu, L. Li, Y.C. Wang, X. Zhang, Correlation Between Emission Behavior and Surface Features of Scandate Cathodes. IEEE Trans. Electron Dev. ED **56**, 776 (2009)

96. G. Miram, M. Cattelino, Life Test Facility for Thermionic Cathodes, Conference Record 1994, Tri-Service/NASA Cathode Workshop, Cleveland, U.S, March 1994, p. 29–31
97. R. L. Ives, G. Collins, M. Read, G. Miram, D. Marsden, Electron Guns for Terahertz Vacuum Electron Sources, Terahertz Science and Technology vol. **4/4**, p. 230 (2011), ISSN 1941–7411
98. M.A. Basten, J.H. Booske, Two-plane focusing of high-space-charge sheet electron beams using periodically cusped magnetic fields. J. Appl. Phys. **85**, 6313 (1999)
99. L. Li, Y. Wang, W. Liu, Y.C Wang, J. Wang, A. Srivastava, J.-K. So, G.-S. Park, Development of high-current sheet beam cathodes for terahertz sources, IEEE Trans. Electron Dev. **ED 56**, p. 762 (2009)
100. A. Srivastava, J.-K. So, Y. Wang, J. Wang, R.S. Raju, S.-T. Han, G.-S. Park, Design of sheet-beam electron gun with planar cathode for terahertz devices. J. Infrared Millim. & Terahertz Waves **30**, 670–678 (2009)
101. R. Forman, Surface studies of barium and barium oxide on tungsten and its application to understanding the mechanism of operation of an impregnated tungsten cathode. J. Appl. Phys. **47**, 5272–5279 (1977)
102. G.A. Haas, A. Shih, C.R.K. Marrian, Interatomic Auger analysis of oxidation of thin Ba film II. Applications to impregnated cathodes. Applications Surf. Sci. **16**, 139–162 (1983)
103. K.G. Eyink, B.C. Lamartine, W.V. Lampert, T.W. Haas, Quantification of the surface coverage of Ba on W substrates using Auger electron spectroscopy. Applications Surf. Sci. **20**, 215–227 (1985)
104. G. Lesny, R. Forman, Surface studies on Scandate cathodes and synthesized scandates. IEEE Trans. Electron Dev. ED **37**, 2595–2604 (1990)
105. S. Yamamoto, S. Taguchi, l. Watanabe, S. Kawase, Impregnated cathode coated with tungsten thin film containing Sc_2O_3. J. Vac. Sci. Technol. **A5,** 1299 (1987)
106. A. Shih, J.E. Yater, C. Hor, Ba and BaO on W and on Sc_2O_3 coated W. Appl. Surf. Sci. **242**, 35–54 (2005)
107. A. P. Makarov, The change of a multilayer film work function of jointly adsorbed atoms of barium, scandium and oxygen on the facet (100) of a tungsten crystal at adsorption and heating, in Proceedings IVEC 2015, Beijing, China, April. 27–29, (2015), p. 41. DOI:10.1109/IVEC.2015.7223742
108. Y. Wang, J. Wang, W. Liu, X. Zhang, L. Li, Emission mechanism of high current density scandia-doped dispenser cathodes, J. Vac. Sci. Technol. **B 29**, p. 04E106-1–9 (2011)
109. Y. Wang, J. Wang, W. Liu, Development of scandate cathode and its prospect_ a review, in Proceedings IVESC, 2012, Monterey, USA, p. 41 (2012)
110. R.W. Speringer, T.A. Haas, Auger electron spectroscopy study of cathode surface during activation and poisoning the Barium on Oxygen on Tungsten dispenser cathode. J. Appl. Phys. **45**, 5260 (1974)
111. A. Shih, G.A. Haas,.R.K. Marrian, "Preparation and oxidation of a thin Ba film", Applications Surf. Sci. **16**, 93–105 (1983)
112. R. Forman, A proposed physical model for the impregnated tungsten cathode based on Auger surface studies of the Ba-O-W system. Appl. Surf. Sci. **2**, 258–274 (1979)
113. T. Kawano, Y. Takai, R. Shimizu, Characterization of Sc-O/W(100) surface as Schottky emitter: work function change for activation processing. Jpn. J. Appl. Phys. **39**, 577–580 (2000)
114. F. Yang, J. Wang, Y. Wang, W. Liu, X. Zhu, Investigation of nanosized-scandia-doped dispenser cathodes with machined surfaces. IEEE Trans. Electron Dev. ED **63**, 1728–1733 (2016)
115. J. Wang, Y. Wang, X. Wang, X. Zhang, F. Yang, W. Liu, M. Zhou, Surface characteristics of scandate dispenser cathodes during life, in Proceedings IVEC, 2013, Paris, France (2013). https://doi.org/10.1109/ivec.2013.6571168
116. D.A. Wright, J. Woods, The emission from oxide-coated cathodes in an accelerating field. Proc. Phys. Soc. **65**, 134–148 (1952)
117. R. Vaughan, A Synthesis of the Longo and Eng Cathode Emission Models. IEEE Trans. Electron Dev. ED **33**, 1925 (1986)

118. R.T. Longo, Physics of thermionic dispenser cathode aging. J. Appl. Phys. **94**, 6966 (2003)
119. Z. Zeng, Q. Su, M. Li, L. Cai, Structure analysis study in emissive materials of the Barium Scandate dispenser cathode. J. Electron. (in Chinese), vol.**12/.2**, 179 (1990)
120. J.M. Vaughn, K.D. Jamison, M.E. Kordesch, In situ emission microscopy of scandium/scandium-oxide and barium/barium-oxide thin films on tungsten, IEEE Trans. Electron Dev. **ED 56**, 794 (2009)
121. Y. Yang, Y. Wang, W. Liu, Z. Pan, J. Li, J. Wang, Robustness investigation on nanosized-scandia-doped dispenser cathodes. IEEE Trans. Electron Dev. ED **65**, 2072–2076 (2018)
122. R.M. Jacobs, J.H. Booske, D. Morgan, Electron emission energy barriers and stability of Sc_2O_3 with Adsorbed Ba and Ba–O. J. Physical Chem. C **118**, 19742–19758 (2014)
123. M.E. Kordesch, J.M. Vaughn, C. Wan, Model scandate cathodes investigated by thermionic-emission microscopy, J. Vac. Sci. Technol. **B 29(4)**, 04E102-1, Jul/Aug 2011
124. V.I. Kapustina, I.P. Lia, A.V. Shumanov, YuYu. Lebedinskii, A.V. Zablotskii, Physical operating principles of scandate cathodes for microwave devices. Phys. Electron. **62**, 116–126 (2017)
125. C.J. Edgcombe, U. Valdre, Microscopy and computational modelling to elucidate the enhancement of factor for field electron emitters. J. Microscopy **203**, 188 (2001)
126. C. Eng, H. Kan, Scanning Auger and work function measurements applied to dispenser cathodes, Aerospace corporation report SD-TR-81-35, (1981)
127. T.C. Back, S. Fairchild et al., Work Function Characterization of Directionally Solidified LaB_6 –VB_2 Eutectic, Ultramicroscopy **183**, May 2017